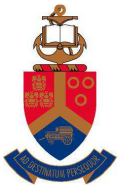

UNIVERSITEIT VAN PRETORIA
UNIVERSITY OF PRETORIA
YUNIBESITHI YA PRETORIA

Heat Transfer Coefficients of Smooth Tubes in the Turbulent Flow Regime

By

Nicole Coetzee

Submitted in partial fulfilment of the requirements for the degree of

MASTER OF ENGINEERING

Supervisor: Prof JP Meyer

Department of Mechanical and Aeronautical Engineering

University of Pretoria

May 2015

I. ABSTRACT

Several well-known equations are available in literature that can be used to determine the heat transfer coefficients of smooth tubes in the turbulent flow regime. When comparing the results of these equations they vary over a considerable range. Although in many cases it is assumed that the Gnielinski equation is one of the most accurate as it is the most recently developed correlation, the uncertainty of this equation has not be quantified as yet. Many of the equations have been developed using the data that was obtained from experimental testing as far back as 80 years ago. As more accurate instrumentation is available, it should be possible to collect more accurate data during experimental testing. The purpose of this study was threefold: to take accurate heat transfer measurements and to quantify the uncertainties of the Nusselt numbers as a function of Reynolds number; to compare the measured data with existing correlations and to develop an accurate Nusselt number correlation from the data. Experiments were conducted on two smooth circular tubes with a heat transfer length 3.75 m with inner tube diameters of 8.3 mm and 14.2 mm using water over a Reynolds number range of 10 000 to 220 000 and a Prandtl number range of 3.2 to 4. Surface roughness analysis was also performed to ensure the tubes can be considered as smooth tubes. Pressure drop measurements were also taken over tube lengths of 4.1 m as a function of Reynolds number. The experiments were conducted using a tube-in-tube heat exchanger with the hot water in the inner tube and the cold water in the annulus operating in a counter flow configuration. The friction factor values were determined from pressure drop measurements and the heat transfer coefficients were determined from the Wilson Plot method using temperature and mass flow rate measurements. The average uncertainties of the friction factors and Nusselt numbers were both less than 3%. The results were compared to the existing literature and it was found that at lower Reynolds numbers the Nusselt numbers deviated slightly to those of Gnielinski with the results comparing more closely with increasing Reynolds number. The friction factor results correlated well with that of Blasius. A new Nusselt number correlation, which is a function of Reynolds number, Prandtl number and friction factor, was developed. The equation predicted all the measured values within 3%. The equation is, however, limited in not taking into consideration large variations in fluid properties.

II. ACKNOWLEDGEMENTS

I would like to take the opportunity to thank the following people:

- My God and Heavenly Father for giving me the opportunity, ability and strength to complete this study.
- My family – thank you for the support and guidance throughout this long journey. Without your support and continuous encouragement, the completion of this study would not have been possible.
- My husband Louw – finding you was the best part of this study. I thank you for your encouragement, motivation, guidance and your regular advice.
- My colleagues and friends – thank you for making this massive learning curve such a fun and rich experience. Through all the good and really bad times, I thank you for seeing me through with humour and unending support. To Kersten, a special word of thanks for all your assistance.
- Prof Meyer and the University – thank you very much for the opportunity to undertake this study and for assisting me in building my education.
- The funding obtained from the NRF, Stellenbosch University/University of Pretoria Solar Hub, EEDSM Hub, RDP and NAC is acknowledged and duly appreciated.

"A man should look for what is, and not for what he thinks should be."
Albert Einstein

III. TABLE OF CONTENTS

IV. LIST OF FIGURES

V. LIST OF TABLES

VI. NOMENCLATURE

SYMBOL	DESCRIPTION	UNITS
A	Surface Area	[m^2]
C_p	Specific Heat Capacity	[J/kg.K]
C	Wilson Plot Coefficient	-
D	Diameter of Tube	[m]
EB	Energy Balance	[%]
h	Convective Heat Transfer Coefficient	[$W/m^2.°C$]
j	j-Factor	-
k	Thermal Conductivity	[W/m.K]
L	Length of Tube	[m]
$\dot{m}$	Mass Flow Rate	[kg/s]
NTU	Natural Transfer Units	-
p	Perimeter	[m]
P	Wilson Plot Variable	-
P	Pressure	[Pa]
$\dot{q}$	Heat Flux	[W/m^2]
$\dot{Q}$	Heat Transfer Rate	[W]
r	Radius of Tube	[m]
R	Thermal Resistance	[°C/W]
s	Standard Deviation	[%]
T	Temperature	[°C]
U	Overall Heat Transfer Coefficient	[W/°C]
U	Uncertainty	-
V	Average Velocity of Fluid Flow	[m/s]

Dimensionless Groups

Gr	Grashof number	-
Nu	Nusselt number	-
Pr	Prandtl number	-
Re	Reynolds number	-
St	Stanton number	-

Greek Symbols

∂	Partial Differential	-

SYMBOL	**DESCRIPTION**	**UNITS**
Greek Symbols		
∂	Partial Differential	-
Δ	Change in Properties	-
ε	Mean Height of the Roughness of a Pipe	-
f	Friction Factor	-
μ	Dynamic Viscosity of Fluid	[N.s/m^2]
ρ	Density of Fluid	[kg/m^3]
τ	Shear Stress	[N]
υ	Kinematic Viscosity of Fluid	[m^2/s]

Subscripts	
a	Annulus
avg	Average
b	Bulk
c	Cold
cs	Cross Sectional
dev	Deviation
e	Exit
exp	Experimental
h	Hot
h	Hydrodynamic
h	Hydraulic
I	Inner Tube
in	Inlet
lm	Log Mean Temperature Difference
max	Maximum
min	Minimum
o	Outer Tube / Annulus
out	Outlet
std	Standard
T	Turbulent
th	Theoretical
w	Wall
∞	Ambient

1. INTRODUCTION

1.1 Background

In the modern world, there is a continuous drive towards an improvement with regards to energy efficiency and the reduced use of limited resources. As the earth's population continues to grow, so do the requirements to live and therefore excessive demand is placed on the natural resources to meet these requirements. This includes the requirement to convert fossil fuels to energy to drive industries to manufacture products required for consumption by an ever increasing world population. In addition to the need for energy to enable these processes, another by-product of these processes are combustion products which negatively impact the environment and add to the devastating effect that global warming is having on our planet. It is due to these factors that research is ongoing to determine a more efficient way to produce energy and to minimise the damaging effects of the process of doing so.

Heat transfer is a physical phenomenon that occurs whenever there is a temperature gradient between two mediums i.e. solids, liquids or gases. Heat transfer has the ability to work in a positive or negative manner whenever any physical process occurs. Positively, it allows for heat to be transferred enabling a reaction that requires heating i.e. saving energy by re-using existing energy/heat that is in an exhaust stream from a previous reaction. It impacts negatively when temperatures rise and heat needs to be exhausted at a higher rate but the physical limits do not allow for it i.e. heat produced by microchips in computing applications. It is due to this that continued research is conducted to determine the most optimal solution within the physical boundaries that exist in heat transfer.

Many of the processes in industry operate in the turbulent flow regime to obtain higher heat transfer rates and therefore higher energy recovery rates. Turbulent heat transfer has been well researched and documented over the past 100 years. Many correlations have been developed and data has been recorded but there is still a considerably large discrepancy in the agreement of these studies and correlations to each other. Dittus and Boelter (1930) performed their experiments with the aim of producing a single equation to accurately predict the heat transfer in both heating and cooling applications using the data of McAdams and Frost (1922) and Morris and Whitman (1928). The resulting equation utilised an exponent to predict the heating and cooling separately which enabled good agreement to the previous data sets obtained.

The first of these studies to make a marked improvement in the prediction of turbulent heat transfer is that of Colburn (1933). Colburn was the first study to make use of the dimensionless numbers such as Stanton, Prandtl and Nusselt to reduce the number of variables in the calculation of the heat transfer coefficients. In addition to this, Colburn recognised the effect that the wall temperature has on the properties of the fluid and that it cannot be assumed that the bulk temperature is sufficient to predict the properties at the tube wall. Sieder and Tate (1936) produced both their own data and used existing data sets to determine an equation which accurately accounts for the difference in temperature between the centre of the fluid stream and that at the tube wall.

The next phase of heat transfer research resulted in more work being undertaken in the field where analytical methods were used to solve for the equations in an effort to predict the turbulent heat transfer behaviour more accurately. Petukhov (1970) performed a considerable amount of analysis using existing data sets as well as producing some data of his own to

determine an equation which also takes into account the effect that the friction factor has on the heat transfer in the system.

The work completed by Gnielinski (1976) utilised that of Petukhov but included the work of Hausen (1959) to improve the ability of the correlation to predict heat transfer in both the transitional and turbulent flow regimes. Of all the studies conducted, Gnielinski produces the best accuracy with the results, lying within 20% of those previously recorded, when compared to existing data sets.

1.2 Problem Statement

In general it should be assumed that the Gnielinski and Petukhov equations are the most accurate as they were the most recently developed and the other older equations developed should be used less and should be phased out. However, a search (January 2015) on Scopus showed that the older equations are being actively used. The citations to these equations are Dittus and Boelter (1930) equation 117 times, the Colburn (1933) equation 262 times, the Chilton-Colburn (1934) equation 345 times, the Sieder and Tate (1936) equation 722 times, the Petukhov (1970) equation 479 times and the Gnielinski (1976) equation 87 times. It therefore seems as if the Sieder and Tate equation is the most utilised equation based on citations. Although it is assumed that the Gnielinski and Petukhov equations are the most accurate of the existing theory, many researchers still utilise the historical equations when verifying smooth tube experimental data, for example: Colburn (1933) and Sieder and Tate (1936). The citations accredited to Gnielinski and Petukhov are most probably not accurate as a large amount of their initial work was published in the German and Soviet literature and in textbooks. The work of Gnielinski (1976) for example, was published in 1976 in the journal of International Chemical Engineering with permission from the VDI-Verlag GmbH, however this paper is not on the Scopus database. Thus, there is no clear evidence from the literature (based on citations) which one of the many equations in general are the most accurate.

In Figure 1, the Nusselt numbers are calculated at a Prandtl number of 7 using the correlations of Dittus and Boelter (1930), Sieder and Tate (1936), Petukhov (1970) and Gnielinski (1976). The coefficient used in the Dittus and Boelter equation is $n = 0.3$ for cooling applications. The Gnielinski and Petukhov correlations compare very well to each other and are within 5% of one another. However at a Reynolds number of 10 000, there is a maximum deviation of over 50% between the Sieder and Tate and Petukhov equations. At a Reynolds number of 200 000 there is a deviation of 40%. The reasons for these deviations are not clear.

Furthermore, in the period of 1922 to 1936, when most of the physical experiments were conducted that formed the basis of the work of many scholars in terms of improvements and refinements, the execution of uncertainty analyses was not a requirement in scholarly journals. Therefore, the uncertainties of convective heat transfer equations in smooth tubes which are widely published in heat transfer textbooks that are used for verification and comparison studies are in general not readily available. With more accurate measuring instrumentation available today than almost a century ago, it should be possible to conduct more accurate experiments and derive a more accurate correlation with a quantified uncertainty. These results can also be used to evaluate the accuracy of existing equations.

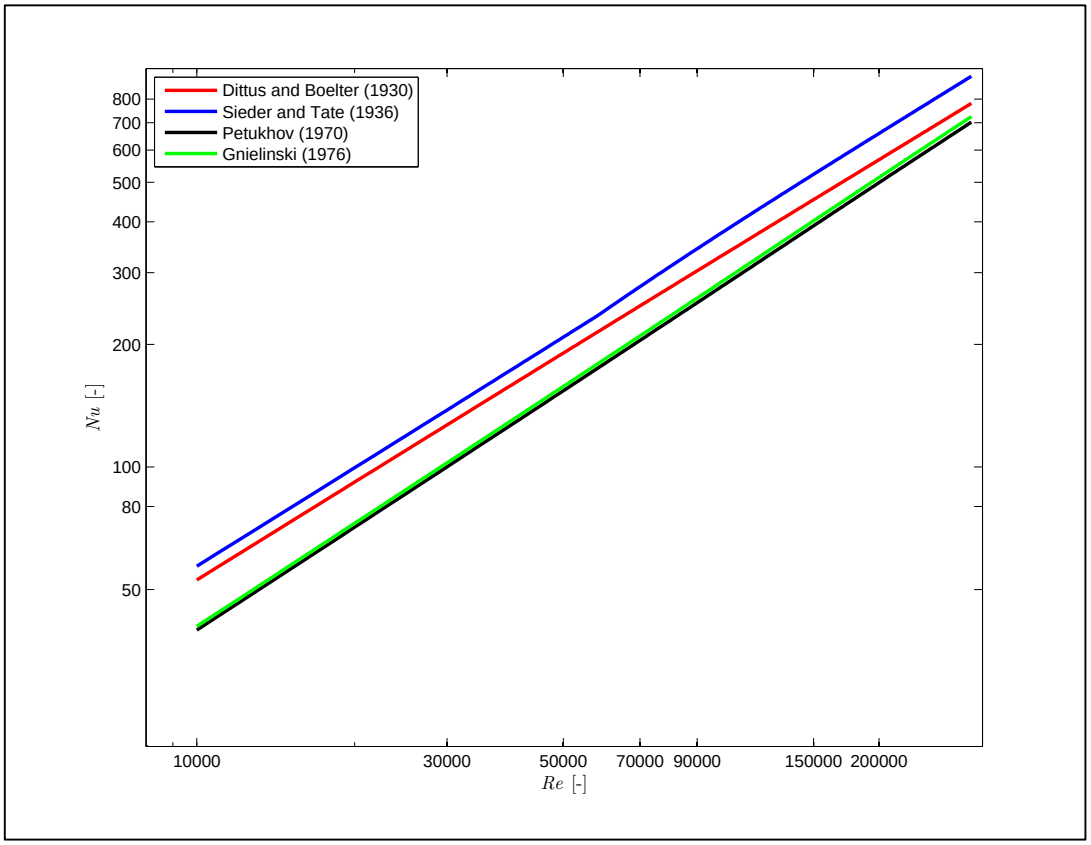

Figure 1: Theoretical comparison of heat transfer correlations for turbulent flow over a Reynolds number range of 10 000 to 250 000 at a Prandtl number of 7. The coefficient used in the Dittus and Boelter equation is n = 0.3 for cooling applications.

1.3 Purpose of Study

The purpose of this study was threefold: to take accurate heat transfer measurements of a circular smooth tube and to quantify the uncertainties of the Nusselt numbers as a function of Reynolds number; to compare the measured data to existing correlations and to develop an accurate Nusselt Number correlation from the data.

The focus was on the turbulent flow regime. The transitional flow regime (Meyer and Olivier 2011) and lower end Reynolds number regimes (Gnielinski 2013) were excluded as work on these regimes was recently conducted.

In terms of the time limitations for a master's dissertation and available experimental facilities and equipment, the experiments were limited to two smooth circular tubes with flow in the horizontal flow direction. Experiments were conducted on two tube diameters and the testing fluid was water only. Experiments were conducted on a Reynolds number range of 10 000 to 230 000 over a Prandtl number range of 3.2 to 4. The work was also limited to exclude the investigation of large variations in fluid properties.

Although pressure drop as a research outcome was not the focus of this study, pressure drop measurements were also taken as several of the existing equations such as Gnielinski and Petukhov make use of the friction factor obtained from pressure drop measurements.

1.4 Organisation of this Dissertation

This dissertation consists of a total of seven chapters. Chapter 2 gives an overview of the existing literature applicable to the study. In Chapter 3 the experimental set-up and test section construction is described and information on the testing process is presented. The data reduction methods used to evaluate the experimental data can also be found in Chapter 3. In Chapter 4 the uncertainty calculation on the experimental data and the results thereof are discussed. Chapter 5 details the results obtained from the experimental testing. In Chapter 6, the conclusions from the study are described and Chapter 7 contains the references used. Appendix A contains detailed information on how the uncertainty of the friction factor and Nusselt Number were calculated. Appendix B contains a sample of the data recorded during experimental testing.

2. LITERATURE STUDY

2.1 Background

The purpose of this chapter is to describe the existing heat transfer theory related to turbulent flow. The theory and properties related to the turbulent flow regime are described. The heat transfer and friction factor theories are addressed. Specific detail on the most important and widely used heat transfer correlations are described which include the studies of: Dittus and Boelter (1930), Colburn (1933), Sieder and Tate (1936), Petukhov (1970) and Gnielinski (1976). The most important experimental data sets that have been utilised in the development of heat transfer correlations are also mentioned.

2.2 Turbulent Flow Regime

The Reynolds number (*Re*) is a dimensionless number used to represent certain fluid flow characteristics. Developed in 1883, the Reynolds number represents the ratio of the inertial forces of a fluid to the viscous forces of a fluid. This can be represented in equation (1) (White 2003) which relates the two fluid forces to each other.

$$Re = \frac{\rho VL}{\mu} = \frac{VL}{\nu} \tag{1}$$

Laminar flow occurs for Reynolds numbers from 0 to approximately 2 300. The flow that occurs in this regime is characterised by smooth and steady flow patterns. Flow in the laminar region is also referred to as streamlined flow.

Laminar flow is characterised by smooth boundary layers with little disturbance between these layers. When dealing with fluid dynamics, flow in the laminar region contains the following physical parameters:

- high momentum diffusion
- low convection heat transfer
- velocity independent of time
- pressure independent of time

Transitional flow occurs as laminar flow becomes turbulent. The Reynolds number range is approximately 2 300 to 10 000 for the transitional flow regime. Transitional flow depends on many factors, these including the surface roughness, type of tube inlet, Reynolds number or fluctuations that may occur in the fluid inlet stream. While numerous data has been collected on the transitional flow regime, the theory required to better understand the behaviour of the fluid while in this regime remains limited.

Turbulent flow occurs for Reynolds numbers in excess of approximately 10 000. Turbulent flow has fluctuating and agitated flow patterns. Initially flow will display occasional natural disturbances as the flow moves through the transition between the laminar and turbulent flow regimes. These fluctuations, which are found in the boundary layer, become more frequent as the flow gets closer to being fully turbulent. At a sufficiently large Reynolds number, the flow fluctuates continuously with eddies and vortices forming. Important to note is that this disorder is not just chaotic motion, it has a definite spatial structure and can be described using the following characteristics (White 2006):

- Fluctuations in pressure, velocity and temperature. Velocity fluctuates in all three directions.
- Eddies that intermingle and fill the shear layer.
- Random fluid property variations.
- Self-sustaining motion by producing new eddies which replace those lost by viscous dissipation.
- Mixing that is much stronger than that found in laminar flow due to the eddies moving in three directions. The movement causes diffusion of mass, momentum and energy.

Due to the consistent tripping and breaking of the boundary layers, considerable mixing occurs in the turbulent flow regime. It is due to this that the heat transfer is enhanced and as a result, the pressure drop over the flow length is also increased.

The physical properties of the turbulent flow regime are:

- low momentum diffusion
- high convection heat transfer
- velocity variations in space and time
- pressure variations in space and time

The turbulent and laminar flow regimes display two distinct variations in heat transfer and pressure drop trends. These trends are discussed in further detail in section 2.3 and 2.4.

2.3 Pressure Drop and Friction Factors in the Turbulent Flow Regime

The pressure drop that occurs during the flow of viscous fluids is usually referred to as an irreversible pressure loss, ΔP. This comes from the term head loss which is associated with fluid mechanics theory. The pressure loss (Cengel 2006) is described by equation (2):

$$\Delta \mathrm{P} = f \frac{L}{D} \frac{\rho V_{avg}^2}{2} \tag{2}$$

where the term $\frac{\rho V_{avg}^2}{2}$ is the dynamic pressure of the system and f is the Darcy friction factor which is defined as:

$$f = \frac{8\tau_w}{\rho V_{avg}^2} \tag{3}$$

The Blasius equation is used to determine the adiabatic friction factor for smooth tubes (White 2006). This is defined in equation (4) as:

$$C_f = 0.0791 Re^{-0.25} \tag{4}$$

When using the friction factor definition, the equation transforms to:

$$f = 0.3164 Re^{-0.25} \tag{5}$$

The Petukhov equation (Petukhov 1970) for smooth tubes is described in equation (6).

$$f = (1.82 \log Re - 1.64)^{-2} \; for \; 3000 < Re < 5 \times 10^6 \qquad (6)$$

Equation (6) is used in conjunction with the Chilton-Colburn analogy to determine the Nusselt number (*Nu*). This is discussed in section 2.4.

Another equation which was developed for the turbulent flow regime is the Colebrook correlation. This correlation is based mainly on experimental data and is applicable for flow with Reynolds numbers in excess of 4 000. This relation led to the development of the Moody chart which is used to determine the friction factor for pipe friction with smooth and rough walls. The chart can be used for various pipe geometries and for open channel flows. The study has proved very valuable in fluid mechanics applications and when calculating the pressure loss of a system.

The Colebrook equation (Colebrook 1939) is an implicit equation as stated in equation (7):

$$\frac{1}{\sqrt{f}} = -2log_{10}\left(\frac{\varepsilon/D_h}{3.7} + \frac{2.51}{Re\sqrt{f}}\right) \qquad (7)$$

There is an alternative formula developed by Haaland (1983) which can be used but it is only found to vary by 2% from the Colebrook correlation.

In Table 1, a summary of friction factors used in the turbulent flow regime can be found.

Table 1: Friction Factors for Turbulent Flow

CORRELATION	**EQUATION**
Blasius (1913) equation	$f = 0.3164Re^{-0.25}$
Petukhov (1970) equation	$f = (1.82 \log Re - 1.64)^{-2}$
Colebrook (1939) equation	$\frac{1}{\sqrt{f}} = -2log_{10}\left(\frac{\varepsilon/D_h}{3.7} + \frac{2.51}{Re\sqrt{f}}\right)$
Haaland (1983) equation	$\frac{1}{\sqrt{f}} = -1.8log_{10}\left(\frac{6.9}{Re} + \left(\frac{\varepsilon/D_h}{3.7}\right)^{1.11}\right)$

2.4 Heat Transfer in the Turbulent Flow Regime

The Nusselt number is a dimensionless number which is used to describe the relationship between the convective heat transfer and the conductive heat transfer that takes place on the surface of an object.

The Nusselt number is defined to be a function of the heat transfer coefficient (*h*), characteristic length (*L*) and thermal conductivity (*k*) of a fluid.

The equation used to describe the Nusselt number (Cengel 2006) is:

$$Nu = \frac{Convective\ \ Heat\ \ Transfer}{Conductive\ \ Heat\ \ Transfer}$$

$$Nu = \frac{hL}{k} \tag{8}$$

Many studies have been undertaken to describe the heat transfer that occurs as a result of the flow of a fluid, known as convective heat transfer. This would lead to the mass flow rate of a fluid being used in relation to the Nusselt number. The Reynolds number is used to characterise the flow of the fluid as it is a simple dimensionless number which takes into account the flow rate, density and viscosity of the fluid. The studies that have been undertaken have mostly been to describe the heat transfer that occurs in either the laminar or turbulent flow regimes.

Another factor which needs to be considered in turbulent heat transfer is the effect that the Prandtl number has on heat transfer. The Prandtl number has little effect on heat transfer in the laminar flow regime but has a significant effect when in the turbulent flow regime.

The Prandtl number is used to relate the molecular diffusivity of momentum to the molecular diffusivity of heat. For example, heat diffuses very quickly in liquid metals which have a Prandtl number of much less than one. In contrast, heat diffuses very slowly in fluids such as oil which has a Prandtl number of much larger than one.

The Prandtl number is defined as (Cengel 2006):

$$Pr = \frac{\nu}{\alpha} = \frac{c_p \mu}{k} \tag{9}$$

For turbulent flow, there are numerous correlations that can be used to calculate the heat transfer that occurs. Each of the correlations that will be investigated are widely recognised and employed when calculating heat transfer coefficients in the turbulent flow regime. It is found that there is a clear variance of results when comparing the heat transfer coefficients calculated by these correlations. This indicates a degree of inaccuracy in the development of these correlations and therefore a more accurate equation needs to be investigated to correctly predict these values and experimentally validate the existing theory.

In Table 2, a summary of all the most important data sets that were produced and utilised in other studies can be found. Included in the table is: the testing fluid that was used, the heat transfer application and which of the important studies utilised these data sets for mathematical manipulation or comparisons to the authors own data set. This gives one a clear representation of what work was undertaken and which works can be compared to each other and where caution should be exercised when Prandtl number differences should be noted due to the varying fluids tested.

Table 2: Summary of Data Sets Employed in Heat Transfer Studies

AUTHOR(S)	TEST MEDIUM	APPLICATION	MAXIMUM REYNOLDS NUMBER TESTED	PRANDTL NUMBER RANGE	EMPLOYED BY
McAdams and Frost (1922)	Water		223 200		Dittus and Boelter (1930)
Morris and Whitman (1928)	Water Gas Oil Gas Oil Straw Oil Straw Oil	Heating Heating Cooling Heating Cooling	38 800 30 000 44 200 12 700 45 300		Colburn (1933) Dittus and Boelter (1930) Sieder and Tate (1936)
Dittus and Boelter (1930)	Oil Water		25 000 20 000		
Sherwood and Petrie (1932)	Water Acetone Benzene Kerosene n-Butyl Alcohol	Heating Heating Heating Heating Heating	113 000 113 000 86 700 31 800 32 500		Colburn (1933) Sieder and Tate (1936)
Petukhov (1970) (Collection of data)					Petukhov (1970)
Allen and Eckert (1964)	Water	-	110 000	8	
Dipprey and Sabersky (1963)	Water	-	150 000	1.2 – 5.9	
Yakovlev (1960)	Water	-	140 000	2 – 12	
Malina and Sparrow (1964)	Water, Oil	-	100 000	3, 48, 75	
Sterman and Petukhov (1965)	Monoisopropyldiphenyl	-	260 000	12 – 35	
Hamilton (1963)	Water and water solutions of Glycerine and Metaxyl	-	100 000	430 – 10^5	

Table 3: Summary of Heat Transfer Correlations

CORRELATION	EQUATION	REYNOLDS NUMBER RANGE	PRANDTL NUMBER RANGE	EXPERIMENTAL DATA SOURCE
Chilton-Colburn Analogy Colburn Equation (1933)	$Nu = 0.125 f Re Pr^{\frac{1}{3}}$ where f is the friction factor from the first Petukhov equation $Nu = 0.023 Re^{0.8} Pr^{\frac{1}{3}}$	$3000 < Re < 5 \times 10^6$ $Re > 10\,000$	$0.7 < \text{Pr} < 160$	McAdams and Frost (1922) Morris and Whitman (1928)
Dittus and Boelter Equation (1930)	$Nu = 0.023 Re^{0.8} Pr^{n}$ where n = 0.3 for cooling n = 0.4 for heating	$2500 < \text{Re} < 10^5$	$0.7 < \text{Pr} < 120$	McAdams and Frost (1922) Morris and Whitman (1928)
Sieder and Tate (1936)	$Nu = 0.027 Re^{0.8} Pr^{\frac{1}{3}} \left(\frac{\mu}{\mu_s}\right)^{0.14}$	$Re > 10\,000$	$0.7 < \text{Pr} < 17600$	Clapp and Fitzsimmons (1928) Keevil and McAdams (1929) Morris and Whitman (1928) Sherwood and Petrie (1932)
Second Petukhov Equation (1970)	$Nu = \frac{\left(\frac{f}{8}\right) \text{Re} Pr}{1.07 + 12.7 \left(\frac{f}{8}\right)^{0.5} \left(Pr^{\frac{2}{3}} - 1\right)}$	$10^4 < Re < 5 \times 10^6$	$0.5 \leq Pr \leq 2000$	Allen and Eckert (1964) Petukhov and Roison (1963) Sterman and Petukhov (1965) Yakovlev (1960)
Gnielinski (1976)	$Nu = \frac{\left(\frac{f}{8}\right)(Re-1000)Pr}{1+12.7\left(\frac{f}{8}\right)^{0.5}\left(Pr^{\frac{2}{3}}-1\right)} \left[1 + \left(\frac{d}{L}\right)^{\frac{2}{3}}\right] K$ where $K = \left(\frac{Pr}{Pr_w}\right)^{0.11}$	$3 \times 10^3 < Re < 5 \times 10^6$	$0.5 \leq Pr \leq 2000$	Clapp and Fitzsimmons (1928) Keevil (1930) Lawrence and Sherwood (1931) Morris and Whitman (1928) Sherwood and Petrie (1932) Sieder and Tate (1936) Hufschmidt (1966)

Important to note is the maximum Reynolds numbers that were tested in the studies. If one compares the Reynolds numbers ranges of the most commonly used heat transfer correlations in Table 2, one can see that most of the experimental data has never exceeded a Reynolds number of 260 000. It is to be noted that the highest Reynolds numbers were never tested using water. The highest Reynolds number tested using water was 230 000 by McAdams and Frost (1922). The correlations that were developed used mathematics and extrapolation to develop the limits of the correlations and therefore there is room for further experimental investigation into higher Reynolds number ranges.

In Table 3, a summary of the most important heat transfer correlations can be found along with the Reynolds number and Prandtl number ranges that are applicable to the specific correlation. Included in the table are the data sets that have been utilised in the development of the correlations.

Although there are many heat transfer correlations that have been developed over the past century, the ones mentioned in Table 3 are those which were proven to be pioneering for their time and those which made a significant difference to the development of heat transfer theory.

2.4.1 The Dittus-Boelter Equation

The first study to change the way heat transfer coefficients were calculated was completed by Dittus and Boelter (1930). The study was completed using a radiator to transfer heat from water to the atmosphere. The study introduced the "Overall Transfer Factor'' which has becoming the Overall Heat Transfer Coefficient (*U*) that is used today. This is utilised when working with the method of representing the heat transfer that occurs in a system as resistance terms, similar to the theory used in electrical circuits. It was found that in turbulent flow, most of the heat is transferred from the liquid to the tube wall by forced convection, and that in the laminar flow regime heat is transferred mainly by conduction.

Dittus and Boelter used the data from previous studies of McAdams and Frost (1922) and Morris and Whitman (1928) to compare their results to. From the results, it was found that previously, there were two separate groups of data points, one for heating of liquids and the other for cooling. It was attempted to plot the heat transfer factors as a function of the various thermal properties of the fluid, using the film temperature instead of the bulk temperature to obtain consensus between the two operating conditions. After doing this, it was found that no agreement was found between the studies when using a single representative equation. It was after this, that a suggestion was made to include a separate exponent for heating and another for cooling. When using this new method and comparing the heat transfer coefficients to Morris and Whitman's (1928) published data, agreement was found between the studies.

In addition to determining the coefficients for heat transfer, an entrance correction factor was proposed by Dittus to eliminate turbulence due to entrance and exit disturbances as little was understood regarding the effects of entrance conditions on heat transfer at that time. McAdams and Frost proposed to use an entrance correction factor to calculate their heat transfer results but this was rejected by Morris and Whitman (1928) on the basis that there was not sufficient data to determine a single accurate correction factor.

The correlation developed by Dittus and Boelter is described by equation (10).

$$Nu = 0.023Re^{0.8}Pr^{n} \tag{10}$$

where n =0.4 for heating applications and n =0.3 for cooling applications.

2.4.2 The Colburn Correlation

While there were many initial attempts to characterise heat transfer as a function of flow rate, few studies were found to make a meaningful contribution in predicting heat transfer coefficients. One of the first studies to contribute to heat transfer in the turbulent flow regime was by Colburn (1933). Colburn found that whilst there were many equations available at that time, every equation was dependent either on types of apparatus, flow conditions or the fluids used. Colburn determined that there was a need for a single equation that could describe heat transfer independently of all those factors. The purpose of Colburn's paper was to simplify the forced convection field by providing a general method of correlating heat transfer data which could be used for the entire flow range, being from laminar to turbulent.

Colburn was one of the first studies which could be noted for fully utilising the dimensionless numbers of Nusselt, Stanton, Reynolds and Prandtl. Colburn understood how utilising these numbers simplify the calculations involved in heat transfer by reducing the number of properties and variables, whilst still allowing for all effects to be represented in an equation.

Colburn's development of his correlation was based on the Reynolds analogy, which was developed to determine the value of C_f which is the shear stress at the wall. Colburn determined that a similar equation needed to be developed to determine heat transfer rates during forced convection. Derived from the non-dimensionalised momentum and energy equations, the Reynolds analogy states that the Stanton number is approximately one half the value of the friction coefficient. The Stanton number is defined as (Cengel 2006):

$$St = \frac{h}{\rho c_p V} = \frac{Nu}{RePr} \tag{11}$$

This is, however, only valid for fluids with Pr ≈ 1 and therefore a more useful analogy was needed to predict heat transfer coefficients that could be applied to fluids with a wide range of Prandtl numbers. Therefore, Colburn added an extra Prandtl number factor and developed what is known as the *j*-factor. The Prandtl number is used as a correction for the differences between the temperature and velocity distributions in the fluid. The *j*-factor is defined in terms of either the overall temperature change of the system or as a heat transfer coefficient. This is represented by (Colburn 1933):

$$j = StPr^{\frac{2}{3}} \quad (0.6 < Pr < 60) \tag{12}$$

The proposed method of presenting the data was helpful as the values of the heat transfer was shown to be a direct function of the temperature change in a heat exchanger and the effect of varying the velocity of the flow on the exit temperature was immediately indicated.

The well-known Chilton-Colburn analogy uses the Petukhov friction factor described in equation (6) to determine the heat transfer using equation (13):

$$Nu = 0.125 f RePr^{\frac{1}{3}} \tag{13}$$

The Colburn equation is a slight mathematical modification of equation (13) and includes the friction factor in the equation which is (Cengel 2006):

$$Nu = 0.023 Re^{0.8} Pr^{\frac{1}{3}} \quad (0.7 \leq Pr \leq 160, \;\; Re > 10\,000) \tag{14}$$

It is important to note that all the system properties are evaluated at the bulk mean fluid temperature which is the average temperature between the inlet and outlet temperature of the fluid. This is represented by:

$$T_b = \frac{T_{in} + T_{out}}{2} \tag{15}$$

2.4.3 The Sieder and Tate Study

The next of the heat transfer studies that were to shape modern theory was that conducted by Sieder and Tate (1936). In addition to developing an extremely accurate and useful correlation to predict heat transfer, the data that was measured has been used extensively by other authors to develop new heat transfer correlations with a considerable degree of accuracy.

During the development of the correlation, two main contributions can be noted. Firstly, the correlation that is developed takes into account the viscosity gradient of the fluid in the tube by means of a viscosity ratio in the form (μ_b/μ_w) where μ_b is the viscosity at the bulk temperature and μ_w is the viscosity of the fluid at tube wall temperature. This observation is of considerable importance as it was the first study to investigate the temperature profile in the radial direction of the tube. Up until this particular study, the temperature profile in the axial direction of the tube was seen to dominate the effect of the profile on heat transfer. It was found that due to the magnitude of the radial temperature gradient, a large viscosity gradient is found in the radial direction and this is what leads to the difference in viscosity at the centre and wall of the tube. It is due to this that the effect of the viscosity gradient needs to be taken into account and therefore the correlation developed by Sieder and Tate (1936) resulted in a far greater accuracy than previous work in heat transfer theory.

The previous correlations fell into two classes – one which used mainstream properties and the other using film properties with these being defined by the temperature which was used to determine the system properties. When using the film properties, one cannot use one correlation to predict heat transfer in heating and cooling applications. If one uses the main stream properties, the temperature difference between the tube wall and fluid are not sufficiently taken into account. Sieder and Tate recognised this and therefore sought to develop a solution to these two problems.

Using their own experimental data and other data sets, from Morris and Whitman (1928) and Sherwood and Petrie (1932), a correlation was developed to predict the heat transfer in the turbulent flow regime for liquids. This equation is shown in (16):

$$Nu = 0.027 Re^{0.8} Pr^{\frac{1}{3}} \left(\frac{\mu}{\mu_w}\right)^{0.14} \tag{16}$$
$$(0.7 \leq Pr \leq 17600, Re \geq 10\,000)$$

The results of the experimental data for testing with water have a deviation of 10% when compared to the theory examined.

2.4.4 The Petukhov Correlation

More complex equations such as the second Petukhov (1970) equation or the Gnielinski (1976) correlation aimed to improve the accuracy of the previous heat transfer studies. It was realised that fluid physical properties greatly depended on temperature. It was due to this phenomenon, that heat transfer was so poorly predicted in previous studies as this was not fully taken into

account. It was therefore necessary to perform an analysis of the flow and heat transfer with the dependence of physical properties on temperature taken into account.

Due to the transient nature of turbulent flow, properties change continuously with time. It is these fluctuations that make turbulent flow so difficult to predict. The difficulty in predicting heat transfer in turbulent flow comes from the inability to determine expressions for the turbulent diffusivities of heat and momentum for variable physical properties.

The Petukhov study uses numerical methods of predicting the heat transfer by using time averaged velocities, densities, enthalpies, temperatures and pressures. Using the energy, momentum and continuity equations, these values can be determined. The solution of turbulent flow is to use expressions for turbulent diffusivities coupled with the analysis of averaged equations for temperature, density and pressure fields. Petukhov restricted his analysis to heat transfer and fluid flow analysis in circular pipes devoid of entrance effects. Petukhov determined that when dealing with large Prandtl numbers, the main temperature change occurs in the vicinity of the tube wall and therefore it is very important to take this phenomenon into account.

To determine the heat transfer with constant physical properties, Petukhov considers a solution for fully developed flow in a circular tube with constant heat flux at the tube wall. The heat transfer coefficient was calculated for Reynolds numbers ranging from 10^4 to 5 x 10^6.

The corresponding solution is found in equation (17), which predicts the heat transfer for fully developed flow (Petukhov 1970).

$$Nu = \frac{\left(\frac{f}{8}\right) RePr}{1.07 + 12.7\left(\frac{f}{8}\right)^{0.5}\left(Pr^{\frac{2}{3}} - 1\right)} \qquad (17)$$

$$(0.5 \leq Pr \leq 2000,\ 10^4 < Re < 5 \times 10^6)$$

It was found by Petukhov (1970) that for the mentioned Reynolds number range, the calculated results had an accuracy of 5-6% when compared to chosen experimental data. Whilst this correlates well, the maximum Reynolds number that was experimentally tested to was 350 000 and the testing fluid was air. The highest Reynolds number tested using water was 140 000. When considering this, it is thought that it would be beneficial to validate the heat transfer coefficients through experimental testing.

2.4.5 The Gnielinski Study

The most recent heat transfer study to significantly contribute to theory on turbulent heat transfer was conducted by Gnielinski (1976). The work that he evaluated was the most recent contribution to heat transfer at that time which was researched by Hausen (1959). Hausen used Sieder and Tate's experimental data to develop a correlation to describe heat transfer in both the transitional and turbulent flow regime. The correlation is (Hausen 1959):

$$Nu = 0.037(Re^{0.75} - 180)Pr^{0.42}\left[1 + \left(\frac{\mathrm{d}}{\mathrm{L}}\right)^{2/3}\right]\left(\frac{\mu}{\mu_w}\right)^{0.14} \qquad (18)$$

$$(0.6 \leq Pr \leq 10^3, 2300 < Re < 10^6)$$

Gnielinski found that the work conducted by Hausen under predicted heat transfer coefficients at high Reynolds numbers. This was found when comparing the theoretical Nusselt numbers calculated using the Hausen equation to the experimental Nusselt numbers obtained by

Hufschmidt *et al* (1966). It was found however, that Hausen's correlation correctly predicted the decrease in the heat transfer coefficient in the transition region between laminar and turbulent flow for Reynolds numbers lower than 10 000. Therefore, Gnielinski determined that to reproduce the experimental values from the existing literature, an equation needed to be developed that correctly described the decrease in heat transfer coefficients in the transitional flow regime and which, for large Reynolds numbers, could account for the dependence of the exponent of the Reynolds number on the Prandtl number.

Gnielinski determined that to achieve this, a generally valid equation should be formulated from the basic form that was developed by Prandtl (1944). Petukhov, as previously mentioned, developed an equation which predicted heat transfer accurately at high Reynolds numbers. The Petukhov equation is based on the original assumptions and correlation of Prandtl (1944). This assumption is that due to the pressure drop, the exponent of the Reynolds number has a noticeable dependence on the Prandtl number. Petukhov takes into account the effect of the friction factor on heat transfer in fully developed turbulent flow in long pipes by using the equation given by Filonenko (1954). Using the Petukhov (1970) equation, it was found that in the region of large Reynolds numbers, the values correspond to the requirements i.e. providing higher Nusselt numbers than the Hausen equation irrespective of the Prandtl number.

$$Nu = \frac{\left(\frac{f}{8}\right)(Re - 1000)Pr}{1 + 12.7\left(\frac{f}{8}\right)^{0.5}\left(Pr^{\frac{2}{3}} - 1\right)} \tag{19}$$

Gnielinski modified the equation by add the correction of $1 + \left(\frac{d}{L}\right)^{\frac{2}{3}}$ as given by Hausen to account for the effect of the length of the tube for which the heat transfer coefficient is being calculated. The ratio of the Prandtl number of the average temperature and the Prandtl number at the wall was added to equation (19) to account for the variation in properties as a result of their temperature dependence, similar to the method of Sieder and Tate (1936) using the viscosity.

The resulting equation is (Gnielinski 1976):

$$Nu = \frac{\left(\frac{f}{8}\right)(Re - 1000)Pr}{1 + 12.7\left(\frac{f}{8}\right)^{0.5}\left(Pr^{\frac{2}{3}} - 1\right)}\left[1 + \left(\frac{d}{L}\right)^{\frac{2}{3}}\right]K \tag{20}$$

where

$$K = \left(\frac{Pr}{Pr_w}\right)^{0.11}$$

The Gnielinski correlation was deemed to be considerably accurate as it was able to reproduce the experimental heat transfer values for transition and turbulent flow over a wide range of Prandtl numbers. In addition to that, nearly 90% of the approximately 800 experimental values taken from existing literature differed by less than ±20% from the theoretical values. However, the uncertainties of the experimental values were not known. Furthermore it is to be noted that the Reynolds number range for this correlation is determined from the validity of the Reynolds number range for the Petukhov equation. The experimental values that are plotted in the Gnielinski article do not exceed a Reynolds number of 640 000. Hufschmidt (1966) produced test results that were used by Gnielinski but his results covered a significant Prandtl number range.

2.5 Conclusion

The calculation of heat transfer and the friction factor in the turbulent flow regime is governed by the use of experimental data due to the fluctuations and agitations found in the fluid stream. The experimental data sets form the basis of heat transfer correlation development.

From the earliest development of correlations used to define turbulent heat transfer, the aim was to simplify the calculation of heat transfer. This led to the introduction of dimensionless numbers. After this development the difference in heat transfer calculation between heating and cooling applications was introduced. This development led to the discovery of the influence of temperature on the thermal properties of a fluid and this introduced the inclusion of the viscosity of a fluid into the calculation of heat transfer. It was discovered that the viscosity would take into account the temperature differences between the tube wall and fluid during experimental testing. After this development, the next discovery was that the friction factor had a considerable effect on the heat transfer and it was therefore included in the calculation of heat transfer in the turbulent flow regime.

There are numerous studies that have been undertaken to quantify the heat transfer in the turbulent flow regime. Many of these studies make use of experimental data sets that were recorded in the early 1920's due to the reliance of the heat transfer correlation development on experimental data. The maximum Reynolds Number that has been tested using water as the testing medium was 223 000. Due to the correlations being developed so many years ago, the accuracy of the correlations has not been required to be quantified by the calculation of the uncertainty of the correlation.

3. EXPERIMENTAL SETUP

3.1 Introduction

The purpose of this chapter is to describe the experimental setup that was used to conduct heat transfer and pressure drop experiments in a smooth horizontal tube over a range of mass flow rates. It also gives an overview of the components of the experimental setup, the test section, as well as the material, equipment and instrumentation used. The experimental procedure and data reduction methods used are also discussed.

3.2 Experimental Setup

The experimental setup was housed in the Thermofluids laboratory at the University of Pretoria and was constructed by myself and is shown schematically in Figure 2. The experimental setup consisted of a tube-in-tube heat exchanger operated using water in a counterflow configuration. It was serviced with two water streams: a hot and cold water fluid stream. The inner tube of the heat exchanger was serviced with hot water and the annulus was serviced with cold water.

The hot water in the system was provided using the municipal water supply and a heater element located in a reservoir. The water was heated using a 36 kW heating element which heated the water to a temperature of 58°C. The hot water was supplied to the system using two pumps due to the large range of flow rates that need to be tested. One positive displacement pump was used to provide a maximum flow rate of 2 700 l/hr. Another positive displacement pump was used to supply the system with a maximum flow rate of 13 200 l/hr. A summary of the equipment specifications of the two water streams is in Table 4.

Table 4: Equipment specifications of the two water streams

Hot Water Stream	
Pump 1: SP 4 Power: Maximum flow rate: Maximum pressure rating: Maximum speed:	Positive displacement pump 0.5 kW 2 700 l/hr 600 kPa (at maximum flow rate) 1 420 rpm
Pump 2: CB 620 Power: Maximum flow rate: Maximum pressure rating: Maximum speed:	Positive displacement pump 11 kW 13 200 l/hr 1 200 kPa (at maximum flow rate) 1 460 rpm
Cold Water Stream	
Pump: CB 410 Power: Maximum Flow Rate: Maximum Pressure Rating: Maximum Speed:	Positive displacement pump 2.2 kW 3 400 l/hr 600 kPa 1 300 rpm

The cold water supply had a similar configuration as the hot water supply loop. The water was stored in a 1 000 litre reservoir which was connected to a 36 kW chilling unit which chilled the water to a temperature of 20°C. The cold water was supplied to the test section using a positive displacement pump which could provide 3 400 l/hr.

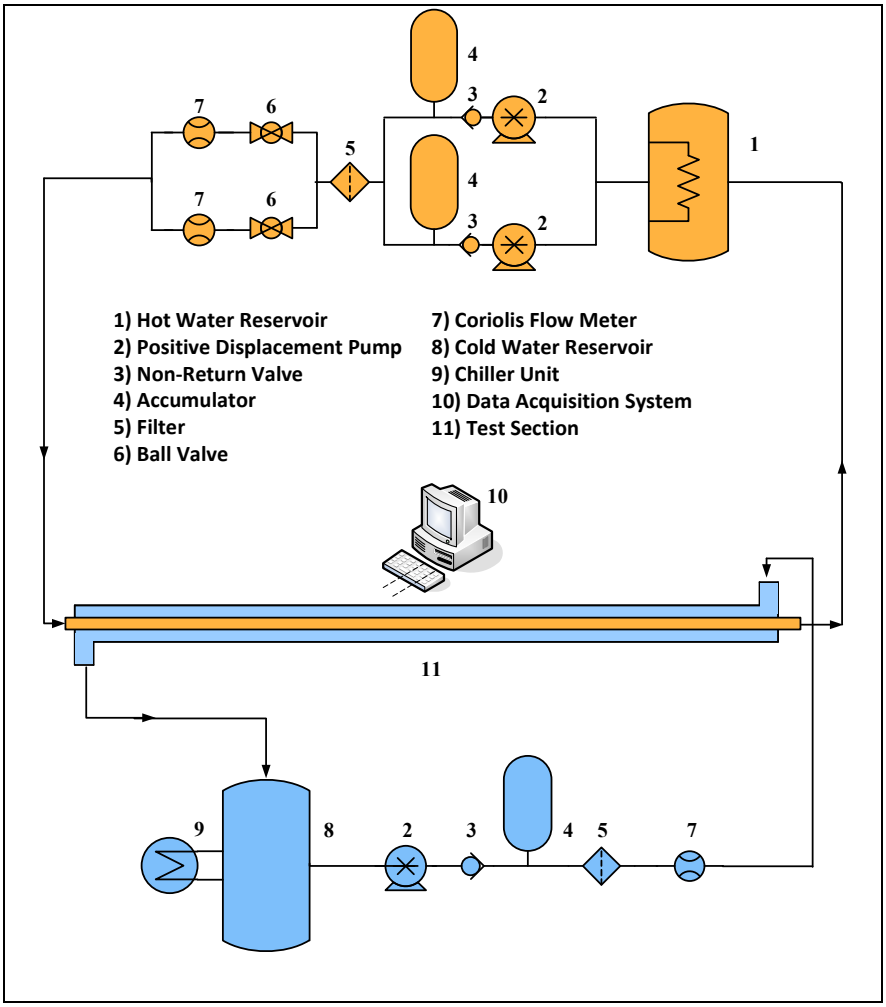

Figure 2: Experimental test setup showing both hot and cold fluid streams with all measuring instrumentation used during testing

Once the water was pumped from the reservoir, it was fed through an accumulator which was used to dampen any pulsations that may have occurred in the system. This was used in an effort to obtain highly accurate flow rate readings and damp pressure fluctuations. Once passed through the accumulator, it was fed through a filter to remove impurities and was then directed to a flow meter. The hot system used two Coriolis flow meters in parallel to measure the extremely low and high flow rates which affects the resolution of the readings taken when a particular flow meter is not suitable for extreme flow rates. The decrease in resolution directly affects the quality of the readings and therefore the accuracy.

Once the flow had been through the flow meter it entered the test section constructed as a heat exchanger. The detail of the design and construction of test section is given in section 3.3.

The piping used for the hot water circuit was high density polyurethane piping (HDPE) as it has a high pressure rating. The connection fittings used were Plasson fittings which offered a pressure rating of 1.6 MPa. In addition to the pressure ratings, the fittings allowed for easy construction and changes that needed to be made to the circuit. The hot water supply lines had an outer diameter of 63 mm with a pressure rating of 1.2 MPa whereas the cold water supply lines had an outer diameter of 25 mm with a pressure rating of 600 kPa.

Both the hot and cold water supply pumps were controlled using variable frequency drives that were operated through a computer system linked to the experimental setup. A data acquisition system was coupled to the computer to log the desired temperature, pressure and mass flow measurements. The data acquisition software also allowed the control of the flow rates of the pumps through the computer. As a result, testing could be performed remotely through the computer and data acquisition system.

3.3 Test Section

Each of the two test sections used to conduct experiments consisted of a tube-in-tube heat exchanger which was tested in the laboratory. A summary of the heat exchangers and their tube diameters can be found in Table 5. The diameters are specified in terms of inner diameter of the tube. In this manuscript reference will be made to the 8.3 mm and 14.2 mm tubes although their diameters are actually 8.29 mm and 14.22 mm respectively.

Table 5: Heat Exchanger Tube Diameters

Inner diameter of inner tube of the heat exchanger	Inner tube wall thickness	Inner diameter of annulus tube of the heat exchanger	Annulus tube wall thickness
Test Section 1 8.29 mm	0.61 mm	17.63 mm	0.71 mm
Test Section 2 14.22 mm	0.81 mm	20.41 mm	0.91 mm

Each of the two test sections consisted of two copper tubes. The heat transfer length of the inner tube was 3.75 m and the pressure drop length was 4.1 m. The inner tubes were made of hard drawn copper tubes and their surface roughness values were measured as 0.0987 µm. The relative surface roughness (ε/D) of the tubes was less than 6×10^{-6} m and can therefore be considered as smooth tubes when compared to a Moody chart (Cengel, 2006). The heat exchanger test sections were covered in Armaflex insulation with a thermal conductivity of 0.034 W/m.K. Due to the cold water running through the annulus and the hot water running through the inner tube, the heat loss to the ambient was minimised when choosing this particular flow configuration.

The selection of the length of the inner tubes was the longest that was commercially available. The reasons for the selection of the long lengths were to assure that fully developed flow will occur in most parts of the tubes and that high of heat transfer rates and pressure drops values could be measured to ensure good energy balances and low uncertainties.

As experiments were only conducted in the turbulent flow regime, no mixers needed to be installed at the inlet and outlet of the inner tubes. All measured wall temperatures on the outside of the tube are assumed be equal to the average temperature of the water in the tube (wall resistance was negligible as discussed in 3.6.4). To ensure that no inlet effects could

disturb the experimental results, a bell mouth inlet with a downstream tube length with the same diameter as the test section and a length of 500 mm was installed upstream of the inlet of the test section.

3.4 Test Section Construction

As explained in the design section of this chapter, the test sections were in the configuration of a tube-in-tube heat exchanger. The inner tube was divided into eight stations, which were used to facilitate the sealing of the annulus pieces over the inner tube when constructing the heat exchanger. Once concentricity was ensured, the outer tube was fitted over the inner tube. The annulus pieces were connected using hydraulic fittings to ensure that they remain intact when testing under high pressure conditions.

An important aspect of the test section construction was the method of maintaining concentricity between the two tubes. The tubes were separated using small pieces of Acetal machined to fit in the annulus of the heat exchanger. Acetal is a plastic which was chosen as it has a high operating temperature, low moisture absorption, low thermal conductivity, good stiffness and is easy to machine. The pieces were attached onto the inner tube at each station to maintain concentricity.

The inlets and outlets of both the annulus and inner tube made use of four T-type thermocouples to measure temperatures accurately. The thermocouples were located 90° from each other around the tube circumference. The average of the four thermocouples was used as a more accurate representation of the temperature at the inlet and outlets of both the inner and outer tubes of the test section. The thermocouples were attached to the tube by soldering the thermocouples onto the outer wall of the tube. A small groove was drilled into the tube and when the groove was filled with solder, the thermocouple was inserted into the groove. The thermocouple configuration is shown in Figure 3.

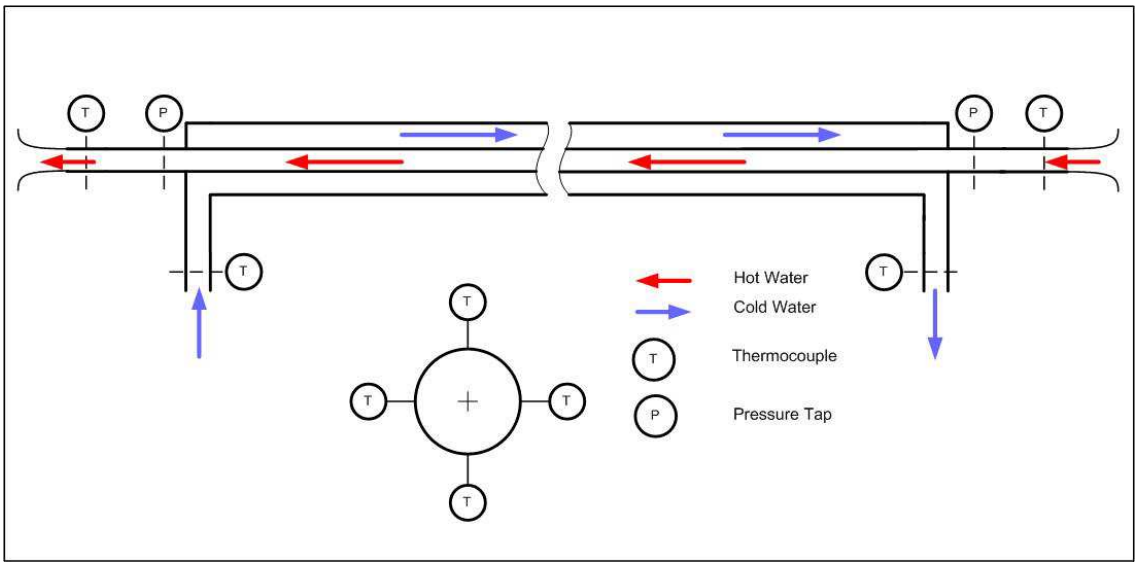

Figure 3: Heat Exchanger Test Section showing the hot and cold fluid flow directions and thermocouple measurement points with a bell mouth entrance

It was important that a high quality bond was made between the thermocouple wire and the tube surface as the wires were handled extensively after the bonding process and there was a risk that the wire would become detached during the handling of the test section. Due to the

wall thickness being so small, the thermal resistance of the wall can be neglected in heat transfer calculations.

Thermocouple calibration was performed using at PT-100 temperature probe which was used to measure a reference temperature over a defined constant temperature range. The accuracy of the PT-100 probe was calibrated to 0.1 °C. The calibration was completed between a minimum and maximum temperature as the difference between the reference temperature and that of the thermocouples was found to be linear. Once the temperatures were logged, calibration coefficients could be determined for each thermocouple to calculate a new temperature reading. This worked as a correction factor to counteract the inherent error in the thermocouple wire and ensure that accurate temperature readings were obtained. During calibration 100 samples were recorded at each temperature and the standard deviation of thermocouples never exceeded 0.1°C.

The pressure drop readings over the length of the inner tube were measured using pressure taps situated at the inlet and outlet of the inner tube. The pressure was measured using three Validyne DP15 Pressure Transducers. Each of the transducers contained a diaphragm which was calibrated to a maximum pressure which could not be exceeded. Each diaphragm was accurate to 0.25% of the rated maximum pressure. The accuracy of each of the pressure ranges was used to calculate the uncertainty of the pressure measurements which is explained in Appendix A. Pressure calibration was completed off site as the pressure ranges that were required to measure experimental data were too high for the equipment in the laboratory. The pressure calibration accuracy is given in Table 6.

Table 6: Pressure Diaphragm Ranges

Diaphragm Number	Pressure Range [kPa]	Error [%]
1	0 – 35	0.25
2	35 – 140	1
3	140 – 860	1.54

Labview software was used to record the measurements during testing. Using the software, 100 samples were recorded at a frequency of 100 Hz for each Reynolds number increment ($\Delta Re = 10\ 000$). The measurements that were recorded were:

- the differential pressure of the inner tube flow stream
- the inlet and outlet temperature measurements of both tube streams
- the mass flow rates of both the inner and outer tube streams

3.5 Testing Procedure

To conduct accurate experiments, the system needed to reach steady state conditions before any measurements were taken. The hot water was circulated through the test section to enable the temperature to stabilise. Once the temperatures were at the desired values, the cold water was circulated through the annulus. Using this circulation process, any excess air in the system was pumped out of the piping and test section and back into the tank. Steady state conditions were determined by monitoring the temperature fluctuations in the system as well as the energy balance readings. The energy balance readings were monitored and once an

approximate reading of 1% was obtained with no temperature or pressure fluctuations, steady state conditions were assured and measurements were recorded.

In Table 7, the maximum testing values can be found for each of the tube diameters.

Table 7: Testing System Properties

Maximum System Properties for Tube Diameters	8.3 mm	14.2 mm
Reynolds number[-]	200 000	220 000
Heat transfer rate [kW]	20	42
Mass flow rate [kg/s]	0.684	1.24
Pressure drop [kPa]	578	134

Upon the start of the experimental system, the pressure transducer valves were closed and remained that way for approximately ten minutes. The pressure transducer valves that were used in the system were opened once the system had been circulating the hot and cold water through the test section for a considerable time. This was done in an effort to prevent the effects of any potential water hammer in the system at start up from damaging the diaphragms in the pressure transducers. Once the system had stabilised, the valves were opened and any excess air in the system was bled out through the pressure transducers. At the end of the testing procedure, the pumps were switched off and the system became static. Once this occurred, the static pressure was recorded. This was done in an attempt to counter any offset that might have occurred in the pressure transducers. This offset was then subtracted from the recorded experimental pressure values to obtain the true reading.

3.6 Data Reduction

To obtain the objectives set out for this study, friction factors, heat transfer coefficients and *j*-factors were required for smooth tubes in the turbulent flow regime. The methods used to calculate these coefficients are described in this section.

3.6.1 General System Variables

The Reynolds number was calculated for the inner tube and annulus mass flow measurements as described in equation (21) and (22).

$$Re_i = \frac{4\dot{m}_i}{\pi D_i \mu_i} \tag{21}$$

$$Re_o = \frac{4\dot{m}_o}{\pi (D_o - D_i)\mu_o} \tag{22}$$

The Prandtl number for the inner tube and annulus flows were defined in equation (23) and (24). The viscosities were calculated using the bulk temperature which is defined in equation (25) and is an average of the inlet and outlet temperature of a fluid stream.

$$Pr_i = \frac{\mu_i C_{pi}}{k_i} \tag{23}$$

$$Pr_o = \frac{\mu_o C_{po}}{k_o} \tag{24}$$

$$T_b = \frac{T_i + T_o}{2} \tag{25}$$

The surface area of the inner tube and annulus were calculated using equations (26) and (27). The heat transfer length was 3.75 m.

$$A_i = \pi D_i L \tag{26}$$

$$A_o = \pi D_o L \tag{27}$$

3.6.2 Pressure Readings

The pressure readings that were obtained were indicative of the pressure drop that occurred over the length of the inner tube of the heat exchanger. Using the pressure drop readings, the friction factor, *f*, was calculated using equation (28). The pressure drop length between the inlet and outlet pressure taps was 4.1 m. The density was calculated at the bulk temperature as defined in equation (25).

$$f = \frac{2\Delta P D}{\rho L V_{avg}^2} \tag{28}$$

The velocity was calculated from the mass flow rate readings that were recorded during testing as well as the cross sectional area of the inner tube. Using equation (29), the average velocity was obtained and using that, the friction factor was calculated.

$$V_{avg} = \frac{\dot{m}}{\rho A_{cs}} \tag{29}$$

3.6.3 *j*-Factor Calculation

When considering the heat transfer results, it was decided to establish what the effect of the Prandtl number would be on the Nusselt number results. As mentioned in chapter 2, Prandtl numbers exhibit a much higher influence on heat transfer results in the turbulent flow regime. It was therefore determined to be important to consider the effects that the Prandtl number has on the Nusselt number.

Using the Colburn analogy of free convection heat transfer and the Stanton number, which is described in chapter 2, a correlation can be made between the *j*-factor and the Nusselt number which is determined experimentally.

The *j*-factor is described using equation (30).

$$j = StPr^{\frac{2}{3}} \tag{30}$$

Replacing the Stanton number with the definition in equation (31), the *j*-factor takes on the form shown in equation (32):

$$St = \frac{Nu}{RePr} \tag{31}$$

$$j = \frac{Nu}{RePr^{\frac{1}{3}}} \tag{32}$$

3.6.4 Heat Transfer Coefficients

The Wilson Plot (WP) method (Briggs and Young 1969) uses only the inlet and outlet temperatures and mass flow rates for both the inner tube and annulus to calculate a heat transfer coefficient. The WP method is traditionally used to calculate the annulus heat transfer coefficients, however, in this case it is used to predict an inner tube heat transfer coefficient using regression analysis. The Wilson Plot analysis utilises the logarithmic mean temperature difference (LMTD) method of calculating the overall heat transfer coefficients of the system.

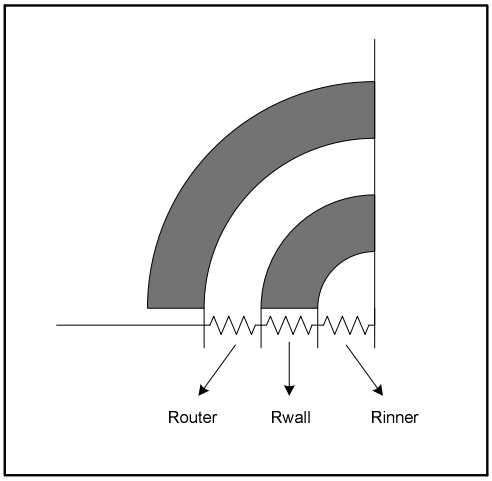

Figure 4: Representation of thermal resistance contributions of the inner, wall and annulus heat transfer

The LMTD method uses an analogy that represents each heat transfer component of the experimental setup as a component of a thermal resistance network. A cross section of the heat exchanger is shown in Figure 4. The thermal resistance theory states that each part of the cross section contributes a resistance which can be related to the overall heat transfer coefficient (U_{ov}).

In this particular case the thermal resistance is equal to the sum of the inner tube, wall and outer tube thermal resistances. This is described by equation (33).

$$R_{ov} = R_i + R_w + R_o \tag{33}$$

The overall heat transfer coefficient of this particular system is affected by the resistance terms of the fluid in inner tube, the inner tube wall and the fluid in the annulus as shown in equation (34). The first term on the right hand side of equation (34) represents the inner wall thermal resistance caused by convection on the inner surface of the inner tube. The term, R_w, represents the conduction through the copper tube wall and the last term represents the annulus side thermal resistance from convection on the outer surface of the inner tube.

$$\frac{1}{U_{ov}A} = \frac{1}{h_i A_i} + R_w + \frac{1}{h_o A_o} \tag{34}$$

The overall heat transfer coefficient was calculated by using the average heat transfer rate between the inner tube and the annulus which was determined using equations (35), (36) and (37).

$$\dot{Q}_i = \dot{m}_i C_{pi}\left(T_{i,in} - T_{i,out}\right) \tag{35}$$

$$\dot{Q}_o = \dot{m}_o C_{po}\left(T_{o,out} - T_{o,in}\right) \tag{36}$$

$$\dot{Q}_{av} = \frac{\dot{Q}_i + \dot{Q}_o}{2} \tag{37}$$

$$\dot{Q}_{av} = \frac{\dot{m}_i\left(C_{pi}\left(T_{i.in} - T_{i,out}\right)\right) + \dot{m}_o\left(C_{po}\left(T_{o.out} - T_{o,in}\right)\right)}{2} \tag{38}$$

Once the average heat transfer rate was calculated, it was used to calculate the overall heat transfer coefficient using equation (39) which utilises the log mean temperature difference (LMTD).

$$U_{ov} = \frac{\dot{Q}_{av}}{A_o \Delta T_{lm}} \tag{39}$$

The log mean temperature was calculated as depicted in equation (40).

$$\Delta T_{lm} = \frac{\left(T_{i,in} - T_{o,out}\right) - \left(T_{i,out} - T_{o,in}\right)}{ln\left(\frac{\left(T_{i,in} - T_{o,out}\right)}{\left(T_{i,out} - T_{o,in}\right)}\right)} \tag{40}$$

The thermal wall resistance term (R_w) was calculated using the conduction equation for heat transfer through the tube wall. This is described in equation (41).

$$R_w = \frac{ln\left(\frac{D_o}{D_i}\right)}{2\pi k_w L} \tag{41}$$

where k is the thermal conductivity of the copper tube wall and L is the length of the tube.

To calculate the thermal conductivity of the copper tube wall, the correlation in equation (42) was used. This correlation calculates the thermal conductivity as a function of the bulk temperature (T_b) of the system (Abu-Eishah 2001), measured in Kelvin.

$$k_w = aT^b e^{cT} e^{\frac{d}{T}} \tag{42}$$

With the constants a = 82.56648, b = 0.262301, c = -4.06701 x 10^{-4} and d =59.72934 for copper.

Although the wall resistance was taken into consideration, the effect of the wall resistance on equation (34) was negligible due to the high thermal conductivity of the copper tube and the thin wall thickness of the tube.

The Wilson Plot method requires the overall heat transfer coefficients of both the inner tube and annulus to be calculated so as to calculate the inner tube heat transfer coefficient. The inner and outer tube Nusselt numbers are solved for using equations (43) and (44). The equations have two coefficients, C and n, which are used to approximate the experimental data through regression analysis using Sieder and Tate (1936) type equations.

$$Nu_i = C_i Re_i^{n_i} Pr_i^{\frac{1}{3}} \left(\frac{\mu_i}{\mu_w}\right)^{0.14} \tag{43}$$

$$Nu_o = C_o Re_o^{n_o} Pr_o^{\frac{1}{3}} \left(\frac{\mu_o}{\mu_w}\right)^{0.14} \tag{44}$$

To calculate the heat transfer coefficient for the inner tube equation (45) was used which is a relation to equation (44) described by the Briggs and Young (1969) method. The thermal conductivity of the water was calculated at the bulk temperature (T_b) which is calculated as the average between the inlet and outlet temperatures of the inner tube.

$$h_i = \frac{Nu_i k_i}{D_i} = C_i Re_i^{n_i} Pr_i^{\frac{1}{3}} \left(\frac{\mu_i}{\mu_w}\right)^{0.14} \frac{k_i}{D_i} \tag{45}$$

This theory can also be applied to the annular heat transfer coefficient as in equation (46).

$$h_o = \frac{Nu_o k_o}{(D_o - D_i)} = C_o Re_o^{n_o} Pr_o^{\frac{1}{3}} \left(\frac{\mu_o}{\mu_w}\right)^{0.14} \frac{k_o}{(D_o - D_i)} \tag{46}$$

The inner tube heat transfer resistance is described using equation (47). The inclusion of h_i^* is the variation of the inner tube heat transfer coefficient and C_i is a correcting constant.

$$R_i = \frac{1}{h_i A_i} = \frac{1}{C_i h_i^* A_i} \tag{47}$$

where

$$h_i = C_i h_i^* \tag{48}$$

The same principle is applied to the outer tube heat transfer resistance as shown in equation (49).

$$R_o = \frac{1}{h_o A_o} = \frac{1}{C_o h_o^* A_o} \tag{49}$$

where

$$h_o = C_o h_o^* \tag{50}$$

Using equation (47) and (49) in equation (34) the total heat transfer resistance takes on the form of equation (51).

$$R_{ov} = \frac{1}{C_i h_i^* A_i} + R_w + \frac{1}{C_o h_o^* A_o} \tag{51}$$

Rearranging the terms, the equation takes on the form of a straight line graph as shown in equation (53).

$$R_{ov} - R_w = \frac{1}{C_i h_i^* A_i} + \frac{1}{C_o h_o^* A_o} \tag{52}$$

$$(R_{ov} - R_w) h_o^* A_o = \frac{1}{C_i} \frac{h_o^* A_o}{h_i^* A_i} + \frac{1}{C_o} \tag{53}$$

The form of equation (53) allows the *y* and *x* values to be determined as described in equation (54) and (55).

$$y = (R_{ov} - R_w) h_o^* A_o \tag{54}$$

$$x = \frac{h_o^* A_o}{h_i^* A_i} \tag{55}$$

When plotting the *x* and *y* values, the new coefficients for C_i and C_o can be calculated by determining the gradient and intercept of equation (53). The gradient, ***a***, determines the C_i value and the intercept, *b*, determines the C_o value as shown in equations (56) and (57).

$$a = \frac{1}{C_i} \tag{56}$$

$$b = \frac{1}{C_o} \tag{57}$$

3.6.5 Wall Temperature Calculation using Wilson Plot

The wall temperature is difficult to measure when conducting experiments using a tube-in-tube heat exchanger test setup configuration due to the construction constraints. Therefore the wall temperature, according to the Wilson Plot, can be calculated and compared to the measured wall temperatures to determine whether there was a possible measurement error during experiments. This can be done using the overall heat transfer coefficient as well as the inner tube heat transfer coefficient calculated using the Wilson Plot. Due to the bulk temperature profile being undefined, it needs to be determined by derivation.

The aim is to determine the inner tube wall temperature T_w along the length of the tube z.

The bulk temperature difference, between the inner and outer tube fluids, at a point along the axial distance of the tube z is defined in equation (58) (Cengel 2006):

$$\Delta T_b(z) = T_i(z) - T_o(z) \tag{58}$$

The energy balance for the inner and outer tube can be determined using equations (59) and (60).

$$\delta\dot{Q} = -\dot{m}_i C_{pi} dT_i \tag{59}$$

$$\delta\dot{Q} = \dot{m}_o C_{po} dT_o \tag{60}$$

Substituting equation (59) and (60) into (61) renders:

$$d\Delta T_b = -\delta\dot{Q} C^* \tag{61}$$

where the term C^* is defined as:

$$C^* = \left(\frac{1}{\dot{m}_i C_{pi}} + \frac{1}{\dot{m}_o C_{po}}\right) \tag{62}$$

Using the definition of the overall heat transfer coefficient, the heat transfer rate takes on the form of equation (63):

$$\delta\dot{Q} = U_{ov}\Delta T_b p_i dz \tag{63}$$

where the perimeter is defined as:

$$p_i = \pi D_i \tag{64}$$

Substituting equation (63) into equation (61) the equation is integrated from 0 to z^*, which is an arbitrary position along the length of the tube, as in equation (65).

$$\int_{\Delta T_b(0)}^{\Delta T_b(z^*)} \frac{1}{\Delta T_b} d\Delta T_b = -\int_0^{z^*} U_{ov} p_i C^* dz \tag{65}$$

$$\ln\left(\Delta T_b(z^*)\right) - ln\left(\Delta T_b(0)\right) = -U_{ov} p_i C^* z^* \tag{66}$$

$$\therefore \Delta T_b(z^*) = e^{[-U_{ov}p_iC^*z^* + ln(\Delta T_b(0))]} \tag{67}$$

From the inner tube energy balance between 0 and z^* it can be obtained:

$$\dot{Q}_{0-z^*} = \dot{m}_i C_{pi}[T_i(0) - T_i(z^*)] \tag{68}$$

Integrating the incremental heat transfer rate from 0 to z^* of the tube renders:

$$\dot{Q}_{0-z^*} = \int_0^{z^*} d\dot{Q}\,(z)dz \tag{69}$$

Substituting equation (63) into (69):

$$\dot{Q}_{0-z^*} = \int_0^{z^*} U_{ov}p_i\Delta T_b\,(z)dz \tag{70}$$

And substituting equation (67) into (70) results in:

$$\begin{aligned}\dot{Q}_{0-z^*} &= \textstyle\int_0^{z^*} U_{ov}p_i\, e^{-U_{ov}p_iC^*z^* + ln[\Delta T_b(0)]}dz \\ &= -\tfrac{\Delta T_b(0)}{C^*}[e^{-U_{ov}p_iC^*z^*} - 1]\end{aligned} \tag{71}$$

Equating equation (71) into (70) results in an equation for the bulk fluid temperature for the inner tube at z^*:

$$\therefore -\frac{\Delta T_b(0)}{C^*}\left[e^{-U_{ov}p_iC^*z^*} - 1\right] = \dot{m}_i C_{pi}\left(T_i(0) - T_i(z^*)\right) \tag{72}$$

$$T_i(z^*) = T_i(0) - \frac{\Delta T_b(0)}{C^*\dot{m}_i C_{pi}}\left(1 - e^{-U_{ov}p_iC^*z^*}\right) \tag{73}$$

From the definition of the inner tube heat transfer coefficient:

$$\delta\dot{Q} = h_i p_i[T_i(z) - T_w(z)]dz \tag{74}$$

Equating equation (74) to (63) results in:

$$U_{ov}p_i\Delta T_b(z)dz = h_i p_i[T_i(z) - T_w(z)]dz \tag{75}$$

The terms are rearranged to obtain T_w:

$$T_w(z) = G_o + G_1 e^{\beta z} \tag{76}$$

where the coefficients G_0, G_1 and β are defined as:

$$G_0 = \left[T_i(0) - \frac{\Delta T_b(0)}{C^*\dot{m}_i C_{pi}}\right] \tag{77}$$

$$G_1 = \Delta T_b(0)\left[\frac{1}{C^* \dot{m}_i C_{pi}} - \frac{U_{ov}}{h_i}\right] \tag{78}$$

$$\beta = -U_{ov} p_i C^* \tag{79}$$

Normally it is not necessary to explicitly determine the wall temperatures when the WP method is used. The reason why it was done in this study was that the wall temperatures were required for the uncertainty analysis.

3.6.6 Energy Balance

The energy balance (*EB*) is calculated using the heat transfer rate of both the inner tube and annulus. The energy balance value is a good indication of the stability and accuracy of the system and measurements. To calculate the energy balance equation (80) is used.

$$EB = \frac{\dot{Q}_i - \dot{Q}_o}{\left(\frac{\dot{Q}_i + \dot{Q}_o}{2}\right)} \times 100 \tag{80}$$

3.7 Conclusion

Experimental data was obtained during tests conducted in the laboratory at the University of Pretoria. Two test sections were constructed in a counterflow arrangement where two different inner tube diameters were used for testing purposes. The inner tube diameters were 8.3 mm and 14.2 mm and the heat transfer length was 3.75 m. Thermocouples were attached along the length of the wall of the tube as well as at the inlet and outlet of the inner tube and annulus. During experimental testing, the following measurements were recorded: temperatures, mass flow rates, pressure drop over the length of the test section. The maximum Reynolds number tested for the 8.3 mm and 14.2 mm tube was 200 000 and 220 000 respectively over a Prandtl number range of 3.2 – 4.

Using the recorded temperature and mass flow measurements, the heat transfer coefficients were determined using the Wilson Plot method. The mass flow rates were used to determine the Reynolds numbers and the friction factors were determined using the pressure drop measurements over the length of the tube. The wall temperature was derived using an energy balance between the inner tube and annulus flows.

4. UNCERTAINTY ANALYSIS

The purpose of this chapter is to describe the method used to determine the uncertainty on all the measured and calculated variables that are used to calculate the heat transfer coefficient for the test section flow. The uncertainty of the system, wall temperature, Nusselt number and friction factor is quantified and the effects of the uncertainty on the experimental data is analysed. The results of the uncertainty analysis are discussed.

4.1 Uncertainty Analysis

During experimental testing, it is impossible to obtain the true value of a measurement due to errors within the equipment and recording of data. Therefore, uncertainty analysis is used as one of the most accurate methods to quantify this error in attempt to obtain the best approximation of the true value. By calculating the uncertainty of the data recorded during testing, the data can be evaluated in its quality and accuracy. One of the primary objectives of this chapter was to quantify the uncertainty on the temperature and pressure drop measurements that were recorded during testing. A full uncertainty analysis was therefore performed on all relevant measurements which were used to determine the Nusselt number and friction factor.

The method of calculating the uncertainty was based on that of Moffat (1988) where the bias and precision values were used to calculate the uncertainty on the measurements recorded during testing. Bias errors are those which are recurring and can be accounted for during measurements. These errors can be attributed to phenomena such as calibration errors, errors during calculation, measurement equipment imperfections etc. Precision errors are those which occur randomly and can be caused by variations in measurement processes, changes in the equipment utilised for measurements etc.

Each uncertainty on a measurement contributes towards a calculated uncertainty for a desired system characteristic such as a Nusselt number or friction factor. Therefore, the uncertainty in a certain system characteristic, for example u, can be determined by quantifying the standard deviation of a measurement and the contribution of the variables in a data reduction step. In equation (81), the standard uncertainty u, is calculated by using the partial derivative of the result, r, with respect to the contributing variable, v and the uncertainty of the contributing variable, $u(v)$.

$$u(r) = \sqrt{\sum_{j=1}^{n}\left[\frac{\partial r}{\partial v_j}u(v_j)\right]^2} \tag{81}$$

Using equation (81), the uncertainty of each variable was calculated and this was used in turn to calculate the next step of the data reduction process. As a result of this, the uncertainty of a certain variable propagates through the process and this information can be used to design systems to reduce the uncertainty of certain parameters.

4.2 System Uncertainty

Each measurement contains a degree of uncertainty and the values for these measurements can be found in Table 8. These uncertainties take into account possible errors during

calibration as well as measurement errors during experimental testing and these consist of bias (B_j) and precision errors (P_j) as shown in equation (82).

$$\partial v_j = \left\{ \left(B_j\right)^2 + \left(P_j\right)^2 \right\}^{\frac{1}{2}} \tag{82}$$

The resulting uncertainty measurements utilise a 95% confidence level that the actual error will not exceed the estimated error. A standard deviation was used in the root sum squared method to calculate the uncertainty of the measurement. A full description of this method can be found in Appendix A.

Table 8: Summary of system uncertainty values

Measurement	Uncertainty
Instrument Uncertainties:	
Temperature (T)	0.01 °C
Inlets, outlets and bulk temperatures (4 Thermocouples)	0.05 °C
Pressure drop (ΔP)	0.25% FS
Mass flow rate ($\dot{m}$)	0.1%
Tube Wall Thermal Conductivity:	3.2%
Fluid Properties:	
Thermal conductivity (k)	2%
Density (ρ)	0.003%
Viscosity (μ)	1%
Specific heat capacity (C_p)	0.06%
Dimension Uncertainties:	
Tube length (L)	2 mm
Tube diameter (D)	20 µm

The thermocouple uncertainty value was calculated from the calibration of the thermocouples using the Pt-100 which had an uncertainty of 0.01°C.

The uncertainties of the fluid properties are obtained from the formulations of Popiel and Wojtkowiak (1998).

4.3 Friction Factor Uncertainty

The friction factor uncertainty was based on equation (28) which determines the friction factor using the pressure drop measurements which were obtained experimentally. As a result, the friction factor uncertainty was determined using equation (83). The term of the equation with the most effect on the friction factor was the pressure drop measurement.

$$\partial f = \left[\left(\frac{\partial f}{\partial \Delta P}\partial \Delta P\right)^2 + \left(\frac{\partial f}{\partial \rho}\partial \rho\right)^2 + \left(\frac{\partial f}{\partial D_i}\partial D_i\right)^2 + \left(\frac{\partial f}{\partial L}\partial L\right)^2 + \left(\frac{\partial f}{\partial \dot{m}}\partial \dot{m}\right)^2 \right]^{\frac{1}{2}} \tag{83}$$

4.4 Nusselt Number Uncertainty

The Nusselt number was calculated using the Wilson Plot theory which is described in section 3.6.2 of Chapter 3. The Wilson Plot method uses the weighted linear least squares (WLS) regression analysis to determine the coefficients, C_o and n, which enable the separation of the overall thermal resistance for the measured experimental data. Each measured variable has its own uncertainty and this propagates through each data reduction step used to determine the heat transfer coefficient. The uncertainty of the linear regression step of the Wilson Plot method also needs to be taken into consideration.

The uncertainty of each of the measured variables is described in section 4.1 and these uncertainties are referred to as base variable uncertainties. The base variable uncertainties need to be determined as they are used in the calculation of the reduced variable uncertainties. The method proposed by Uhia *et al.* (2013) was used to calculate the uncertainty of the heat transfer coefficients when using the Wilson Plot data reduction method. The method proposed by Uhia *et al.* is based on the general uncertainty equation described by equation (82).

By arranging the data reduction equations as described in Chapter 3, the uncertainty was be calculated on each of the reduction steps and the contribution of each step on the total uncertainty was taken into account. The uncertainty analysis was performed on equation (53) which arranged the Wilson Plot data reduction in the form of a straight line graph equation. The *x* and *y* axis values are stated in equation (54) and (55).

$$y = (R_{ov} - R_w)h_o^* A_o \tag{54}$$

$$x = \frac{h_o^* A_o}{h_i^* A_i} \tag{55}$$

By applying equation (81), the uncertainty in the *y*-axis values derived from the Wilson Plot was calculated using equation (84).

$$u(y) = \sqrt{\left[\frac{\partial y}{\partial R_{ov}} u(R_{ov})\right]^2 + \left[\frac{\partial y}{\partial h_o^*} u(h_o^*)\right]^2} \tag{84}$$

Similarly, the uncertainty for the *x* axis values was calculated using equation (85).

$$u(x) = \sqrt{\left[\frac{\partial x}{\partial h_o^*} u(h_o^*)\right]^2 + \left[\frac{\partial x}{\partial h_i^*} u(h_i^*)\right]^2} \tag{85}$$

The uncertainty of the coefficients used in the Wilson Plot method was determined from the uncertainty of the gradient, *a*, and intercept, *b*, of equation (53). This is shown in equations (86) and (87).

$$u(C_i) = \frac{\partial C_i}{\partial a} u(a) \tag{86}$$

$$u(C_o) = \frac{\partial C_o}{\partial b} u(b) \tag{87}$$

The uncertainty of the gradient and intercept was calculated as described in Appendix A. Using the uncertainty of the coefficients, the uncertainty of the heat transfer coefficients could be determined from the definition found in equations (48) and (50) and using equation (81). The inner tube heat transfer coefficient uncertainty was determined using equation (88).

$$u(h_i) = \sqrt{\left[\frac{\partial h_i}{\partial h_i^*} u(h_i^*)\right]^2 + \left[\frac{\partial h_i}{\partial C_i} u(C_i)\right]^2} \tag{88}$$

The annulus heat transfer coefficient uncertainty was calculated using equation (89).

$$u(h_o) = \sqrt{\left[\frac{\partial h_o}{\partial h_o^*} u(h_o^*)\right]^2 + \left[\frac{\partial h_o}{\partial C_o} u(C_o)\right]^2} \tag{89}$$

A coverage factor was included by Uhia to increase the confidence level of the results to 95%. The recommended coverage factor is $CF = 2$ to obtain the 95% confidence level while assuming a normal distribution in the heat transfer coefficient results. The final uncertainty of the heat transfer coefficients was calculated by equations (90) and (91) which includes the coverage factor.

$$U(h_i) = CFu(h_i) \tag{90}$$

$$U(h_o) = CFu(h_o) \tag{91}$$

4.5 Wall Temperature Uncertainty

Due to the wall temperature being difficult to measure during experiments, the wall temperature was calculated according to the Wilson Plot as described in section 3.6.5. As with the heat transfer coefficients, the general uncertainty equation can be applied to the data reduction steps used to determine the wall temperature. The uncertainty of the wall temperature is be described by equation (92).

$$\begin{aligned} U_{T_w} = \Bigg[& \left(\frac{\partial T_w}{\partial T_i(0)} U_{T_i(0)}\right)^2 + \left(\frac{\partial T_w}{\partial \Delta T_b(0)} U_{\Delta T_b(0)}\right)^2 + \left(\frac{\partial T_w}{\partial C^*} U_{C^*}\right)^2 \\ & + \left(\frac{\partial T_w}{\partial \dot{m}_i} U_{\dot{m}_i}\right)^2 + \left(\frac{\partial T_w}{\partial C_{pi}} U_{C_{pi}}\right)^2 + \left(\frac{\partial T_w}{\partial U_{ov}} U_{U_{ov}}\right)^2 \\ & + \left(\frac{\partial T_w}{\partial h_i} U_{h_i}\right)^2 + \left(\frac{\partial T_w}{\partial p_i} U_{p_i}\right)^2 + \left(\frac{\partial T_w}{\partial z} U_z\right)^2 \Bigg]^{\frac{1}{2}} \end{aligned} \tag{92}$$

A detailed explanation of how the uncertainty terms are calculated can be found in Appendix A.

4.6 Uncertainty Analysis Results

4.6.1 Friction Factor Uncertainty

The friction factor was determined by using the pressure drop readings that were experimentally recorded during testing. By evaluating the uncertainty of the components of equation (28) in Table 9, it can be seen that the two highest individual contributors to the uncertainty are the mass flow rate and the pressure drop readings. The pressure drop readings are considerably higher in contribution than that of the mass flow rate.

Table 9: Factors Contributing to Friction Factor Uncertainty

Property	Minimum Uncertainty	Maximum Uncertainty
$\dot{m}_i$	0.18%	1.5%
D	0.2%	1%
dP	0.38%	12%
ρ	-	0.03%
L	0.2%	1%

The uncertainty values are shown plotted along with the friction factors for a data set for the 8.3 mm tube in Figure 5. From Figure 5, it can be seen that most of the friction factor values fell within the uncertainty values for the entire Reynolds number range. The uncertainty was highest at the lowest Reynolds number which decreases with increasing Reynolds number.

The uncertainty was highest at two points which represent the lowest recorded values on a particular pressure diaphragm. The accuracy of the measurement was lowest at the low end of the diaphragm pressure range. The switch from one pressure diaphragm to the next occurred at a Reynolds number of 110 000 as can be seen from the increase in uncertainty in Figure 5. The maximum uncertainty value of the friction factor for tube 8.3 mm was 11% and the minimum was 1.3%. This is shown in Table 10.

As most of the experimental values lie within the calculated uncertainties it is determined that the measurement of the pressure drop and mass flow rates was accurate and credible. The friction factors for the 14.2 mm tube were plotted with the uncertainty on each of the values in Figure 6. Once again, the uncertainty was high at low Reynolds number and steadily decreased as the pressure drop values approached the full range pressure values of each diaphragm.

Table 10: Friction factor uncertainties

Friction Factor Uncertainty	Minimum Uncertainty	Maximum Uncertainty	Average Uncertainty
Tube diameter 8.3 mm	0.58%	4.48%	2.46%
Tube diameter 14.2 mm	0.61%	19.25%	2.81%

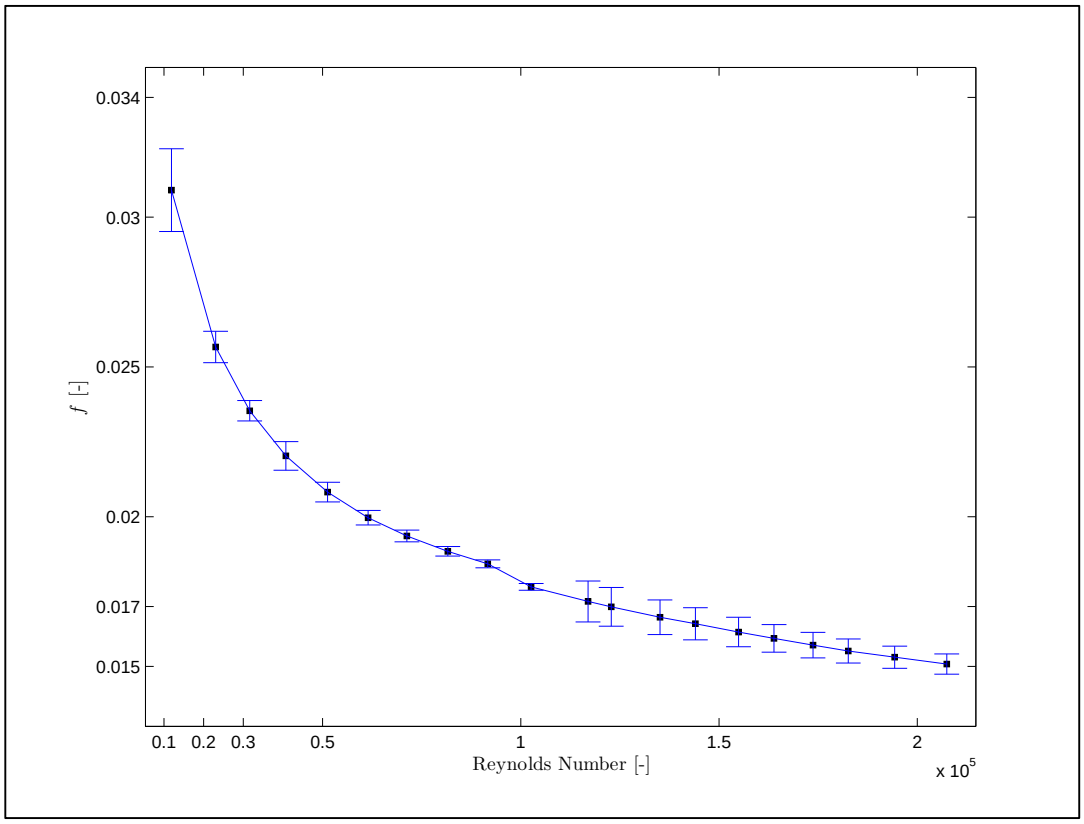

Figure 5: Friction factor measurements with calculated uncertainties for a Reynolds number range of 10 000 to 200 000 for the 8.3 mm tube

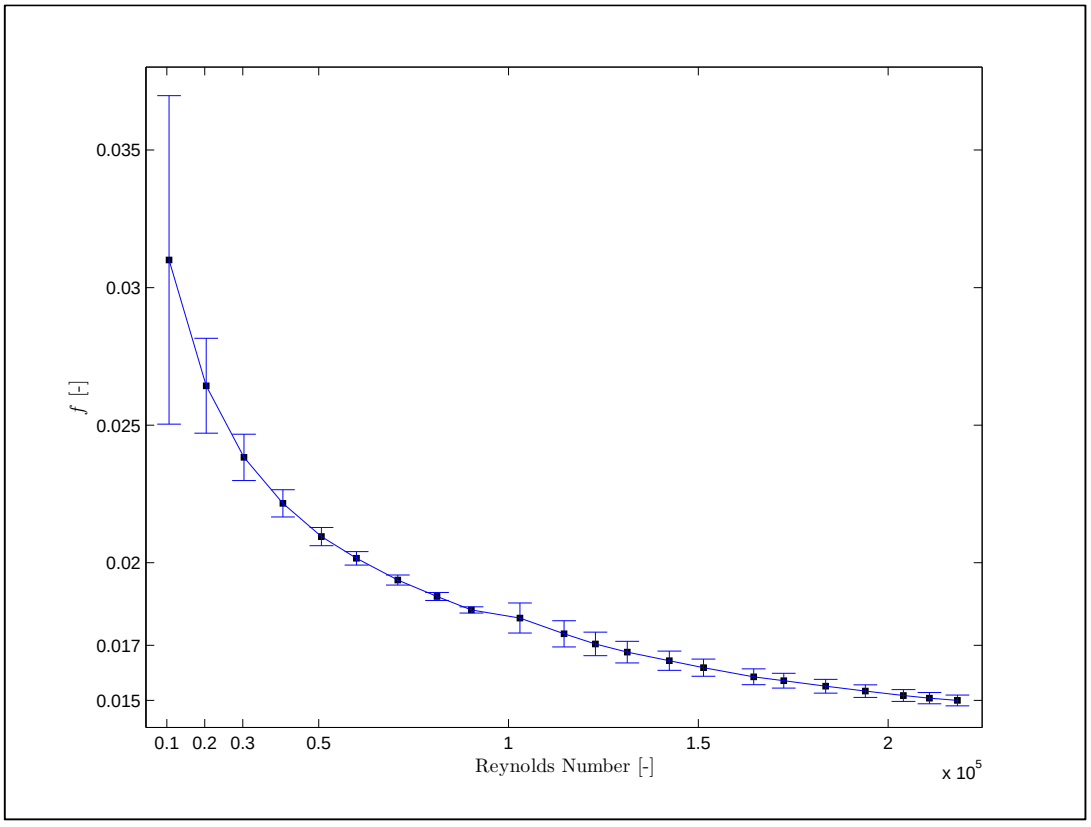

Figure 6: Friction factor measurements with calculated uncertainties for a Reynolds number range of 10 000 to 220 000 for the 14.2 mm tube

It was observed that at a Reynolds number of 100 000, the uncertainty values increased again as a new diaphragm was used to measure the next pressure drop range and it also decreased as the Reynolds number increased. All the friction factor data points were found to lie within the uncertainty band for the entire range of Reynolds numbers.

Figure 7 displays the friction factor uncertainties for both tube diameters as a function of Reynolds number. All the uncertainty values lie below 20% while the average uncertainty of all the measurement points was less than 3%.

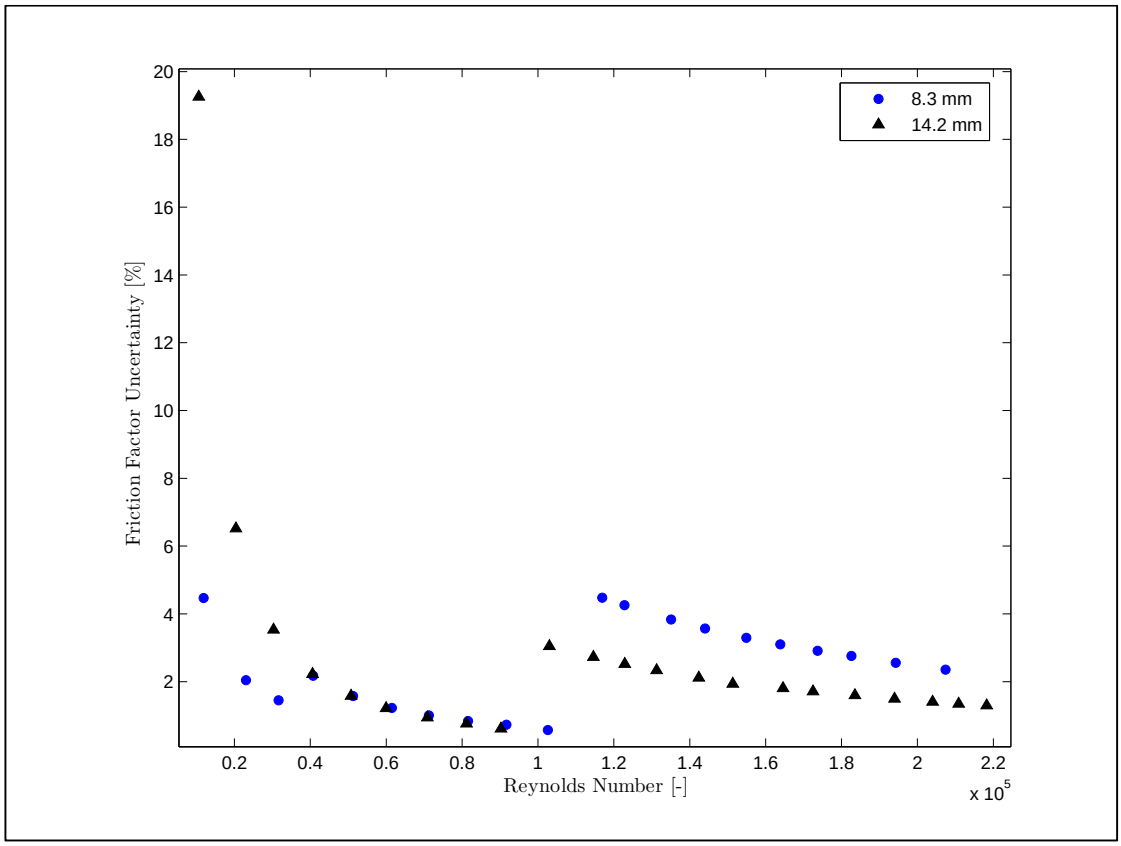

Figure 7: Friction factor uncertainty results for both 8.3 and 14.2 mm tube diameters as a function of Reynolds number

4.6.2 Nusselt Number Uncertainty

The uncertainty analysis of the Nusselt number is described in detail in Appendix A. The method proposed by Uhia *et al* (2013) was used to determine the uncertainty of the Nusselt number which is calculated using the Wilson Plot method.

The uncertainty was calculated for all the measurements obtained during experimental testing. These measurements were used to determine other system variables such as the Reynolds Number, Prandtl number etc. Once these were determined, the heat transfer coefficients were determined for the system. The uncertainty was calculated in a similar fashion starting with the uncertainty on the measurements and then using the method described in Chapter 4 to determine the calculated variables' uncertainty.

4.6.2.1 Relative Uncertainty

The first step was to determine the uncertainty of the measurements that were recorded during testing which are referred to as base variable uncertainties. The base variable measurements were used in a number of data reduction steps to obtain the heat transfer coefficients. Taking each of the individual variables from each equation, the uncertainty contribution of each one was calculated.

The uncertainty was determined using the following steps:

- Level 1 – Base Variables: Measured values during testing – mass flow rate, viscosity, thermal conductivity, diameter, inlet and outlet temperatures
- Level 2: Reduction of Level 1 – calculation of Reynolds number, Prandtl number, area, thermal resistance of the tube, Log Mean Temperature Difference, heat transfer rate.
- Level 3: Reduction of Level 2 – calculation of unscaled heat transfer coefficients, overall thermal resistance
- Level 4: Reduction of Level 3 – calculation of heat transfer coefficients, Wilson Plot coefficients

The relative uncertainty of a variable was calculated as a percentage of the total calculated value. The base variable relative uncertainty values were plotted as a function of the inner tube Reynolds number in Figure 8. From the plotted uncertainties, it can be see that the highest relative uncertainty belonged to that of the thermal conductivity of the water (k) in the annulus and the inner tube at a relative uncertainty of 2%. The second highest contributor of the base variable relative uncertainty was the scaling coefficient used in the regression analysis of the Wilson Plot (C_i) at a value of just under 1.5%. The uncertainty in the viscosity of the fluid also made a considerable contribution with a relative uncertainty of approximately 1%.

The relative uncertainty values of the reduced system variables are shown in Figure 9. Each of the base variable uncertainties had an effect on the reduced uncertainties depicted in Figure 9. Each of the calculated values had their own measure of relative uncertainty which was plotted against the inner tube Reynolds number. The lowest uncertainty values belonged to the uncertainty of the calculated tube areas. This is due to the low uncertainty that existed when measuring the diameter and that being the only contributor to the uncertainty of the calculated length.

The Reynolds number uncertainty was considerably low for both the inner and outer tube flows with the average uncertainty being relatively constant between 1-1.1%. A similar trend was seen for the Prandtl number with the average uncertainty being between 2.25-2.3% for the inner and outer tube Prandtl number.

It was found that the inner tube heat transfer coefficient relative uncertainty stayed approximately constant at 2% over the Reynolds number range. The annulus tube heat transfer coefficient relative uncertainty stayed constant at a value of 2.35% over the Reynolds number range.

4.6.2.2 Identification of Dominating Factors on Heat Transfer Coefficient Uncertainty

The uncertainties of all the measurements taken during experimental testing contributed towards the uncertainty of the heat transfer coefficient. It was important to determine which of the system characteristic uncertainties displayed a dominating effect on the heat transfer.

To calculate the uncertainty propagation of a certain variable, the general expression in equation (93) was used. The value of x_i represents a measured variable and F is a function of x_i .

$$u(F)^2 = \sum_{i=1}^{n} \left[\frac{dF}{dx_i} u(x_i)\right]^2 \tag{93}$$

Dividing equation (93) by the term $u(F)^2$ renders:

$$1 = \sum_{i=1}^{n} \left[\frac{dF}{dx_i} u(x_i)/u(F)\right]^2 \tag{94}$$

The fractional uncertainty component could then be calculated using equation (95). This represents the contribution of the variable to the total uncertainty found in the variable determined by the function F.

$$R_u = \left[\frac{dF}{dx_i} u(x_i)/u(F)\right]^2 \tag{95}$$

Using equation (95) it was determined which variable exhibits the dominating uncertainty on the function F.

Figure 10 is a visual representation of the contribution in uncertainty of each variable to the function F.

According to Figure 10, the main contributor to the uncertainty of the inner tube heat transfer coefficient, h_i, was the unscaled heat transfer coefficient, h_i^*, and the scaling factor C_i. The uncertainty in the scaling factor was caused by the regression analysis in the Wilson Plot method.

The main contributor to the unscaled heat transfer coefficient, h_i^*, was the thermal conductivity of the water in the inner tube (k_i). The two other significant contributors were the inner tube Reynolds number and Prandtl number, where the uncertainty of the thermal conductivity contributed significantly to the latter. The main contributor of the uncertainty in the Reynolds number was the viscosity of the water in the inner tube (μ_i).

Taking all these into account, it can be deduced that the main contributors to the uncertainty in the inner tube heat transfer coefficient were the Wilson Plot regression analysis, and the water's thermal conductivity and viscosity measurements.

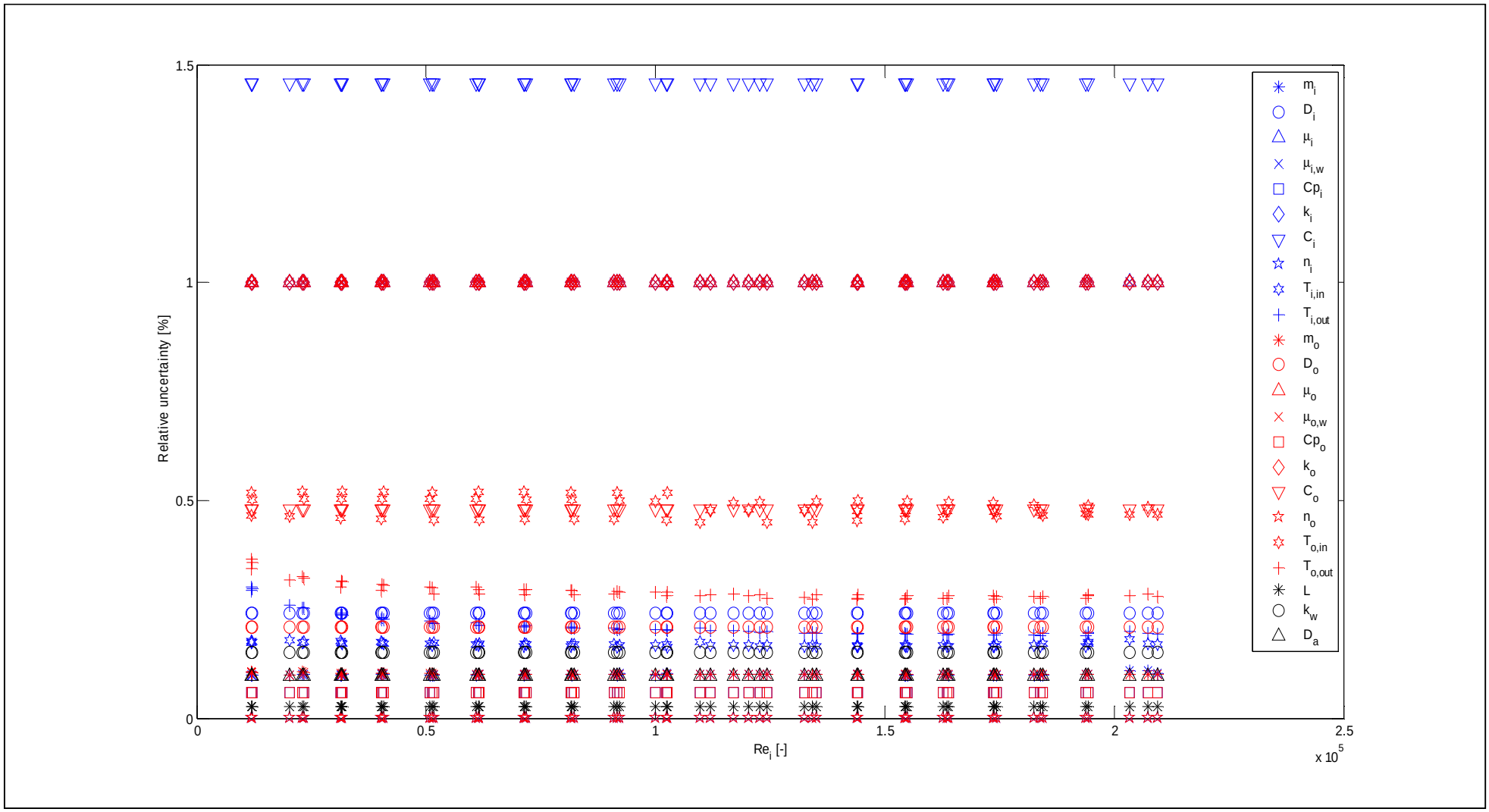

Figure 8: Relative uncertainty of the base variables measured during experimental testing as a function of Reynolds number

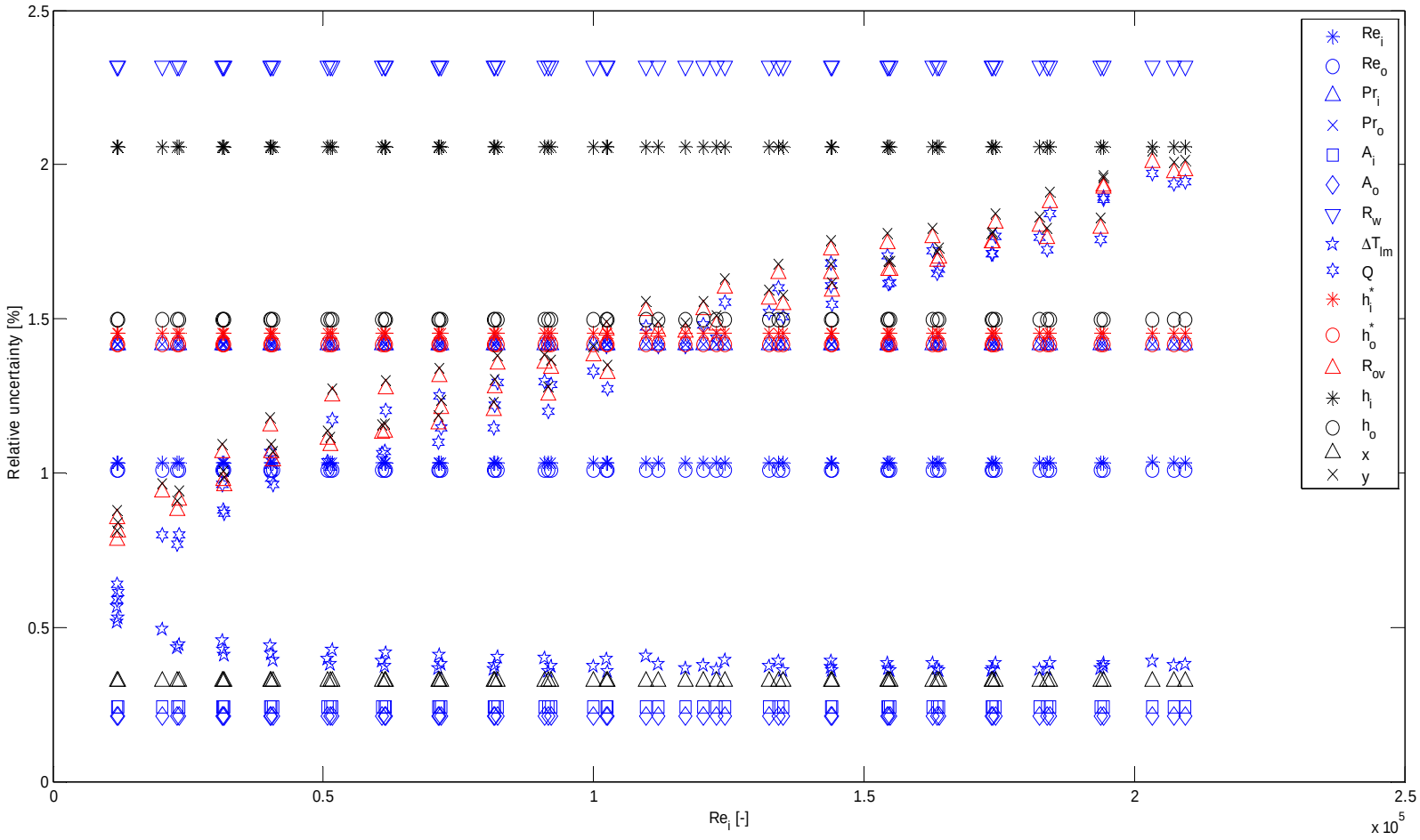

Figure 9: Relative uncertainty of the reduced variables calculated from the measured uncertainty for a Reynolds number range of 10 000 to 210 000

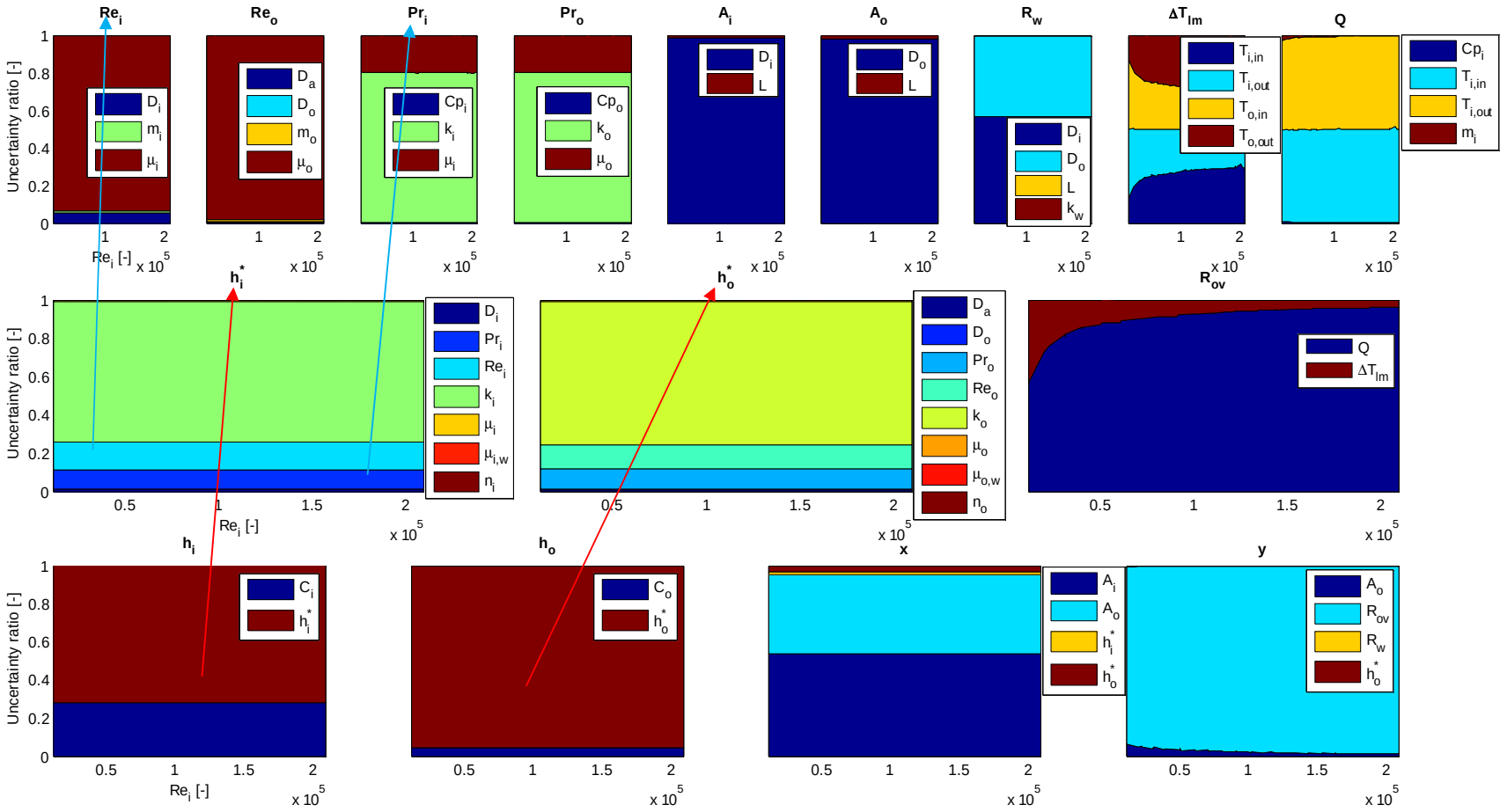

Figure 10: Relative uncertainty of the measured and calculated variables for 8.3 mm tube. The effect of each of the measured and calculated variables on the heat transfer coefficient is shown for the test Reynolds number range.

4.6.2.3 Wall Temperature Measurements

The wall temperature was measured during experimental testing and this was compared to the wall temperature calculated using the Wilson Plot as described in Chapter 3.6.5. The inner tube wall temperature measurements were recorded along the axial length of the tube at 8 different positions. This is depicted in Figure 11. Each of the positions were measurements were recorded were an equal distance of 0.45 m apart.

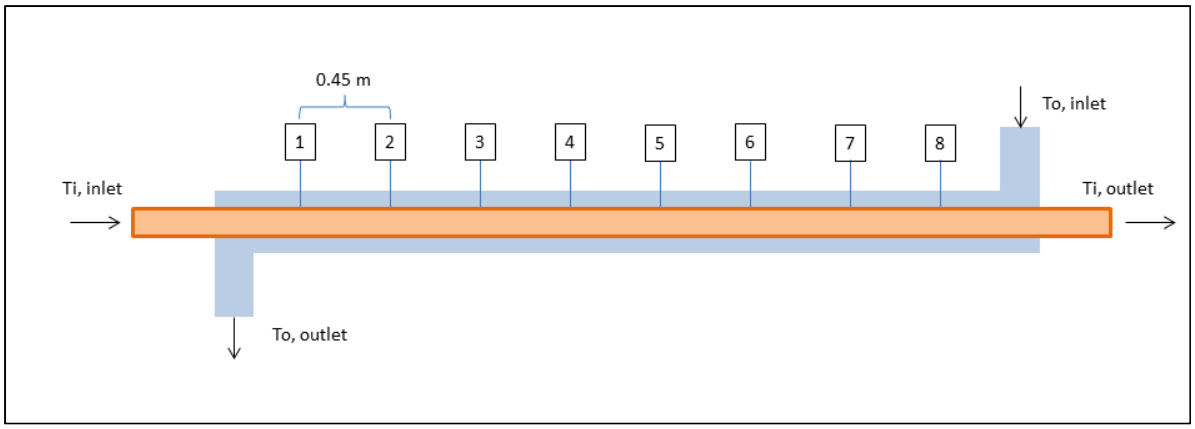

Figure 11: Inner tube wall temperature schematic showing the temperature measurement positions along the length of test section

The measured and calculated wall temperatures were plotted for the highest and lowest Reynolds number along the axial length of the tube as is shown in Figure 12.

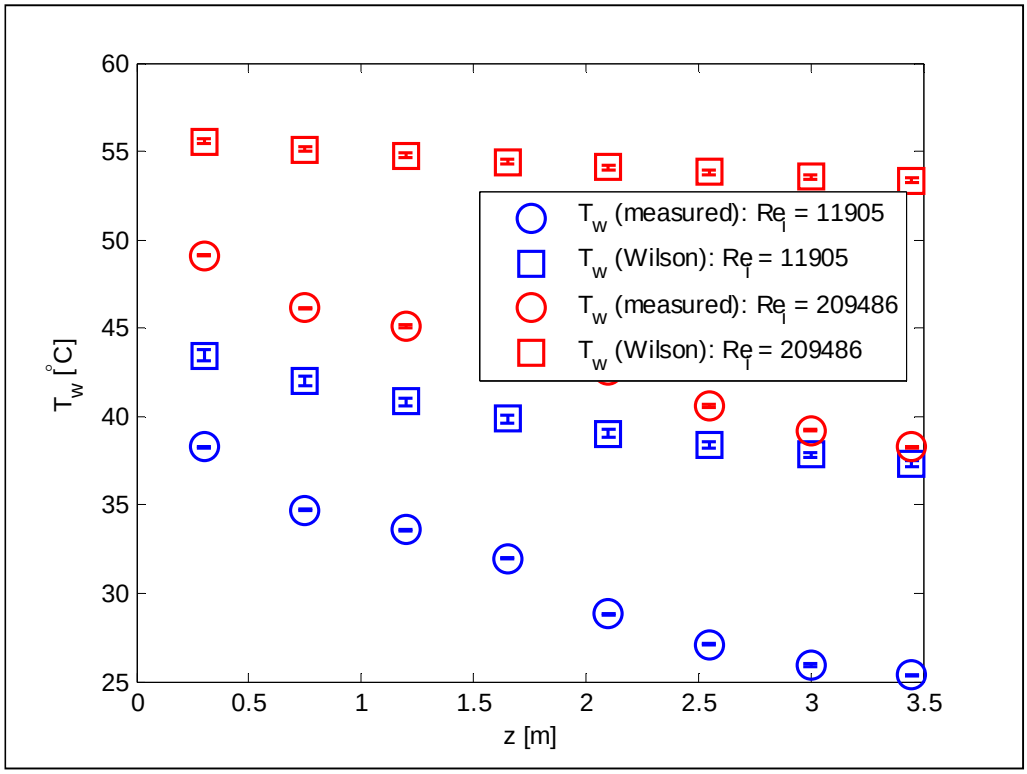

Figure 12: Comparison of the measured wall temperature to the calculated wall temperature using the Wilson Plot method along the length of the test section for the 8.3 mm tube

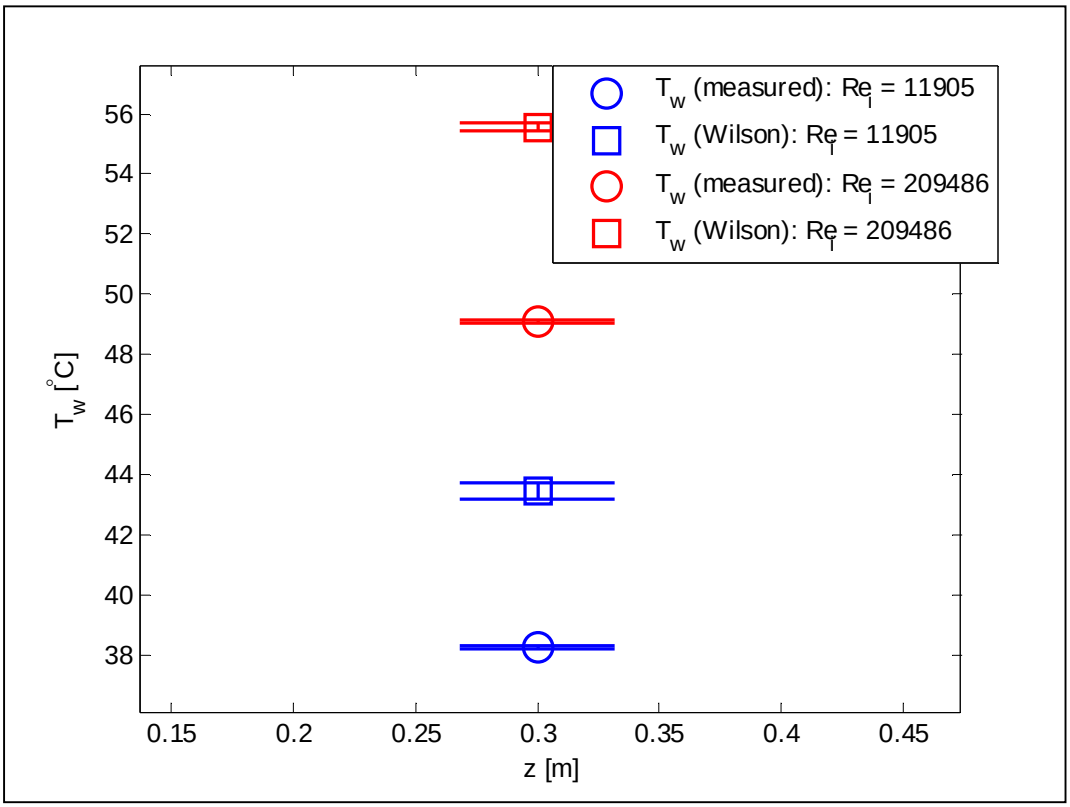

Figure 13: The difference between the measured and calculated wall temperature for a Reynolds number of 11 905 and 209 486 at a position of 0.3 m along the length of the 8.3 mm

The Wilson plot does not only serve as a method to obtain the inner tube heat transfer coefficient. Once the Wilson Plot uncertainty was calculated on the inner tube heat transfer coefficient, the deduced Wilson plot wall temperature as derived in equation (76) could be used to validate a measured wall temperature.

The measured wall temperature, if measured correctly, normally produces inner tube heat transfer coefficient values with lower uncertainty in comparison with that of the Wilson plot method. It, however, requires the correct design of the test section as well as the correct method of attaching a thermocouple to the tube wall. The correct design of the heat exchanger requires that the ratio of the overall-to-inner-tube heat transfer coefficient to be high enough in order to obtain a large enough value for $T_i - T_w$ and consequently a low uncertainty on $h_i = \frac{\dot{Q}}{\pi D_i dz(T_i - T_w)}$. The latter issue requires that sufficient precautions are taken in the attachment of the thermocouple to the measured wall surface. This is in order to avoid measurement errors that sometimes occur if the temperature of a surface with a convective stream over it is measured. The measurement errors could be as a result of heat conducted away from the thermocouple junction and/or electrical error due to a large thermal gradient in the thermocouple wires. It could also be as a result of a thermocouple junction that is big enough to measure an average of a large range of temperatures occurring in the thermal boundary layer. In high Reynolds number turbulent flow, the temperature gradient in the thermal boundary layer can be very steep and the latter error large if not eliminated by design of the heat exchanger.

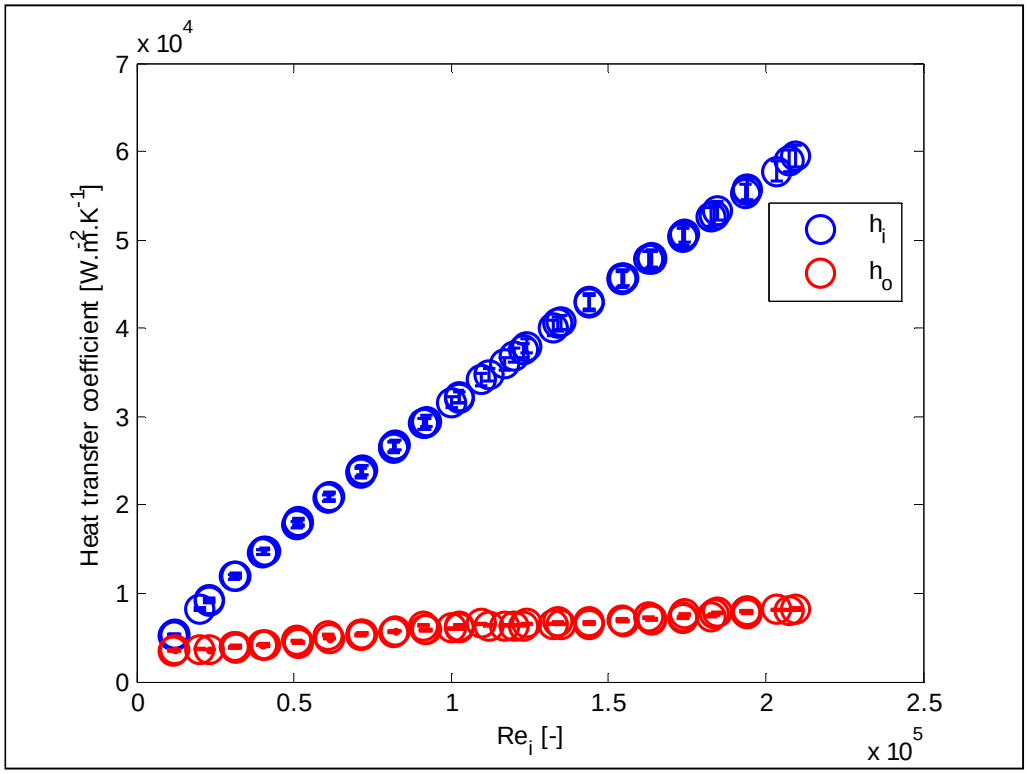

Figure 14: The Wilson Plot results of the inner and outer tube heat transfer coefficients for the 8.3 mm test section over a Reynolds number range of 10 000 to 210 000

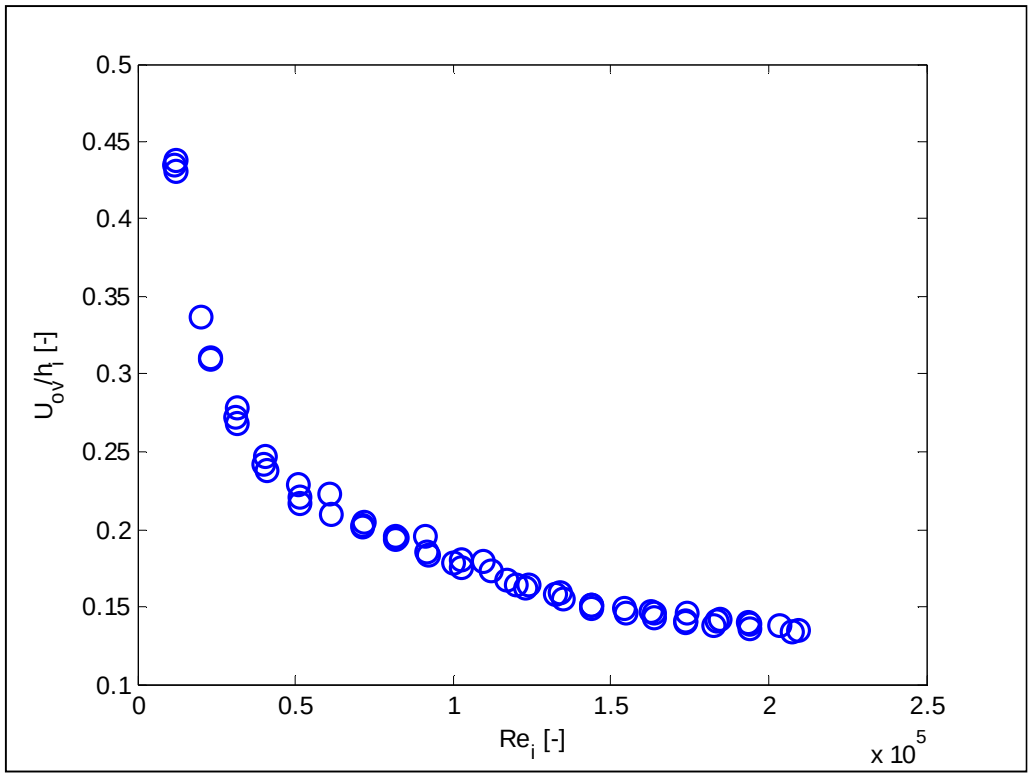

Figure 15: The ratio of the overall heat transfer coefficient to the inner tube heat transfer coefficient for the 8.3 mm tube

If the uncertainty in the Wilson plot wall temperature was quantified correctly, the measured wall temperature, $T_{w,meas}$, should not deviate from the Wilson plot temperature, $T_{w,Wilson}$, by more than $2U_{T_{w,meas}} + 2U_{T_{w,Wilson}}$. The wall- and Wilson plot uncertainties were labelled as $U_{T_{w,meas}}$ and $U_{T_{w,Wilson}}$ respectively. The values of $T_{w,meas} \pm U_{T_{w,meas}}$ and $T_{w,Wilson} \pm U_{T_{w,Wilson}}$ were plotted in Figure 12 and Figure 13 at the lowest and highest values of Re_i. The deviation between $T_{w,Wilson}$ and $T_{w,meas}$ was always higher than about 5 °C, which was much higher than $2U_{T_{w,meas}} + 2U_{T_{w,Wilson}}$. This indicated that the wall temperature was most likely measured incorrectly.

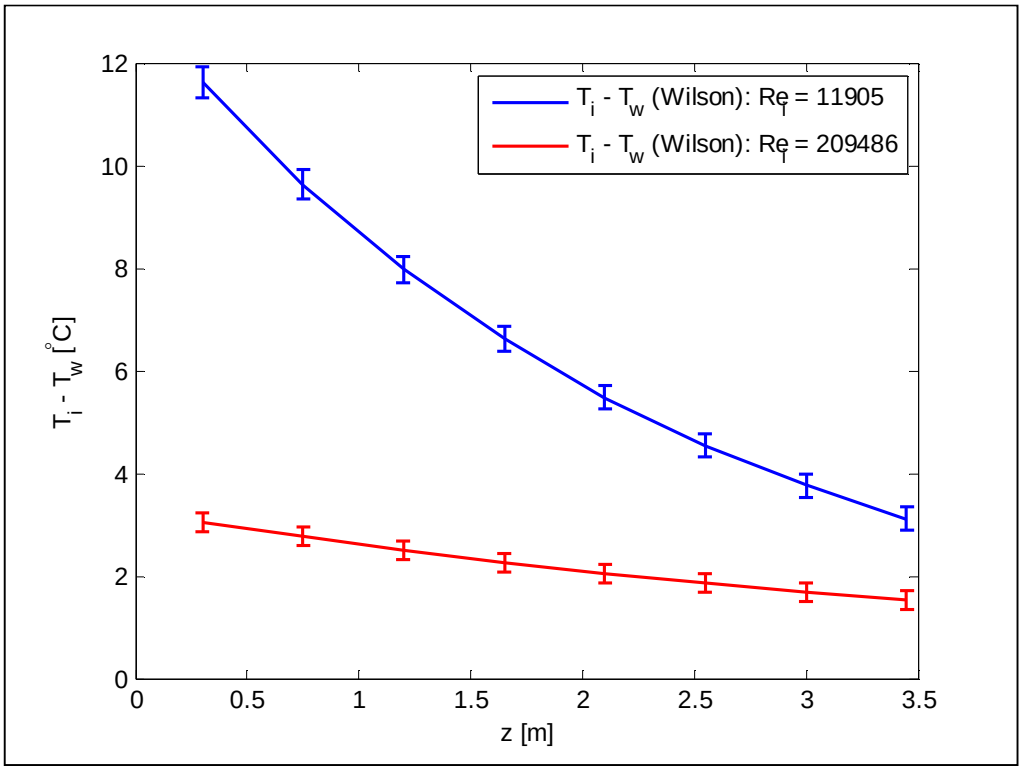

Figure 16: The difference between the bulk inner tube temperature and the wall temperature calculated using the Wilson Plot method for a Reynolds number of 11 905 and 209 486

The results in Figure 14, Figure 15 and Figure 16 can be used in order to determine if the measurement error was partly due to the incorrect design of the test section. Figure 14 shows that the heat transfer coefficient was much higher in the inner tube in comparison with that in the annulus at increasing values of Reynolds number. Figure 15 shows the same result when looking at U_{ov}/h_i, the ratio of the overall heat transfer coefficient to the inner tube heat transfer coefficient. The ratio U_{ov}/h_i has a direct influence on the wall temperature, as is shown in equation (76). By increasing the mass flow rate in the annulus or finning the outside of the inner tube this ratio could have been increased. The mass flow rate was, however, limited to the capability of the annulus pump. When considering Figure 16, $T_i - T_w$ according to the Wilson plot along the heat exchanger length, it can be seen that increasing values of Re_i had a substantial influence on $T_i - T_w$. The lowest values of $T_i - T_w$ were however still about 20 times higher than the measurement uncertainty of $T_i - T_w$. The low U_{ov}/h_i values obtained as a result of the heat exchanger design can therefore not explain the large difference between $T_{w,meas}$ and $T_{w,Wilson}$. The large difference can be attributed to the

method and location of attaching the wall temperature thermocouple. It was for this reason that the measured wall temperature data was excluded from this study.

4.7 Conclusion

The general uncertainty equation was used to determine the uncertainty of all the variables that were recorded during experimental testing and used in data reduction steps to obtain the friction factor, heat transfer coefficient and wall temperature of the inner tube. The uncertainty analysis is performed on all measured and reduced variables. The friction factor uncertainty was calculated using the method of Moffat and the results show a higher uncertainty measurement on the low range measurements of each diaphragm used to measure the pressure and reducing as approaching the full scale measurement.

The heat transfer coefficient uncertainty was determined using the method proposed by Uhia *et al.* (2013) which produced a low average relative uncertainty over the Reynolds number range. It was determined that the main contributors of the uncertainty in the heat transfer coefficient were the result of the Wilson Plot regression analysis and the inner tube water thermal conductivity and viscosity.

The Wilson Plot method was used to validate the wall temperature measurements that were recorded during experimental testing. When compared to one another, the wall temperature measurements were found to under predict the temperature of the tube wall. It was also found that the heat transfer coefficient in the inner tube was much higher than that of the annulus over the Reynolds number range. This is confirmed by evaluated the ratio of the overall heat transfer coefficient to the inner tube heat transfer coefficient. As a result, the measured wall temperature data was excluded from the results.

5. RESULTS

5.1. Introduction

The purpose of this chapter is to present the results of the experimental testing. The energy balance of the system is discussed. The friction factor and heat transfer coefficient results are presented. The effect of the *j*-factor on the heat transfer results is evaluated and a new correlation to predict the heat transfer based on the experimental data is determined.

5.2. Energy Balance Results

The energy balance of the system was calculated using the heat transfer rates of both the inner and outer fluid streams in the heat exchanger as shown in equation (80). The energy balance is a good indication of whether the system is experiencing excessive heat losses at any point and whether the system is stable. The energy balance will stabilise once the inlet and outlet temperatures and mass flow rates have reached steady state conditions. It is important to have a stable system when recording experimental data.

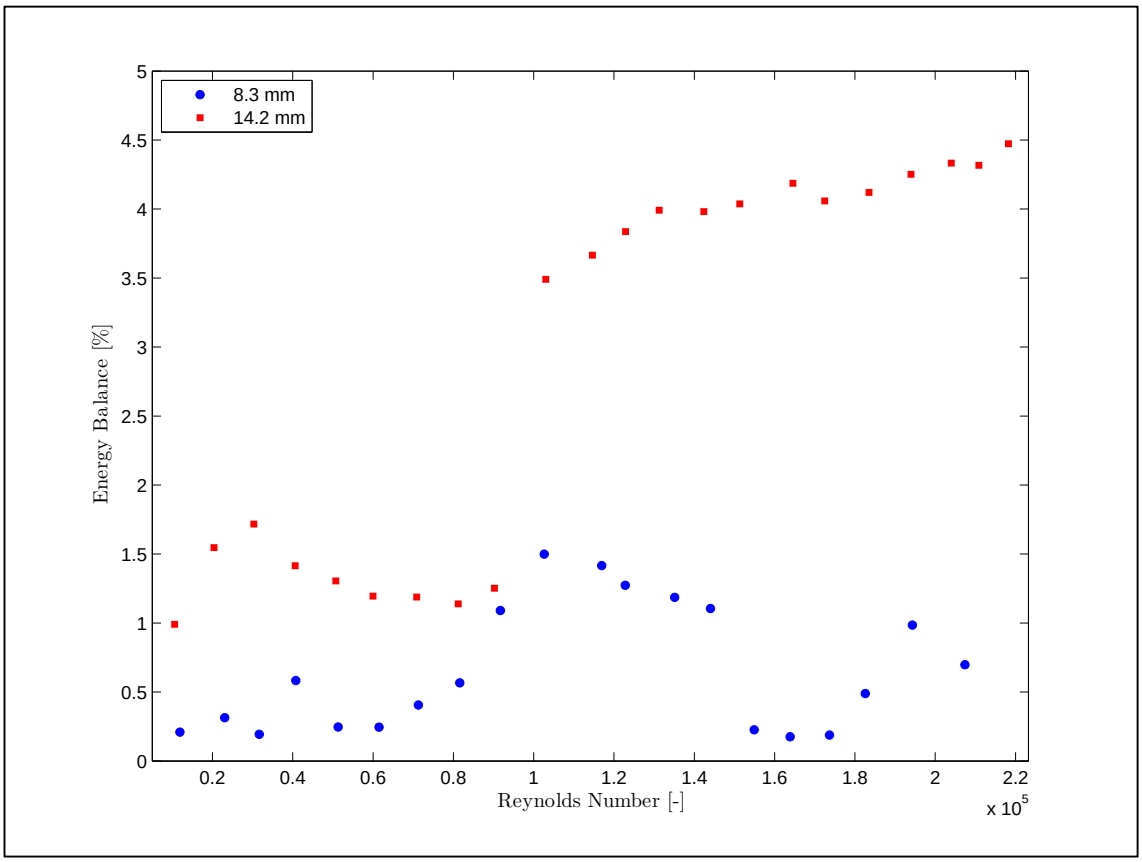

Figure 17: Energy balance results for 8.3 mm and 14.2 mm tube diameters over a Reynolds number range of 10 000 to 220 000

The energy balance results for one data set of each tube diameter are displayed in Figure 17. The energy balance values of each data set of each tube diameter were averaged to obtain the overall average of the test results for each tube. This is tabulated in Table 11. The energy

balance values were on average less than 0.7% for the 8.3 mm tube and less than 3% for the 14.2 mm tube respectively.

Table 11: Energy Balances for all Tube Diameters

Tube Diameter	**8.3 mm**	**14.2 mm**
Data Set 1	0.66%	2.86%
Data Set 2	0.67%	2.98%
Data Set 3	0.68%	2.79%
Average	**0.67%**	**2.88%**

5.3. Friction Factor Results

The friction factors were compared to the Blasius (1913) and Petukhov (1970) equations as these are accurate and well utilised equations used to predict the friction factor in the turbulent flow regime.

For the 8.3 mm tube, the friction factor graph shown in Figure 18 displays good agreement to both the Blasius and Petukhov correlations. At the lowest Reynolds numbers, the results lie slightly above the correlations but with increasing Reynolds number the results converged to the Blasius equation. The Petukhov and Blasius equations are not equal in parts but the results fell in between the two equations at a Reynolds number of 20 000 - 50 000. The same trend is seen from Reynolds numbers of 100 000 – 200 000.

The results deviated slightly from a Reynolds number of 150 000 where a possible reason for this could be due to a change of the diaphragm used to measure the largest pressure range. Since the values are low compared to the full scale value of the transducer, which is 860 kPa, the uncertainty was the highest at this range of the pressure readings. The accuracy was expected to improve as the pressure values increased and approached the full scale value of the diaphragm. The pressure readings for the 8.3 mm tube were the higher of the two test sections due to the diameter being the smaller of the two tubes. During testing, this was the limiting factor on the maximum Reynolds number that could be achieved.

The friction factor results for the 14.2 mm tube are shown in Figure 19. When considering the results for the 14.2 mm tube, it is once again seen that the values for the friction factor resembled those predicted using the Blasius equation. There was an outlier point at a Reynolds number of approximately 100 000, this is due to the same reason explained for the 8.3 mm tube, that was the changing of the pressure diaphragm and being on the low range of the diaphragm.

The friction factor deviation data for both of the tube diameters is found in Table 12. The deviation results were calculated as a comparison between the experimental data and the Blasius equation. The deviation percentage is the amount that the experimental data deviated from the Blasius correlation using equation (96).

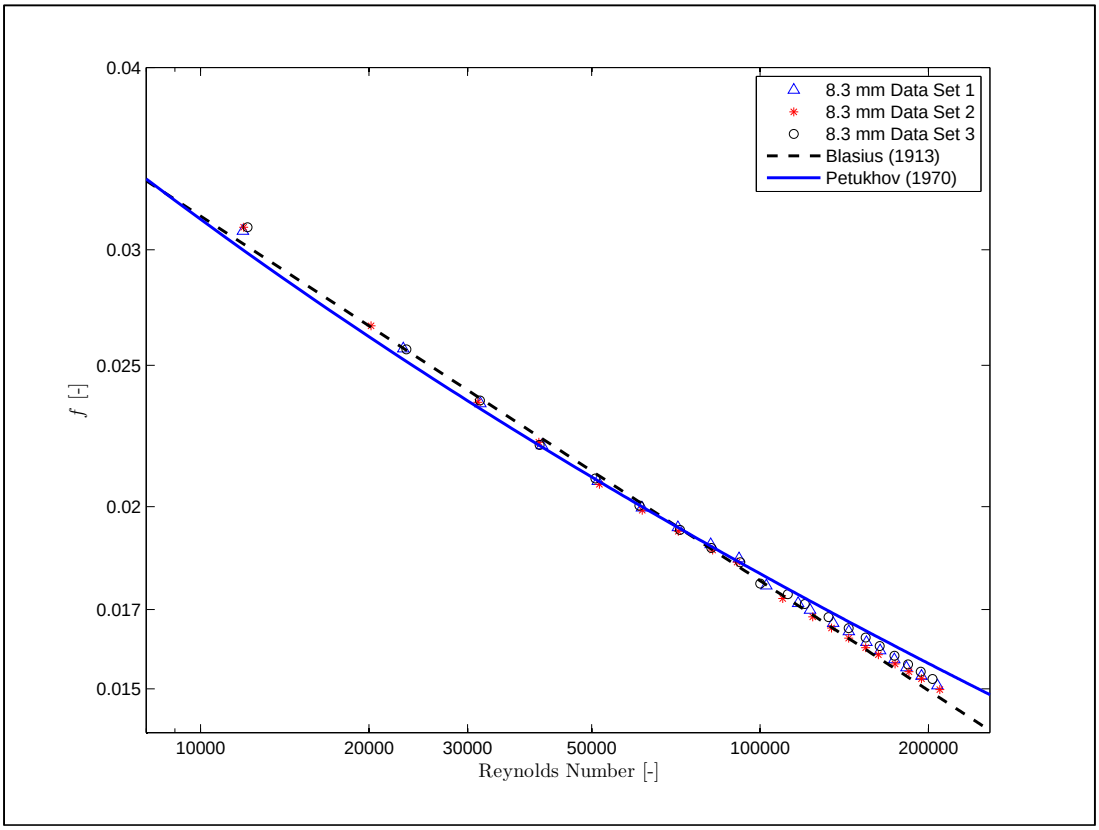

Figure 18: Friction factor results for 8.3 mm tube compared to Blasius (1913) and Petukhov (1970)

The maximum of this data set was taken and that is the value stated in Table 12 as the maximum deviation.

$$s_{dev}(\%) = \frac{f_{blasius} - f_{experimental}}{f_{experimental}} \times 100 \tag{96}$$

The relative mean deviation of the data, s_{mean}, is the average value of the deviation calculated using equation (96). The relative absolute deviation, s_{abs}, is the absolute value of the relative mean deviation. The relative absolute deviation can be used to determine the average value of the deviation whether the data is over or under predicted in comparison to the theory.

The standard deviation of the data in comparison to that predicted by Blasius was calculated using equation (97). The value of *M* represents the number of data points in the experimental data set.

$$s_{std} = \sqrt{\frac{\sum_{i=1}^{M} |s_{dev} - s_{mean}|^2}{M - 1}} \tag{97}$$

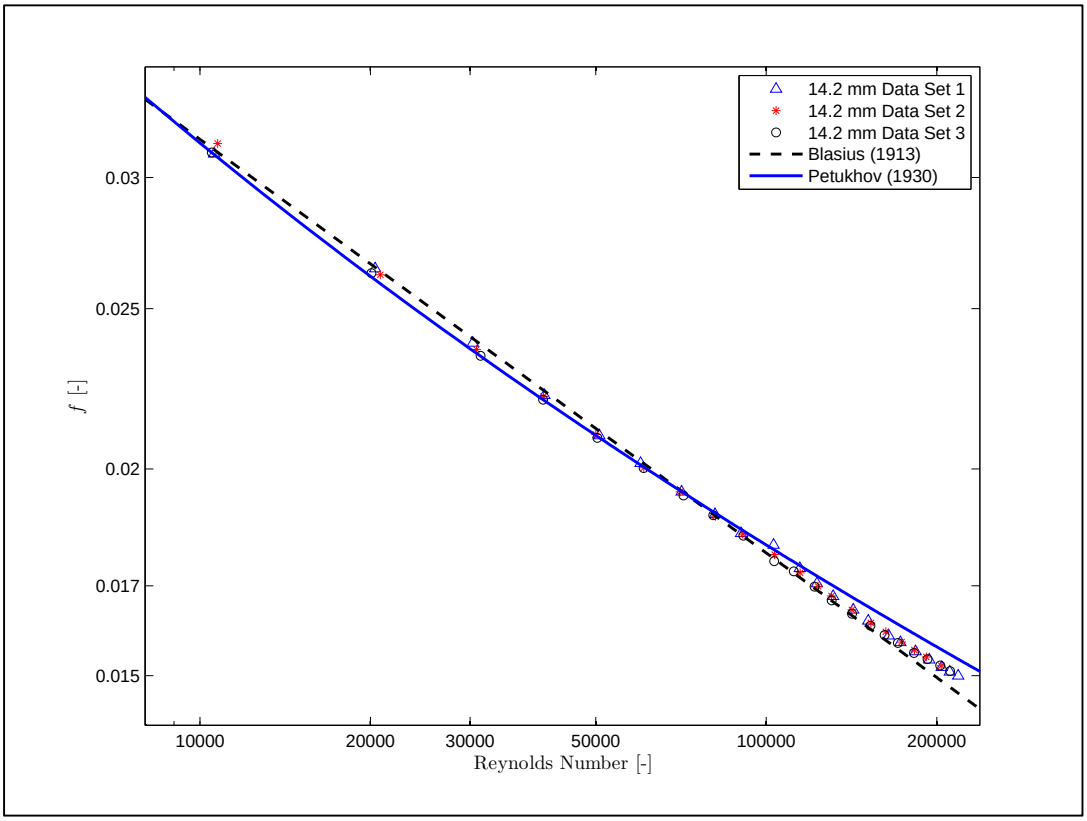

Figure 19: Friction factor results for 14.2 mm tube compared to the Blasius (1913) and Petukhov (1970) correlations

As shown in Table 12, the maximum deviation of the data of both tube diameters was less than 5% when compared to that predicted by Blasius. The majority of the experimental data was over predicted when comparing to Blasius which results in negative values of the relative mean deviation. The relative absolute deviation shows the average deviation fell within a range of 0.5-3%. The standard deviation of the data was low with most data falling below 2% for both tube diameters.

Table 12: Friction Factor Deviation Data

Friction Factor Deviation	**Maximum Deviation [%]**	**Relative Mean Deviation [%]**	**Relative Absolute Deviation [%]**	**Standard Deviation [%]**
8.3 mm Tube:				
Data Set 1	-1.7	-0.6	1.0	1.0
Data Set 2	-2.6	-0.1	0.8	0.6
Data Set 3	-3.0	-0.9	1.2	1.2
14.2 mm Tube:				
Data Set 1	-4.6	-1.6	2.2	2.1
Data Set 2	-4.3	-1.3	2.0	2.0
Data Set 3	-4.5	-1.4	2.1	2.1

5.4. Heat Transfer Coefficient Results

The Nusselt number was calculated using the heat transfer coefficients which are solved for using regression analysis as described in Chapter 3.6.4. The result of the Wilson Plot calculation of the *x* and *y* values that are described by equations (54) and (55) can be found in Figure 20.

The results for the 8.3 mm tube are displayed in Figure 21 for all three experimentally recorded data sets. The experimental data was compared to that of that of Dittus and Boelter (1930), Sieder and Tate (1936) and Gnielinski (1976). The Dittus and Boelter correlation was used with $n = 0.3$ for cooling applications when calculating the heat transfer coefficients for comparison. The study of Petukhov (1970) is a well utilised equation as those previously mentioned for comparison, but in this case has not been used as it compares very closely to that of Gnielinski (1976) with an average deviation of only 3%. Therefore it is omitted for comparison to the Nusselt number results. It can be seen in Figure 21 that all three experimental data sets resembled the Nusselt number results predicted using the Gnielinski correlation in equation (19). This trend is seen throughout the higher Reynolds number range with a slight deviation at the lower Reynolds number range. At the lower Reynolds number range the results were found to correlate closely to that of Sieder and Tate. The Dittus and Boelter approximations were much lower than the others and this is thought to be due to the fact that the correlation does not account for viscosity effects at the wall as the other two equations do.

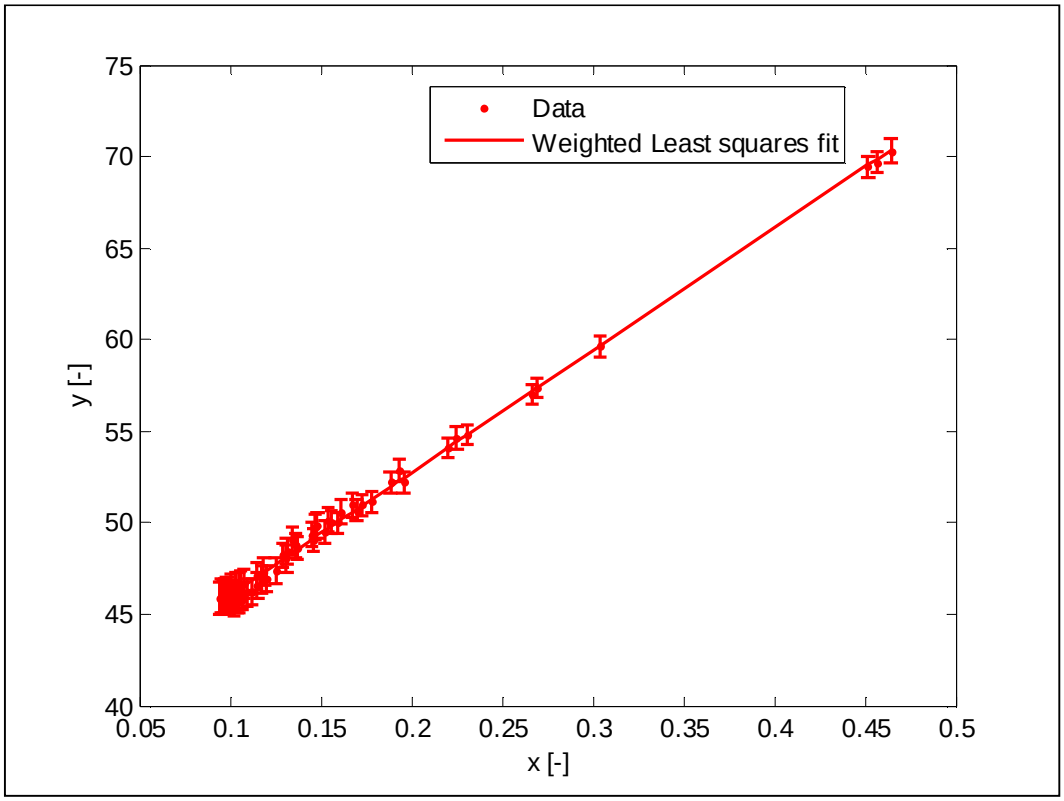

Figure 20: Wilson Plot results plotted with uncertainties for 8.3 mm tube test section

In Figure 22, an alternative representation of the data compared to that of Gnielinski's is shown. The data was compared with that of Gnielinski in a ratio format with a value of 1

representing the experimental data being equal to that of Gnielinski. As shown in this form, the data correlated very closely to that of Gnielinski (average difference is 3%). Gnielinski states that his equation has an accuracy of 20%. The dashed lines are added at 10% higher and lower than Gnielinski's values. From the representation in Figure 22, it is observed that the data was very close to being equal to Gnielinski's predictions, especially as the Reynolds number increased where errors were approximately 1%. The largest differences occurred at low Reynolds numbers with errors of up to 6.2%. Throughout the Reynolds number range, it is shown that the experimental heat transfer coefficients fell within the 20% accuracy range that is applied to the Gnielinski correlation.

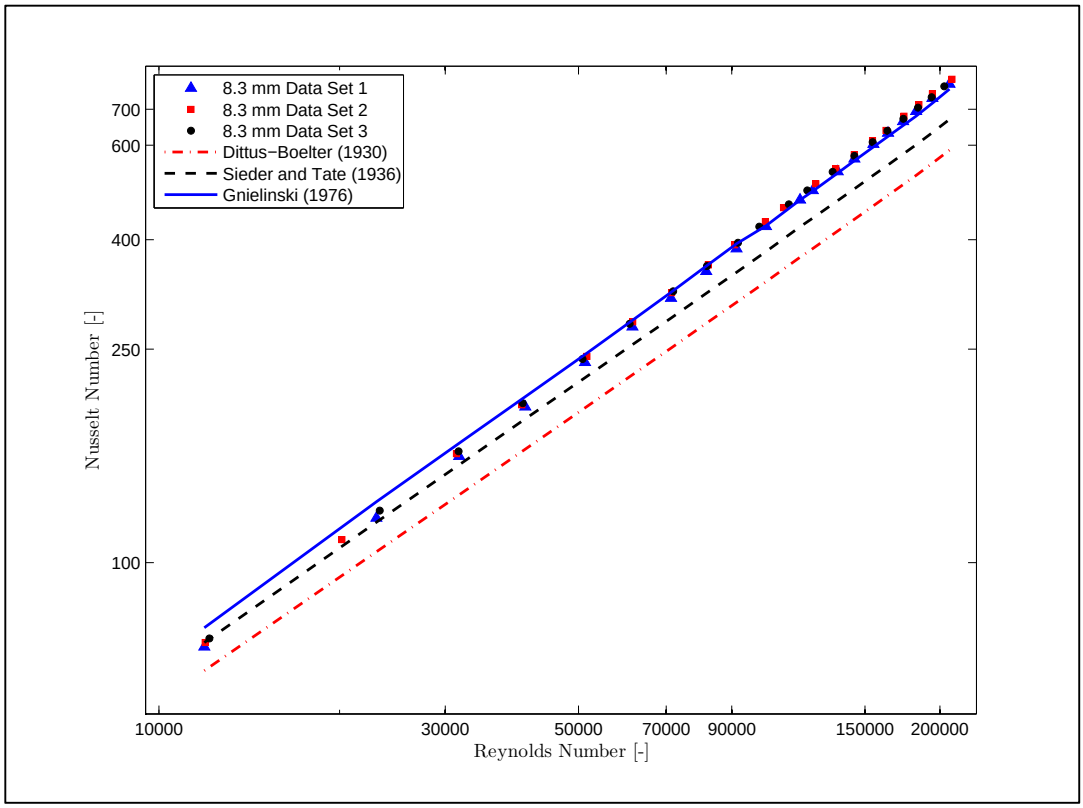

Figure 21: Nusselt number results calculated using the Wilson Plot method for 8.3 mm tube compared to the Gnielinski (1976), Sieder and Tate (1936) and Dittus and Boelter (1930) correlation. The Prandtl number range is 3.2 to 3.9 over the Reynolds number range.

As with the friction factor deviation data, a similar process was followed to calculate the Nusselt number deviation of the experimental data to that of Gnielinski. The maximum, relative mean, relative absolute and standard deviations are the same as defined in section 5.3 and were calculated in the same way.

The deviation of the experimental data to that predicted by Gnielinski was calculated using equation (98).

$$s_{dev}(\%) = \frac{Nu_{Gnielinski} - Nu_{experimental}}{Nu_{experimental}} \times 100 \qquad (98)$$

The maximum deviation is found to be 6.2% for the 8.3 mm tube when comparing the experimental results to those of Gnielinski. The maximum value of the standard deviation is found to be 2.1% which can be found in Table 13.

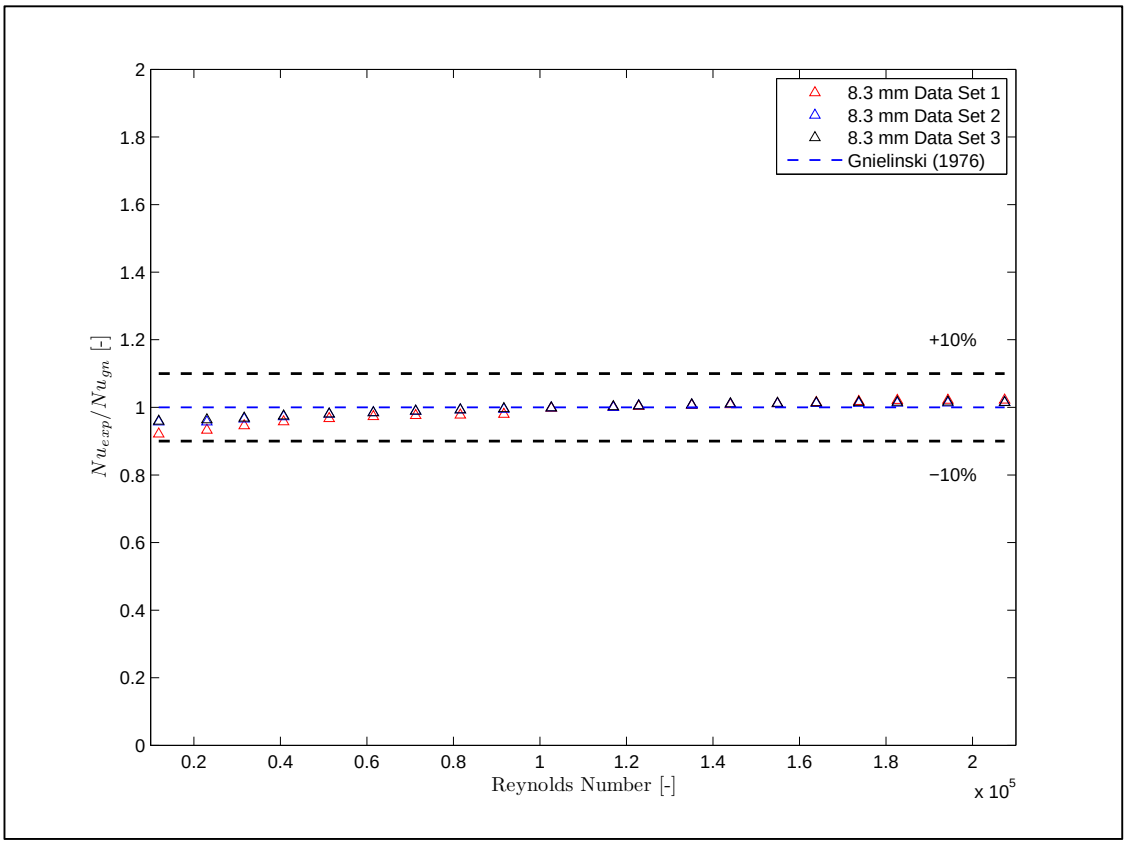

Figure 22: Experimental data compared to the theoretical results predicted by the Gnielinski correlation for the 8.3 mm tube over a Reynolds number range of 10 000 to 200 000

When using the corrected Gnielinski equation (20), there are two additional factors added. The first is the addition of by Hausen which takes into account the length of the tube and the second is the variation of the Prandtl number as a result of its dependence on temperature is taken into account in the form of the *K*-factor. The *K*-factor is a ratio of the Prandtl number at the average temperature and at temperature at the tube wall.

The value of the dimensional factor proposed by Hausen of $1 + \left(\frac{d}{L}\right)^{\frac{2}{3}}$ is equal to 1.017 which remains constant for all the experimental data. As a result of the value being so close to 1, the effect of the dimensional factor is expected to be minimal.

The *K*-factor is plotted against the Reynolds number for all three data sets of the 8.3 mm tube as seen in Figure 23. As can be seen from the results, the *K*-factor values lie between 0.986 and 0.996.

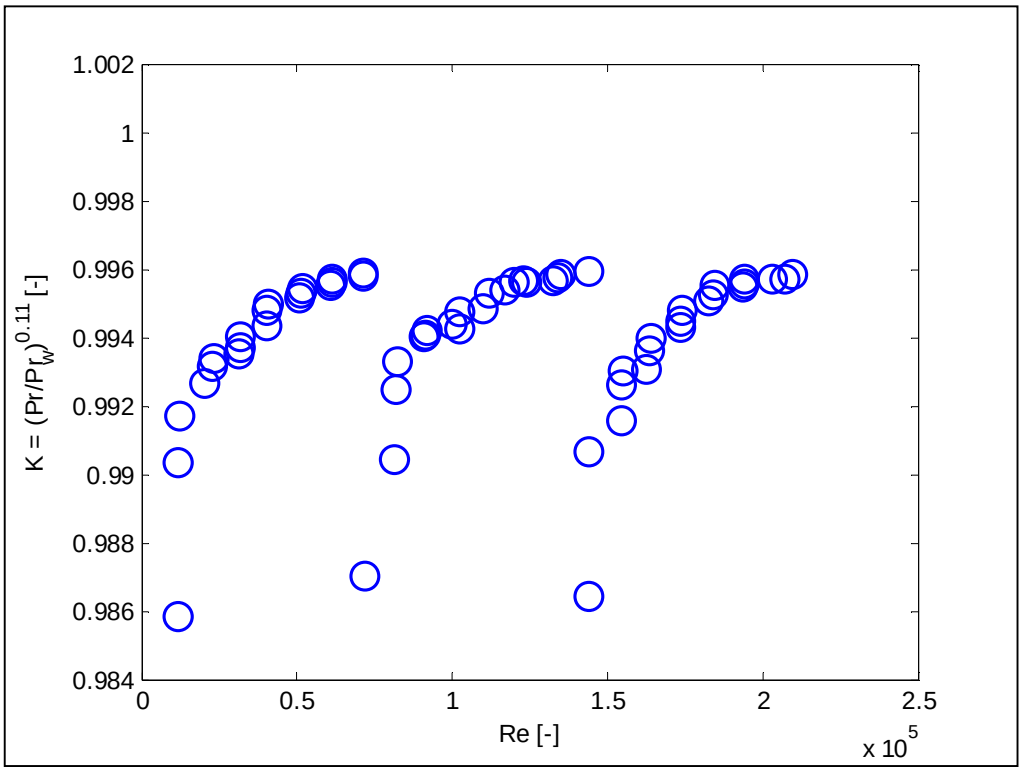

Figure 23: Ratio of Prandtl number at the average tube temperature and wall temperature versus Reynolds number for the 8.3 mm tube. Prandtl number ranges from 3.2 – 3.9 over the Reynolds number range.

The *K*-factor is calculated for both the minimum and maximum Reynolds numbers along the length of the tube as can be seen in Figure 24. It can be seen that the *K*-factor is still close to equal to one but that the variation in the fluid and wall temperature varies along the length of the tube. This is expected when considering the difference in the wall and fluid temperature as seen in Figure 16.

The *K*-Factor is applied to the Gnielinski results that are calculated using equation (19) as well as the dimensional correction from Hausen to see what the effect thereof would be on the results. The Gnielinski values calculated using equation (19) are plotted in Figure 25 along with those that have been corrected using equation (20). The values are plotted for both the minimum and maximum Reynolds numbers along the length of the tube wall. As can be seen in Figure 25, the difference between the two calculated Nusselt numbers is minimal. This can be attributed to the *K*-factor being close to equal to one as seen in Figure 23.

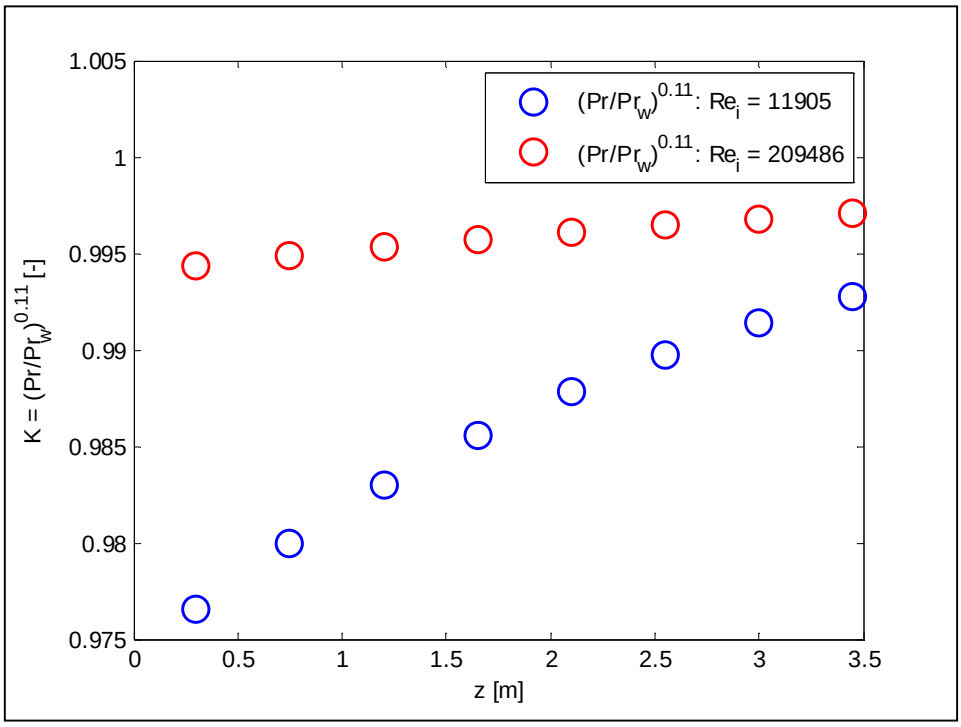

Figure 24: The K-factor which is representative of the Prandtl number at the average tube temperature and wall temperature at the mimimum and maximum Reynolds number over the length of the 8.3 mm tube. Prandtl number ranges from 3.2 – 3.9 over the Reynolds number range.

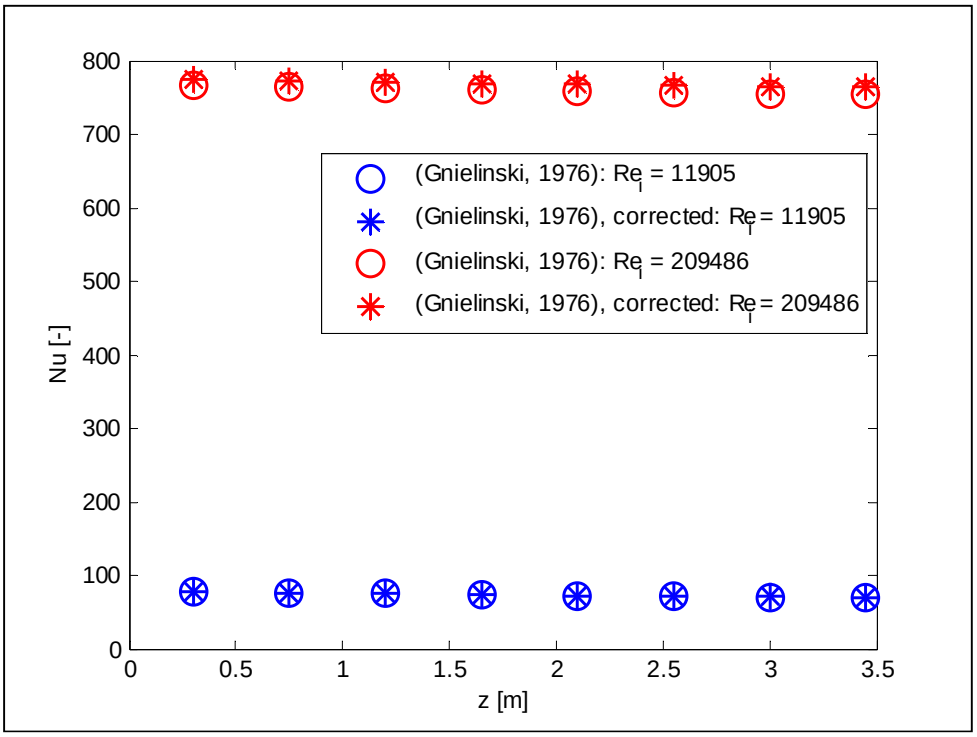

Figure 25: Nusselt Number calculated using the Gnielinski equation (19) and the corrected equation (20) at the minimum and maximum Reynolds numbers along the length of the tube wall. Prandtl number ranges from 3.2 – 3.9 over the Reynolds number range.

The results for the 14.2 mm tube are found in Figure 26. It is shown that the data also deviated from that of Gnielinski at lower Reynolds numbers as seen with the 8.3 mm tube results. All three data sets correlated very well with one another as seen in Figure 26. As the Reynolds number increased, the data converged to that of Gnielinski with the deviation being the least at the maximum Reynolds number of 220 000. The experimental results tended to be lower than Gnielinski and Sieder and Tate at the beginning of the test but improved as the Reynolds number increased. Once again the results of Dittus and Boelter under predicted the heat transfer coefficients throughout the Reynolds number range.

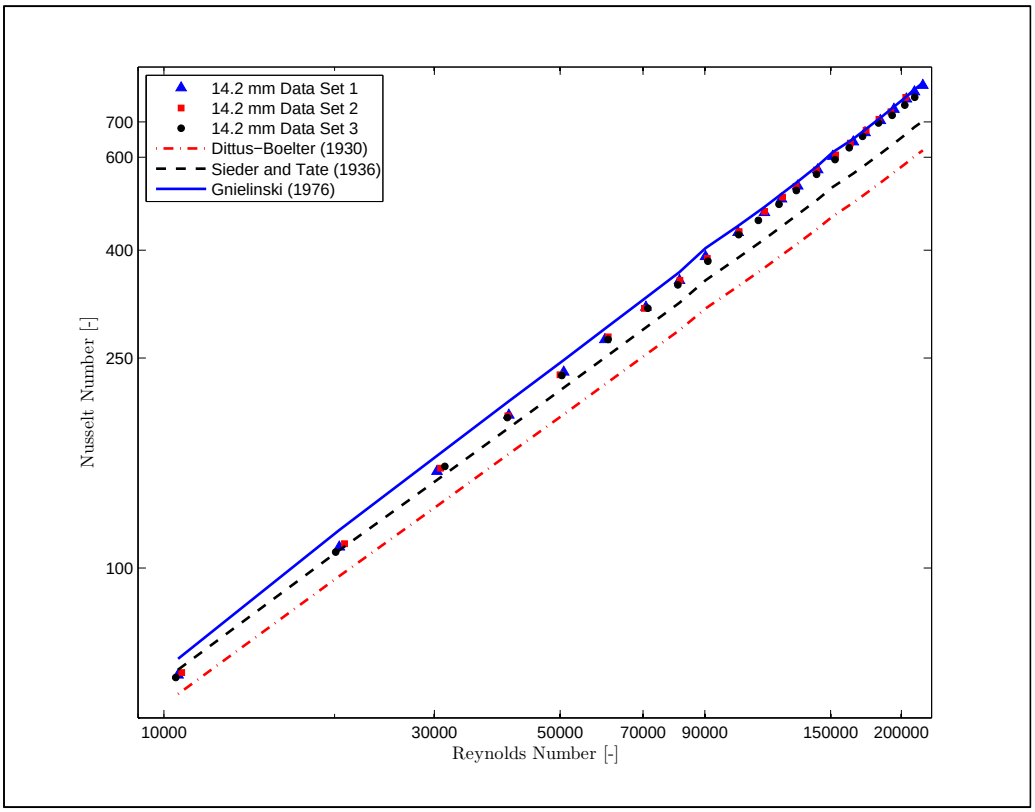

Figure 26: Nusselt number results calculated using the Wilson Plot method for the 14.2 mm tube compared to the correlations of Gnielinski (1976), Sieder and Tate (1936) and Dittus and Boelter (1930). The Prandtl number range is 3.3 to 4 over the Reynolds number range.

When comparing the data to that of Gnielinski in Figure 27, it is observed how the data deviated at lower Reynolds numbers once again, but correlated very well as the Reynolds number increases. Throughout the range, the experimental data was found to lie within the 20% limit that is applied to the Gnielinski correlation and therefore is considered to be a good estimate of the heat transfer coefficient in the turbulent flow regime. The maximum deviation for the 14.2 mm tube was found to be 8.3% at low Reynolds numbers when compared to Gnielinski. At high Reynolds numbers the minimum deviation was found to be 1%. The standard deviation was found to be 2.3%.

To summarise, it was therefore found that the maximum deviation for the 8.3 mm and 14.2 mm tube diameters lies below 10%. The relative mean deviation shows that the majority of the data for the two diameters lay below that of Gnielinski. The relative absolute deviation of both tube diameters was found to lie below 7% when compared to Gnielinski. This once

again fell within the 20% accuracy band of the Gnielinski correlation. The standard deviation of both tube diameters was found to lie below 3%.

Table 13: Nusselt number deviation data

Nusselt Number Deviation	Maximum Deviation [%]	Relative Mean Deviation [%]	Relative Absolute Deviation [%]	Standard Deviation [%]
8.3 mm Tube:				
Data set 1	6.2	1.9	1.9	2.1
Data set 2	4.5	0.6	1.6	2.0
Data set 3	4.3	0.5	1.6	1.9
14.2 mm Tube:				
Data set 1	7.7	3.2	3.2	2.3
Data set 2	6.8	3.0	3.0	2.0
Data set 3	8.3	5.0	5.0	1.7

When considering the Gnielinski equation, the friction factor that was used to calculate the Nusselt number is the Petukhov friction factor. This was observed when equations (6) and (19) were used to calculate the Nusselt number. The Petukhov friction factor was used in conjunction with the Gnielinski correlation to obtain the heat transfer coefficient which was used for comparison to the experimental results.

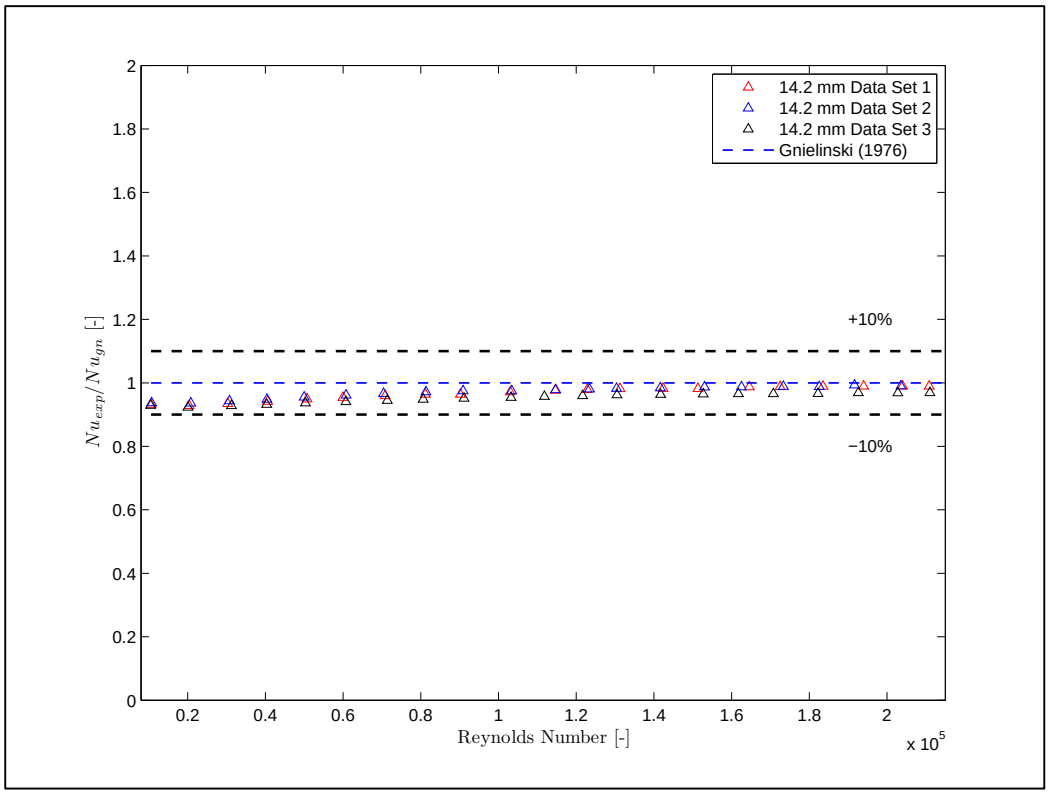

Figure 27: Experimental data compared to the theoretical results calculated using the Gnielinski (1976) correlation for the 14.2 mm tube test section

When comparing to the Blasius equation in Chapter 5.4, it is shown that there are minor variations in the experimental friction factor when comparing it to the existing theory on friction factors. Taking this into account, the experimental friction factor was used to predict the Nusselt number using the Gnielinski correlation to determine whether there is an effect of the friction factor on the heat transfer coefficients predicted by Gnielinski. This was performed for both tube diameters and compared to the original predictions by Gnielinski using the Petukhov friction factor using only one data set for each tube diameter.

Slight deviations occurred at lower Reynolds numbers but these deviations are minimal being less than 2%. The deviations that occur at the highest Reynolds numbers are less than 3%. Taking these values into consideration, it can be deduced that the difference between the use of the theoretical or the experimental friction factor is minimal. The deviation was less than 2% and therefore deemed acceptable when concluding that the difference between the theoretical and experimental friction factors in the use of the Gnielinski correlation is minimal.

5.5. *j*-Factor Results

As described in Chapter 2, the *j*-factor was developed by Colburn (1933) which was based on the Reynolds analogy. The Reynolds analogy combines the heat and momentum transfer in a fluid. The Reynolds analogy uses the Stanton number which represents the relationship between the shear force at the wall and the total heat transfer at the wall. Colburn introduced the *j*-factor as a correlation using the Stanton number and the Prandtl number to represent the heat transfer in a fluid for a range of Prandtl numbers. This is shown in equations (31) and (32).

A plot was generated of the friction factor and the *j*-factor as a function of the Reynolds number, as shown in Figure 28. From Figure 28, it can be concluded (take note that log scales are used) that both sets of coefficients decline in value at a similar gradient with increasing Reynolds number. The friction factor was divided by the *j*-factor to determine whether the relationship between the two coefficients could be predicted mathematically using the Reynolds analogy modified by Colburn.

The result of this is shown in Figure 29. Both of the data sets plotted for each of the tube diameters follow a similar trend when plotted against the Reynolds number. A curve fit was performed using a power function and an equation is developed which can predict the ratio of *f/j* as a function of Reynolds number.

Equation (99) presents a correlation coefficient (R^2 value) of 98% using a power function fit to the data.

$$\frac{f}{j} = 22.59Re^{-0.11} \tag{99}$$

By using equation (31) and (32) the Reynolds-Colburn analogy can be applied to equation (99). As a result, a new equation is proposed to simply predict the Nusselt number using the Reynolds number, Prandtl number and friction factor, all of which can be determined experimentally. This simplifies the calculation of the Nusselt number considerably.

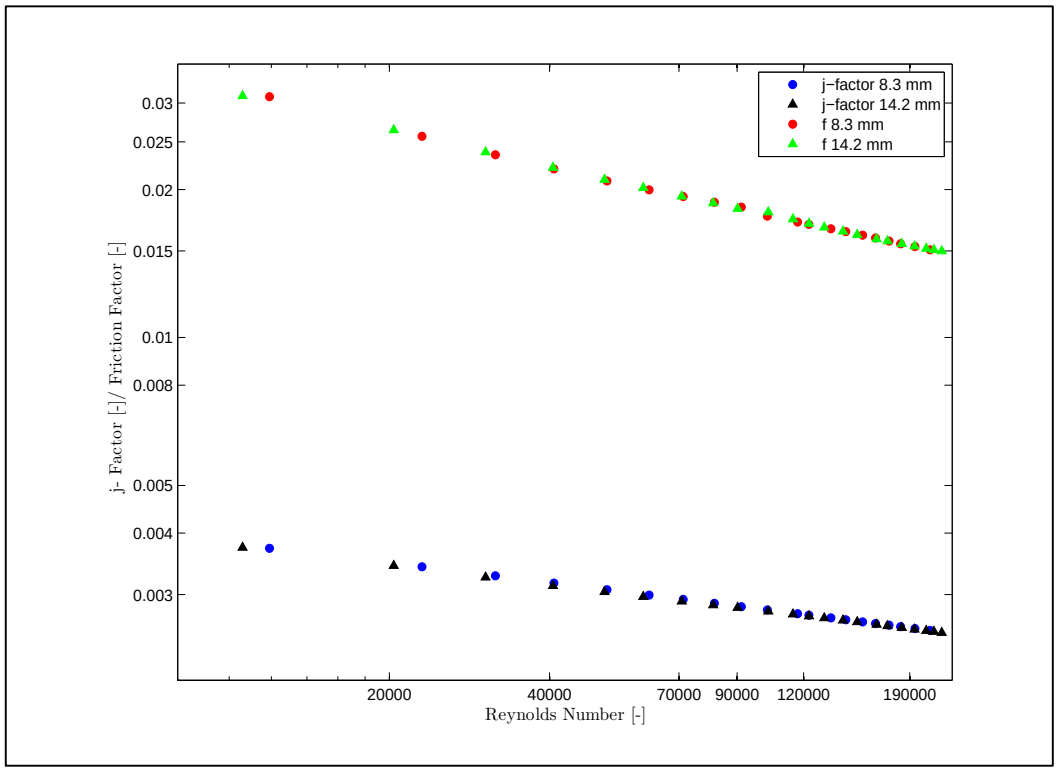

Figure 28: Plot of j-factor and friction factor as a function of Reynolds number for both test sections showing similar gradients over the Reynolds number range

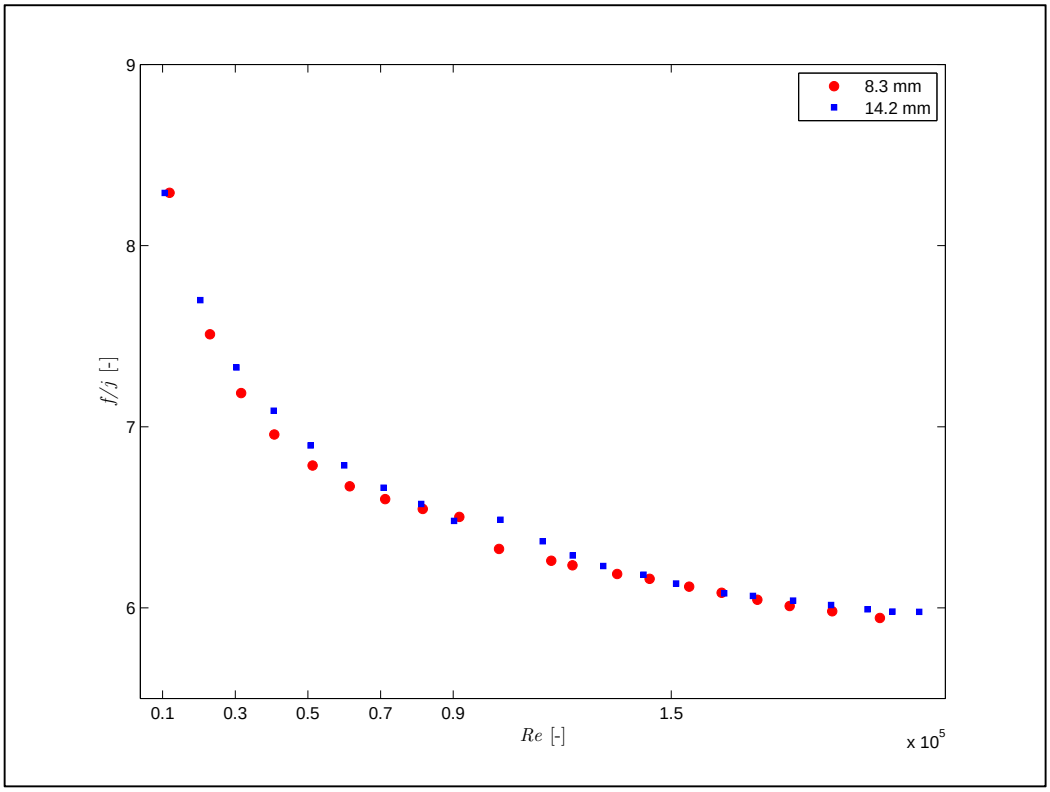

Figure 29: The calculated ratio between friction factor and j-factor as a function of Reynolds number for both test sections

The resulting correlation is described in equation (100).

$$Nu = 0.0443 f Re^{1.11} Pr^{\frac{1}{3}} \tag{100}$$

Since the friction factor in Equation (100) can be determined using the Blasius correlation as in Equation (5), it can be simplified to:

$$Nu = 0.014017 Re^{0.86} Pr^{\frac{1}{3}} \tag{101}$$

$$10\,000 \leq Re \leq 220\,000, \qquad 3.2 \leq Pr \leq 4$$

$$d = 8.3\ mm\ and\ 14.2\ mm$$

The proposed equation is valid for the tested Reynolds and Prandtl number ranges as the experimentally recorded data form the basis for the equation. As only two tube diameters have been tested, further testing should be performed to determine an accurate diameter range for the validity of the proposed equation. The newly developed Nusselt number equation is compared to the measurements and the Gnielinski equation in Figure 30 for the 8.3 mm tube and in Figure 31 for the 14.2 mm tube.

The work of Friend and Metzner (1958) demonstrates that on a large set of data, the exponent of the Prandtl number is not 1/3 but 0.42 in the turbulent flow regime. Equation (101) is amended to include the updated Prandtl number exponent as seen in equation (102).

$$Nu = 0.014017 Re^{0.86} Pr^{0.42} \tag{102}$$

Figure 30 shows data plotted using equation (101) and equation (102) compared to the measurements recorded during testing and those calculated using the Gnielinski equation. The data plotted using equation (101) follows the trend of the experimental data very well. The average error is 2.2% and the maximum error occuring at a Reynolds number of 12 000 was 5.7 %. When compared to the Gnielinski equation, equation (101) underpredicts the Nusselt number at the low Reynolds number range but converges very well at the high Reynolds number range. The plot of equation (102) shows the Nusselt number being higher than that of the experimental data, Gnielinski equation and equation (101) with an average deviation of 10% and a maximum deviation of 13% for the 8.3 mm tube.

Similarly this is plotted for the 14.2 mm tube as can be seen in Figure 31. The data plotted using equation (101) follows the trend of the experimental data and Gnielinski very well. The maximum error is 5.6% at a Reynolds number of 20 000 and the average error over the full range is 2.6%. Once again it can be seen the low Reynolds number range shows a larger deviation from the Gnielinski and experimental data than at higher Reynolds numbers. The results converge as the Reynolds number increases. As seen with the results of the 8.3 mm tube, the plotted equation (102) predicts a higher Nusselt number than the other plots on Figure 28 with an average deviation of 11% and a maximum deviation of 14%.

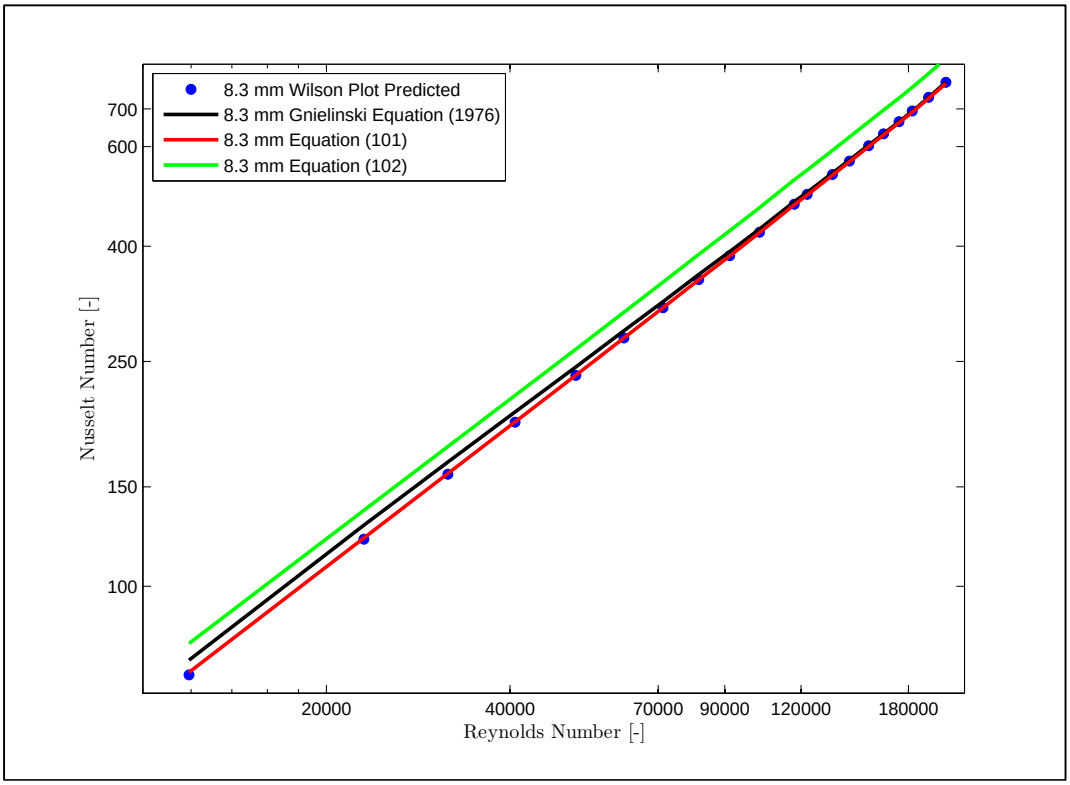

Figure 30: Results of the 8.3 mm Tube using the Wilson Plot method, Gnielinski equation and data calculated using equation (101) and (102) using a Prandtl number range of 3.2 to 4

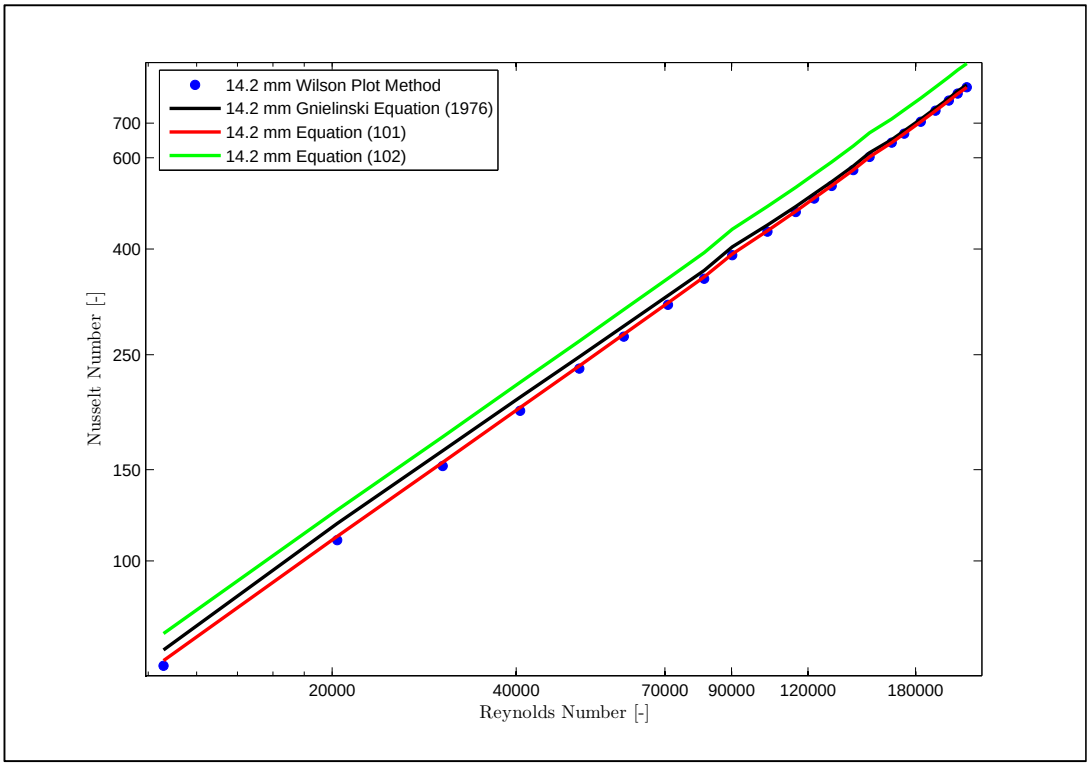

Figure 31: Results of the 14.2 mm Tube using the Wilson Plot method, Gnielinski equation and data calculated using equation (101) and (102) using a Prandtl number range of 3.2 to 4

In Figure 32, the results are shown in the form of ratio when compared to the Gnielinski results. The results all fall within the 10% range of deviation to Gnielinski. The results deviate at the lower Reynolds number range and show convergence to the Gnielinski results as the Reynolds number increases. This is seen for both the 8.3 and 14.2 mm tube diameters.

It can therefore be concluded that the newly developed equation produces results within an average of 2.5% of the Gnielinski equation.

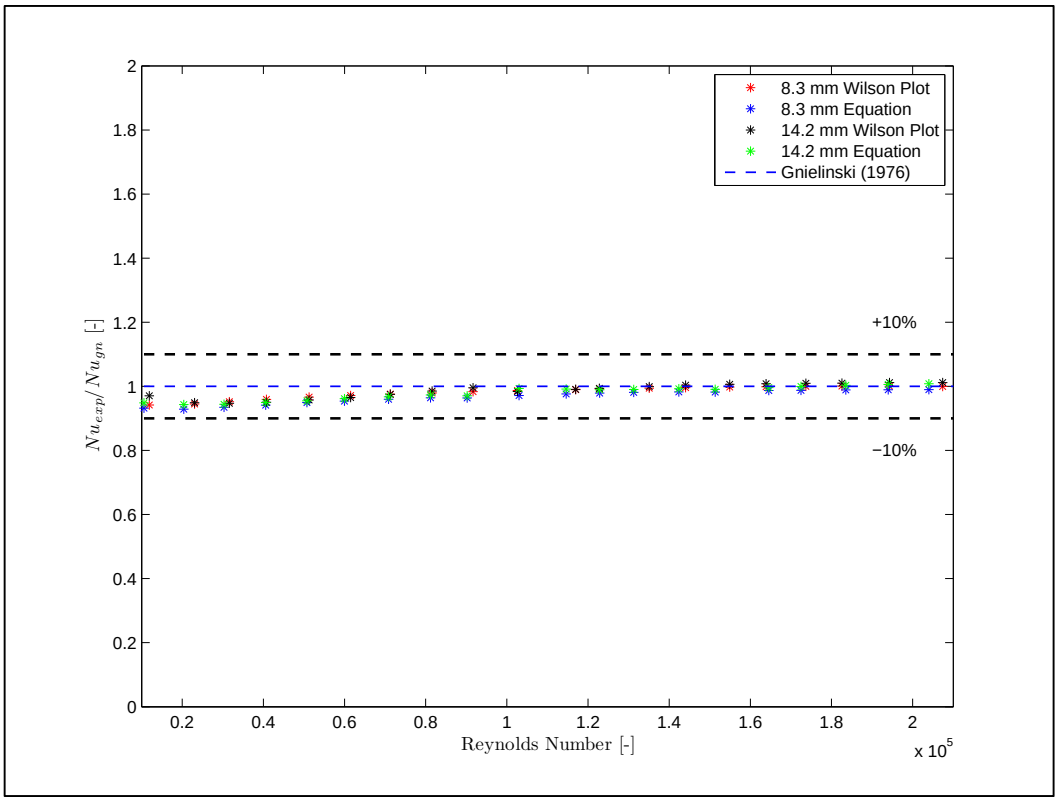

Figure 32: Results of equation (101) for both test sections compared to Gnielinski which displays all results fall within 10% to that of Gnielinski

With the experimental data that was obtained, the *j*-factor values and Nusselt numbers of each point were also compared to the *j*-factors calculated using equation (30) and the Nusselt numbers predicted using equation (101). For the calculations performed using equations (30) and (101), the Reynolds number, friction factors and Prandtl number values obtained using the experimental measurements were used. When the measured and calculated *j*-factor values were compared for the two tubes it was found that the *j*-factor errors and Nusselt number errors were the same, as they were expected to be.

Figure 33 shows the error between the Nusselt number calculated using equation (101) and those determined using the data recorded during experimental testing. The error is displayed in the form of a ratio where the average deviation is 0.04% for the 8.5 mm tube and 0.4% for the 14.2 mm tube.

It was found that the newly developed Nusselt number equation (101) could predict all 123 measuring points of both the 8.3 and 14.2 mm tube within 1%. As the uncertainties of the measured Nusselt numbers were 3%, the accuracy claim of equation (101) would be within 3% of measured data.

Although it has been shown that equation (101) is very accurate for the estimation of Nusselt numbers, the Prandtl number range of experiments was low and more experiments need to be conducted so that changes in fluid properties can be taken into consideration.

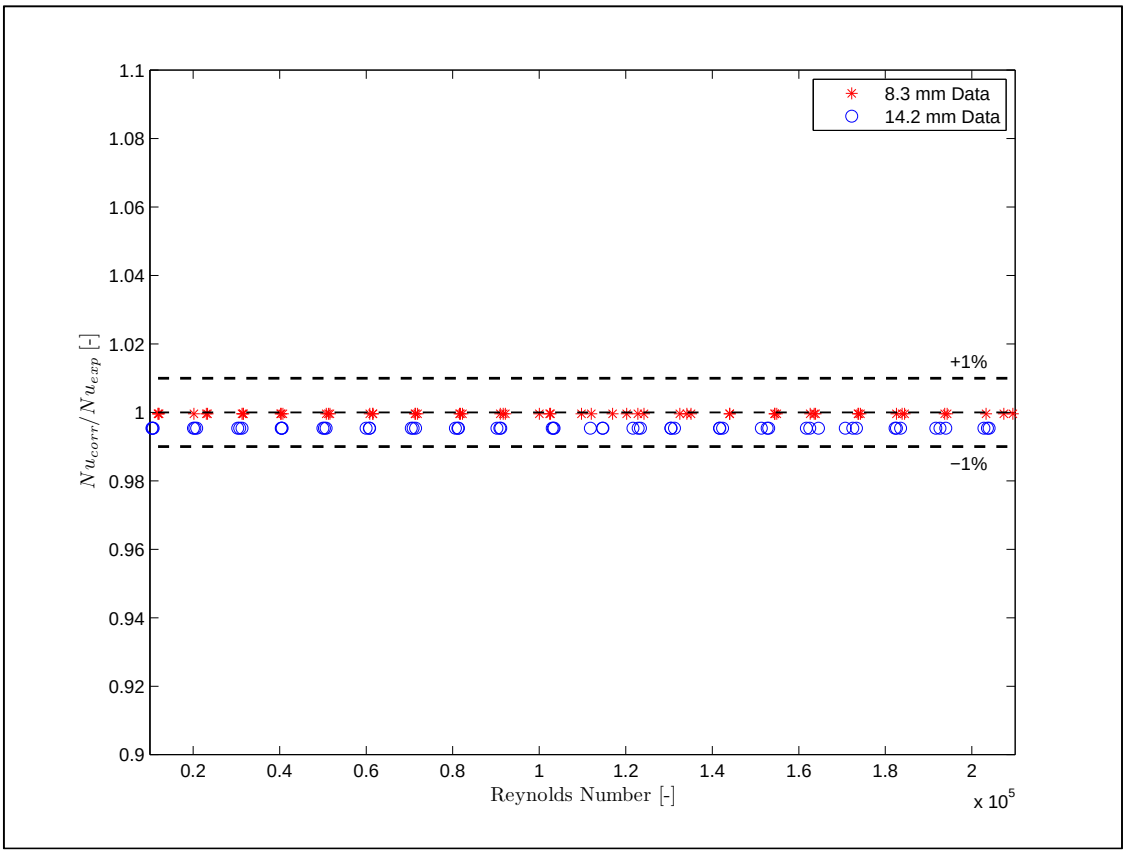

Figure 33: Comparison of Nusselt Number calculated using Equation (101) to the experimental Nusselt Numbers depicted as a ratio plotted against Reynolds Number.

5.6. Conclusion

The purpose of this chapter was to present the results of the experimental data that was recorded during testing. The testing method was followed as described in Chapter 3. For each tube diameter, a set of three data recordings were used for comparison to each other. Each data set consisted of set number of data points which were averaged. Using the methods described in Chapter 3.6, the data recorded was used to determine the energy balance, friction factor, Nusselt number, Reynolds number, uncertainty and the *j*-factor of each tube diameter.

The friction factor results displayed good agreement with well-known correlations. The heat transfer coefficient results all showed good agreement with the most utilised correlations for turbulent flow. The *j*-factor was used to determine a correlation to calculate the heat transfer coefficient using only dimensionless numbers calculated from the experimentally measured data. When compared to existing theory, the correlation predicts the heat transfer within a comparably close range.

When the newly developed equation was compared to the measurements of this study it was found that it can accurately predict all values within the uncertainty of the measurements. The newly developed equation also compared very well with the Gnielinski equation.

6. CONCLUSION

6.1 Summary

Existing heat transfer theory contains many correlations that have been developed and improved on over the last 100 years. Studies were developed by Dittus and Boelter (1930), Colburn (1933), Sieder and Tate (1936), Petukhov (1970) and Gnielinski (1976) which all contributed to the improved accuracy of heat transfer correlations. All of these studies have found to be varying in accuracy with no study quantifying uncertainty on any experimental data recorded. Further investigation showed that a number of the studies were based on the same set of data recorded up to 100 years ago. The purpose of this study was: to take accurate heat transfer measurements on a circular smooth tube and to quantify the uncertainties of the Nusselt numbers as a function of Reynolds number; to compare the measured data with existing correlations and to develop an accurate Nusselt number correlation from the data.

Two circular and smooth horizontal test sections were used to test a Reynolds number range of 10 000 to 220 000 using water as the testing medium. Each of the inner tubes of a tube-in-tube heat exchanger configuration was tested. During testing, the mass flow rate, pressure drop and temperatures were recorded over the length of the test section. Using these measurements the dimensionless numbers of Reynolds, Nusselt and the friction factor were determined. The Nusselt numbers were determined using the Wilson Plot method. The uncertainties of the measured and reduced variables were determined.

6.2 Conclusions

The uncertainty analysis was performed on all measured and reduced variables. The friction factor uncertainty was calculated using the method of Moffat (1988) and the results show a higher uncertainty measurement on the low range measurements of each diaphragm used to measure the pressure and reducing as approaching the full scale measurement. The heat transfer coefficient uncertainty was determined using the method proposed by Uhia *et al.* (2013) which produced an average relative uncertainty of less than 3% over the Reynolds number range. It was determined that the main contributors of the uncertainty in the heat transfer coefficient were the result of the Wilson Plot regression analysis and the inner tube water thermal conductivity and viscosity. The measured wall temperature was compared to the derived wall temperature using the Wilson Plot results and it was found that there was a considerable difference in the two values. The measured wall temperature displayed a deviation greater than the uncertainty on the Wilson Plot wall temperature. It was determined that the method and location of the wall temperature thermocouples attributed to a measurement error during experiments and therefore the measured wall temperatures were not used to calculate the heat transfer coefficient.

The results of the experimental testing displayed a good agreement to the well-known correlations used in turbulent heat transfer theory. The energy balance results displayed a low average value under 3% and showed that there was good system stability and low heat losses during testing. The results of the friction factor experiments displayed a low deviation when compared to the existing theory, below 3% and both the tube diameter results fall within the calculated uncertainty for the experimental data. The Nusselt number results displayed good agreement with the Gnielinski (1976) correlation, falling within 10% of the predicted results. The correlations of Dittus and Boelter (1930) and Sieder and Tate (1936) are not found to

compare well to the experimental data but both correlations do not take the friction factor into account which may contribute to the accuracy of the heat transfer coefficient calculation.

When plotting the *j*-factor it was found that a relationship existed between the friction factor and *j*-factor with both sets of data following a similar gradient when plotted against the Reynolds number. Using the relationship, a power equation was used to plot the ratio of friction factor and *j*-factor against the Reynolds number. As a result, an equation was developed where the Nusselt number can be calculated using the friction factor, Prandtl number and Reynolds number which are all determined experimentally. When comparing the correlation to the calculated data using the Gnielinksi (1976) correlation it was found that the data fell within 10% of Gnielinski (1976). However when compared to the measurements recorded, the newly developed equation could predict all the measurements within the experimental uncertainty which was 3%.

6.3 Recommendations

As a result of the testing and experimental data obtained, some future recommendations can be determined. One of the future recommendations would be to test a range of different tube diameters to determine whether there is an effect of the diameter on the method used to determine the correlation to predict the Nusselt number. Once the effect of different tube diameters has been determined and developed, it would be beneficial to have experimental data recorded for fluids with varying Prandtl numbers over a very large range so that fluid property variations can also be investigated. The uncertainty should also be calculated using a different proposed numerical method to verify the results found in this study.

7. REFERENCES

1. Abu-Eishah, S.I., 2001. Correlations for the Thermal Conductivity of Metals as a Function of Temperature. International Journal of Thermophysics, 22(6), p. 1855–1868.

2. Allen, R.W. and Eckert, E.R.G, 1964. Journal of Heat Transfer, Volume 86, No 2.

3. Blasius, P. R. H. 1913. Das Aehnlichkeitsgesetz bei Reibungsvorgangen in Flüssigkeiten. Forschungsheft 131, p. 1-41.

4. Briggs, D.E. and Young E.H., 1969. Modified Wilson Plot Techniques for Obtaining Heat Transfer Correlations for Shell and Tube Heat Exchangers. Chem. Eng. Prog. Symp. Ser., No 92, Vol. 65, p. 35-45.

5. Cengel, Y.A., 2006. Heat and Mass Transfer: A Practical Approach Third., McGraw-Hill.

6. Clapp, M.H. and Fitzsimmons, O.F., 1928. The Effect of Heat Transfer of Friction Factors in Fanning's Equation, Thesis, Massachusetts Institute of Technology.

7. Colebrook, C.F., 1939. Turbulent flow in Pipes, with Particular Reference to the Transition between the Smooth and Rough Pipe Laws, Journal of the Institute of Civil Engineers London, No 11, p. 133-156.

8. Colburn, A.P., 1933. A Method of Correlating Forced Convection Heat Transfer Data and a Comparison with Fluid Friction, American Institute of Chemical Engineers.

9. Dipprey, D.F. and Sabersky, R.H., 1963. International Journal of Heat Mass Transfer, Volume 6, No 5, p. 329-353.

10. Dittus, F. and Boelter, L.M.K., 1930. Heat Transfer in Automobile Radiators of the Tubular Type. University of California Publications in Engineering, 2(13), p. 443-461.

11. Filonenko, G.K. ,1954. Hydraulic Resistance in Pipes. Teploenergetika 1, No 4, p. 40-44.

12. Friend, W.L. and Metzner, A.B., 1958. Turbulent Heat Transfer inside Tubes and the analogy among Heat, Mass, and Momentum Transfer. AIChE Journal, 4(4), p. 393 - 402.

13. Gnielinski, V., 1976. New Equations for Heat and Mass Transfer in Turbulent Pipe and Channel Flow. International Chemical Engineering, 16(2), p. 359 - 368.

14. Gnielinski, V., 2013. On Heat Transfer in Tubes. International Journal of Heat Mass Transfer, 63 p.134-140.

15. Haaland, S.E., 1983. Simple and Explicit Formulas for the Friction Factor in Turbulent Pipe Flow. Journal of Fluids Engineering, Transactions of the ASME, 105(1), p.89-90.

16. Hamilton, R.M., 1963. Ph.D Thesis, Cornell University.

17. Hausen, H., 1959. Neue Gleichungen für die Wärmeübertragung bei freier und erzwungener Strömung. Allg. Wärmetechnik, 9, p. 75 - 79.

18. Hufschmidt, W., Burck, E. and Riebold, W., 1966. Determination of Local and Average Heat Trasnfer Coefficients in Tubes at High Heat Fluxes. International Journal of Heat Mass Transfer, Volume 9, No. 6, p.539 - 565.

19. Keevil, C.S., 1930. Heat Transfer and Friction for Heating and Cooling of Fluids in Pipes, Thesis, Massachusetts Institute of Technology.

20. Lawrence, A.E. and Sherwood, T.K., 1931. Industrial Engineering Chemistry, Volume 23, No. 3, p. 301 - 309.

21. Malina, J.A. and Sparrow, E.M., 1964. Chemical Engineering Science, No 19, p. 953-962.

22. McAdams, W.H. and Frost, T.H., 1922. Heat Transfer by Conduction and Convection II- Liquids Flowing through Pipes. Journal of Industrial and Engineering Chemistry, 14(12), p. 1101-1104.

23. Meyer, J.P. and Olivier, J.A., 2011. Heat Transfer in the Transitional Flow Regime. Evaporation, Condensation and Heat Transfer, p. 245-260.

24. Moffat, R.., 1988. Describing the uncertainties in experimental results. Experimental Thermal and Fluid Science, 1(1), p. 3 - 17.

25. Morris, F.H. and Whitman, W.G., 1928. Heat Transfer for Oils and Water in Pipes. Industrial and Engineering Chemistry, 20(3), p. 234-240.

26. Petukhov, B.S., 1970. Heat Transfer and Friction in Turbulent Pipe Flow with Variable Physical Properties. In J. P. Hartnett and J. Thomas F. Irvine, eds. Advances in Heat Transfer. Elsevier, p. 503 - 564.

27. Petukhov, B.S. and Roison, L.I., 1963. Teplofiz. Vysoc. Temperatur 1, No. 3.

28. Popiel, C.O. and Wojtkowiak, J., 1998. Simple Formulas for Thermophysical Properties of Liquid Water for Heat Transfer Calculations [from O°C to 150°C. Heat Transfer Engineering, 19(3), p. 87-101.

29. Prandtl, L., 1944. Fuhrer durch die Stromungslehre, Verlag Vieweg, Braunschweig, Germany.

30. Sherwood, T.K. and Petrie, J., 1932. Heat Transmission to Liquids Flowing in Pipes. Industrial and Engineering Chemistry, 24(7), p. 736-745.

31. Sieder, E.N. and Tate, G.E., 1936. Heat Transfer and Pressure Drop of Liquids in Tubes. Industrial and Engineering Chemistry, 28(12), p. 1429-1435.

32. Sterman, L.S. and Petukhov, V.V., 1965. Tplo i Massoperenos (Heat and Mass Transfer), Volume 1.

33. Uhia, F.J, Campo, A. and Fernandez-Seara, J., 2013. Uncertainty Analysis for Experimental Heat Transfer Data Obtained by the Wilson Plot Method. Thermal Science, Volume 17, No. 2, p. 471-487.

34. White, F.M., 2003. Fluid Mechanics Fifth., McGraw-Hill.

35. White, F.M., 2006. Viscous Fluid Flow Third., McGraw-Hill.

36. Yakovlev, V.V., 1961. Local and Mean Heat Transfer for a Turbulent Flow of Nonboiling Water in a Tube with High Heat Loads. Soviet Journal of Atomic Energy, Volume 8, No 3, p. 221-224.

A. APPENDIX A – UNCERTAINTY ANALYSIS

A1. Uncertainty Theory

According to the theory of Moffat (1988), the uncertainty of a measurement can be determined by using two types of errors that occur during experimental measurements. These are the bias and precision errors. Bias errors are known as fixed errors and arise from calibration errors, defects in measuring equipment, incorrect theory and the associated assumptions with theory. The precision error occurs as a random error and these can be as a result of changing conditions in the experimental environment or equipment being used. Therefore, the uncertainty in a measurement can be approximated as:

$$\partial v_j = \left\{ \left(B_j\right)^2 + \left(P_j\right)^2 \right\}^{\frac{1}{2}} \quad \text{A1.}$$

Each uncertainty on a measurement contributes towards a calculated uncertainty for a desired system characteristic such as a Nusselt number or friction factor. Therefore, the uncertainty in a certain system characteristic, for example *u*, can be determined by quantifying the standard deviation of a measurement and the contribution of the variables in a data reduction step.

The precision error P_j is defined by equation (A2) which is determined by the standard deviation and coverage factor for a defined number of samples per data point. During experiments, 100 samples were recorded per data point. The coverage factor CF is a function of the t-distribution of the data at a 95% confidence level.

$$P_j = CF \frac{S_i}{\sqrt{N}} \quad \text{A2.}$$

where

$$CF = f(t_{95\%,N-2}) \quad \text{A3.}$$

In equation (A4), the standard uncertainty *u*, is calculated by using the partial derivative of the result, *r*, with respect to the contributing variable, *v* and the uncertainty of the contributing variable, *u(v)*.

$$u(r) = \sqrt{\sum_{j=1}^{n} \left[\frac{\partial r}{\partial v_j} u\left(v_j\right) \right]^2} \quad \text{A4.}$$

Using equation (A2), the uncertainty of each variable is calculated and this is used in turn to calculate the next step of the data reduction process. As a result of this, the uncertainty of a certain variable propagates through the process and this information can be used to design future systems to reduce the uncertainty of certain systems.

To calculate the uncertainty of each of the recorded measurements, a standard deviation with a confidence level of 95% was used in the root sum squared method to calculate the

uncertainty of the measurement. A full description of this method can be found in Appendix A.

A2. System Uncertainty

Instruments

Each of the instruments that are used to measure experimental readings have a manufacturer specified accuracy. This is used as the bias value when determining the uncertainty of the instruments.

Table A1: Measurement Uncertainties

Instrument	Range	Uncertainty
Temperature (T)	-200 – 350 °C	0.01 °C
Inlets, outlets and bulk temperatures		0.05 °C
Annulus temperatures		0.1 °C
Pressure Drop (ΔP)		
Transducer 1	0 – 35 kPa	0.25% FS
Transducer 2	35 – 140 kPa	0.25% FS
Transducer 3	140 – 860 kPa	0.25% FS
Mass Flow Rate ($\dot{m}$)		
Inner tube low	0 – 0.667 kg/s	0.1%
Inner tube high	0.667 – 1.38 kg/s	0.1%

The thermocouple bias value is calculated from the calibration of the thermocouples using the Pt-100 which had an uncertainty of 0.01°C.

The pressure transducers each have one diaphragm which is used for testing both tube diameters. The bias values are calculated using the full scale values of each diaphragm. The bias values are obtained from the calibration values provided when the transducers were calibrated. Due to the high pressure values that are measured, the calibration is done using an external company as it cannot be done in the laboratory.

Fluid Properties

The uncertainties of the fluid properties are obtained from the formulations of Popiel and Wojtkowiak (1998), which can be found in Table A2.

Table A2: Thermal Property Uncertainties

Property	Uncertainty
Thermal Conductivity (k)	2%
Density (ρ)	0.003%
Viscosity (μ)	1%
Specific Heat Capacity (C_p)	0.06%

The thermal conductivity of the tube wall, k_w, is stated as 3.2% in the study of Abu-Eishah (2001).

Dimension Measurements

The uncertainties for the measurement of the dimensions of the tubes are stated below in Table A3. The uncertainty for the measurement of the dimensions of the length and diameter of the tubes used in the construction of the heat exchanger is used to calculate the heat transfer area uncertainty.

Table A3: Uncertainty of Dimension Measurements

Dimension	Uncertainty
Length of tube (L)	0.2%
Tube diameter (D)	1%

A3. Friction Factor Uncertainty

The friction factor is calculated using the measured pressure difference (ΔP) as follows:

$$f = \frac{\rho \pi^2 D_i^5 \Delta P}{8 L \dot{m}^2} \tag{A5.}$$

The uncertainty is therefore calculated using the equation (A6):

$$\partial f = \left[\left(\frac{\partial f}{\partial \Delta P} \delta \Delta P \right)^2 + \left(\frac{\partial f}{\partial \rho} \partial \rho \right)^2 + \left(\frac{\partial f}{\partial D_i} \partial D_i \right)^2 + \left(\frac{\partial f}{\partial L} \partial L \right)^2 + \left(\frac{\partial f}{\partial \dot{m}} \partial \dot{m} \right)^2 \right]^{\frac{1}{2}}$$

$$\partial f = \left[\left(\frac{\rho \pi^2 D_i^5}{8 L \dot{m}^2} \partial \Delta P \right)^2 + \left(\frac{\pi^2 D_i^5 \Delta P}{8 L \dot{m}^2} \partial \rho \right)^2 + \left(\frac{5 \rho \pi^2 D_i^4 \Delta P}{8 L \dot{m}^2} \partial D_i \right)^2 + \left(-\frac{\rho \pi^2 D_i^5 \Delta P}{8 L^2 \dot{m}^2} \partial L \right)^2 + \left(-\frac{\rho \pi^2 D_i^5 \Delta P}{4 L \dot{m}^2} \partial \dot{m} \right)^2 \right]^{\frac{1}{2}} \tag{A6.}$$

A4. Heat Transfer Measurement Uncertainties

Inlet and Outlet Temperatures

The inlet, outlet and annulus wall temperatures were all measured using four thermocouples placed at points situated 90° apart around the outer wall of the tube. To calculate the temperature at a specific point, the average of the four thermocouples is calculated as represented in equation (A7):

$$\bar{T}_{i,in} = \frac{T_{i,in1} + T_{i,in2} + T_{i,in3} + T_{i,in4}}{4} \quad \text{A7.}$$

The uncertainty is calculated using equation (A8):

$$\partial \bar{T}_{i,in} = \left(\left(\frac{\partial \bar{T}_{i,in1}}{4} \right)^2 + \left(\frac{\partial \bar{T}_{i,in2}}{4} \right)^2 + \left(\frac{\partial \bar{T}_{i,in3}}{4} \right)^2 + \left(\frac{\partial \bar{T}_{i,in4}}{4} \right)^2 \right)^{\frac{1}{2}} \quad \text{A8.}$$

The uncertainties for all the thermocouples are the same so therefore equation (A9) can be simplified to:

$$\partial \bar{T}_{i,in} = \sqrt{\frac{1}{4}} \partial T \quad \text{A9.}$$

The inlet and outlet temperatures are used to determine the heat transfer rate and Nusselt number.

Heat Transfer Coefficient Uncertainty

The uncertainty analysis of experimental data was established to determine what error is included during testing and how this affects the quality and accuracy of the data recorded. Experimental testing inherently contains errors that are attributed to the accuracy of the measuring instrumentation, the method of record data, and the variation in the experimental environment. Due to these and other factors, it is not possible to record the true value of the experimental data and therefore the uncertainty estimates how well the data has estimated the true value.

The Wilson Plot method is used to determine the Nusselt number from the experimental data. The motivation for using the Wilson Plot method is due to the difficulty in obtaining accurate temperature readings from the tube wall during testing. The Wilson Plot method uses only the inlet and outlet temperatures and mass flow rates for both the inner tube and annulus to calculate a heat transfer coefficient. The Wilson Plot method is traditionally used to calculate an inner tube wall temperature using regression analysis. Using this predicted wall temperature, the inner tube heat transfer coefficient can be calculated.

The standard uncertainty equation is shown in (A4) where u is the standard uncertainty and v_j represents the variable that causes the uncertainty in result r which is applied to a data reduction correlation. The method of data reduction requires that the uncertainty of each of the input variables is quantified and taken into account when calculating the uncertainty of the Nusselt number.

The uncertainty of each of the input variables is compounded during the data reduction process and this leads to a very complex method in determining the final uncertainty of the Nusselt number.

The theory that is used to determine the Nusselt number has been determined by Uhia *et al.* (2013). The theory is based on the Wilson Plot method which is "based on the separation the overall thermal resistance from appropriate experimental data by means of a linear regression analysis" (Uhia *et al.* 2013). The technique of thermal resistances is used to determine an overall heat transfer coefficient as described in Chapter 3.6.

$$\frac{1}{R_{ov}} = \frac{1}{h_i A_i} + R_w + \frac{1}{h_o A_o} \qquad \text{A10.}$$

The Wilson Plot method uses an unknown constant to fit the experimental data to the predicted model and this is shown in equations (A11) and (A12) where C_i and C_o are the correcting constants and h_i^* and h_o^* are the heat transfer coefficient variation models. A correction factor is used by Uhia to obtain a 95% confidence interval assuming a normal distribution in the experimental results used to determine the heat transfer coefficient.

$$h_i = C_i h_i^* \qquad \text{A11.}$$

$$h_o = C_o h_o^* \qquad \text{A12.}$$

Using the definition of the system in terms of thermal resistances in equation (A10) and equations (A11) and (A12), the calculation can be rearranged in a linear form of $y = ax + b$ as shown in equation (A13).

$$(R_{ov} - R_w) h_o^* A_o = \frac{1}{C_i} \frac{h_o^*}{h_i^*} \frac{A_o}{A_i} + \frac{1}{C_o} \qquad \text{A13.}$$

Where the *x* and *y* values are calculated as follows:

$$x = \frac{h_o^*}{h_i^*} \frac{A_o}{A_i} \qquad \text{A14.}$$

$$y = (R_{ov} - R_w) h_o^* \mathrm{A_o} \qquad \text{A15.}$$

Each of the terms has a degree of uncertainty due to the data reduction of each of the experimental values that are recorded. Each uncertainty value needs to be determined by applying equation (A4) to each of the terms in equations (A14) and (A15).

The uncertainty of the *x*-value is described in equation (A16).

$$U_x = \left[\left(\frac{\partial x}{\partial h_o^*} U_{h_o^*} \right)^2 + \left(\frac{\partial x}{\partial A_o} U_{A_o} \right)^2 + \left(\frac{\partial x}{\partial h_i^*} U_{h_i^*} \right)^2 + \left(\frac{\partial x}{\partial A_i} U_{A_i} \right)^2 \right]^{\frac{1}{2}} \qquad \text{A16.}$$

The various terms of the uncertainty equation are described in equations (A17-A20).

$$\frac{\partial x}{\partial h_o^*} = \frac{A_o}{h_i^* A_i} \tag{A17.}$$

$$\frac{\partial x}{\partial A_o} = \frac{h_o^*}{h_i^* A_i} \tag{A18.}$$

$$\frac{\partial x}{\partial h_i^*} = -\frac{h_o^* A_o}{h_i^{*2} A_i} \tag{A19.}$$

$$\frac{\partial x}{\partial A_i} = -\frac{h_o^* A_o}{h_i^* {A_i}^2} \tag{A20.}$$

Similarly the uncertainty for the y-value is calculated using equation (A21).

$$U_y = \left[\left(\frac{\partial y}{\partial R_{ov}} U_{R_{ov}}\right)^2 + \left(\frac{\partial y}{\partial R_w} U_{R_w}\right)^2 + \left(\frac{\partial y}{\partial h_o^*} U_{h_o^*}\right)^2 + \left(\frac{\partial y}{\partial A_o} U_{A_o}\right)^2\right]^{\frac{1}{2}} \tag{A21.}$$

The various terms of the uncertainty equation are described in equations (A22-A25).

$$\frac{\partial y}{\partial R_{ov}} = h_o^* A_o \tag{A22.}$$

$$\frac{\partial y}{\partial R_w} = -h_o^* A_o \tag{A23.}$$

$$\frac{\partial y}{\partial h_o^*} = (R_{ov} - R_w) A_o \tag{A24.}$$

$$\frac{\partial y}{\partial A_o} = (R_{ov} - R_w) h_o^* \tag{A25.}$$

The uncertainty of h_o^* is calculated using equation (A26).

$$U_{h_o^*} = \left[\left(\frac{\partial h_o^*}{\partial Re_o} U_{Re_o}\right)^2 + \left(\frac{\partial h_o^*}{\partial Pr_o} U_{Pr_o}\right)^2 + \left(\frac{\partial h_o^*}{\partial \mu_o} U_{\mu_o}\right)^2 + \left(\frac{\partial h_o^*}{\partial \mu_{wo}} U_{\mu_{wo}}\right)^2 + \left(\frac{\partial h_o^*}{\partial k_o} U_{k_o}\right)^2 + \left(\frac{\partial h_o^*}{\partial D_i} U_{D_i}\right)^2 + \left(\frac{\partial h_o^*}{\partial D_o} U_{D_o}\right)^2\right]^{\frac{1}{2}} \tag{A26.}$$

The definitions of the various terms of equation (A26) are defined in equations (A27-A33).

$$\frac{\partial h_o^*}{\partial Re_o} = n_o Re_o^{n-1} Pr_o^{\frac{1}{3}} \left(\frac{\mu_o}{\mu_w}\right)^{0.14} \frac{k_o}{D_i - D_o} \quad \text{A27.}$$

$$\frac{\partial h_o^*}{\partial Pr_o} = \frac{1}{3} Re_o^{n_o} Pr_o^{-\frac{2}{3}} \left(\frac{\mu_o}{\mu_w}\right)^{0.14} \frac{k_o}{D_i - D_o} \quad \text{A28.}$$

$$\frac{\partial h_o^*}{\partial \mu_o} = 0.14 Re_o^{n_o} Pr_o^{\frac{1}{3}} \left(\frac{\mu_o}{\mu_w}\right)^{-0.86} \frac{1}{\mu_w} \frac{k_o}{D_i - D_o} \quad \text{A29.}$$

$$\frac{\partial h_o^*}{\partial \mu_w} = -0.14 Re_o^{n_o} Pr_o^{\frac{1}{3}} \left(\frac{\mu_o}{\mu_w}\right)^{-0.86} \frac{1}{{\mu_w}^2} \frac{k_o}{D_i - D_o} \quad \text{A30.}$$

$$\frac{\partial h_o^*}{\partial k_o} = Re_o^{n_o} Pr_o^{\frac{1}{3}} \left(\frac{\mu_o}{\mu_w}\right)^{0.14} \frac{1}{D_i - D_o} \quad \text{A31.}$$

$$\frac{\partial h_o^*}{\partial D_i} = -Re_o^{n_o} Pr_o^{\frac{1}{3}} \left(\frac{\mu_o}{\mu_w}\right)^{0.14} \frac{k_o}{(D_i - D_o)^2} \quad \text{A32.}$$

$$\frac{\partial h_o^*}{\partial D_o} = Re_o^{n_o} Pr_o^{\frac{1}{3}} \left(\frac{\mu_o}{\mu_w}\right)^{0.14} \frac{k_o}{(D_i - D_o)^2} \quad \text{A33.}$$

The uncertainty of the outer tube area is described by equation (A34).

$$U_{A_o} = \left[\left(\frac{\partial A_o}{\partial D_o} U_{D_o}\right)^2 + \left(\frac{\partial A_o}{\partial L} U_L\right)^2\right]^{\frac{1}{2}} \quad \text{A34.}$$

$$\frac{\partial A_o}{\partial D_o} = \pi L \quad \text{A35.}$$

$$\frac{\partial A_o}{\partial L} = \pi D_o \quad \text{A36.}$$

The uncertainty of the inner tube heat transfer correction factor h_i^* is calculated using equation (A37).

$$U_{h_i^*} = \left[\left(\frac{\partial h_i^*}{\partial Re_i}U_{Re_i}\right)^2 + \left(\frac{\partial h_i^*}{\partial Pr_i}U_{Pr_i}\right)^2 + \left(\frac{\partial h_i^*}{\partial \mu_i}U_{\mu_i}\right)^2 + \left(\frac{\partial h_i^*}{\partial \mu_{wi}}U_{\mu_{wi}}\right)^2 + \left(\frac{\partial h_i^*}{\partial k_i}U_{k_i}\right)^2 + \left(\frac{\partial h_i^*}{\partial D_i}U_{D_i}\right)^2\right]^{\frac{1}{2}} \quad \text{A37.}$$

The definitions of the terms in equation (A37) are described in equations (A38-A43).

$$\frac{\partial h_i^*}{\partial Re_i} = n_i Re_i^{n_i-1} Pr_i^{\frac{1}{3}}\left(\frac{\mu_i}{\mu_w}\right)^{0.14}\frac{k_i}{D_i} \quad \text{A38.}$$

$$\frac{\partial h_i^*}{\partial Pr_i} = \frac{1}{3} Re_i^{n_i} Pr_i^{-\frac{2}{3}}\left(\frac{\mu_i}{\mu_w}\right)^{0.14}\frac{k_i}{D_i} \quad \text{A39.}$$

$$\frac{\partial h_i^*}{\partial \mu_i} = 0.14 Re_i^{n_i} Pr_i^{\frac{1}{3}}\left(\frac{\mu_i}{\mu_w}\right)^{-0.86}\frac{1}{\mu_w}\frac{k_i}{D_i} \quad \text{A40.}$$

$$\frac{\partial h_i^*}{\partial \mu_w} = -0.14 Re_i^{n_i} Pr_i^{\frac{1}{3}}\left(\frac{\mu_i}{\mu_w}\right)^{-0.86}\frac{1}{{\mu_w}^2}\frac{k_i}{D_i} \quad \text{A41.}$$

$$\frac{\partial h_i^*}{\partial k_i} = Re_i^{n_i} Pr_i^{\frac{1}{3}}\left(\frac{\mu_i}{\mu_w}\right)^{0.14}\frac{1}{D_i} \quad \text{A42.}$$

$$\frac{\partial h_i^*}{\partial D_i} = -Re_i^{n_i} Pr_i^{\frac{1}{3}}\left(\frac{\mu_i}{\mu_w}\right)^{0.14}\frac{k_i}{{D_i}^2} \quad \text{A43.}$$

The uncertainty of the inner tube area is defined by equation (A44).

$$U_{A_i} = \left[\left(\frac{\partial A_i}{\partial D_i}U_{D_i}\right)^2 + \left(\frac{\partial A_i}{\partial L}U_L\right)^2\right]^{\frac{1}{2}} \quad \text{A44.}$$

$$\frac{\partial A_i}{\partial D_i} = \pi L \quad \text{A45.}$$

$$\frac{\partial A_i}{\partial L} = \pi D_i \quad \text{A46.}$$

The uncertainty of the total heat transfer resistance is calculated using equation (A47).

$$U_{R_{ov}} = \left[\left(\frac{\partial R_{ov}}{\partial \dot{Q}} U_{\dot{Q}}\right)^2 + \left(\frac{\partial R_{ov}}{\partial \Delta T_{lm}} U_{\Delta T_{lm}}\right)^2\right]^{\frac{1}{2}} \quad \text{A47.}$$

$$\frac{\partial R_{ov}}{\partial Q} = \frac{1}{\Delta T_{lm}} \quad \text{A48.}$$

$$\frac{\partial R_{ov}}{\partial \Delta T_{lm}} = -\frac{\dot{Q}}{(\Delta T_{lm})^2} \quad \text{A49.}$$

The uncertainty of the tube wall resistance is calculated using equation (A50). The various terms of equation (A48) are described using equations (A51-A54).

$$U_{R_w} = \left[\left(\frac{\partial R_w}{\partial D_o} U_{D_o}\right)^2 + \left(\frac{\partial R_w}{\partial D_i} U_{D_i}\right)^2 + \left(\frac{\partial R_w}{\partial L} U_L\right)^2 + \left(\frac{\partial R_w}{\partial k_w} U_{k_w}\right)^2\right]^{\frac{1}{2}} \quad \text{A50.}$$

$$\frac{\partial R_w}{\partial D_o} = \frac{\frac{D_i}{D_o} \cdot \frac{1}{D_i}}{2\pi L k_w} = \frac{1}{D_o 2\pi L k_w} \quad \text{A51.}$$

$$\frac{\partial R_w}{\partial D_i} = \frac{-\frac{D_i}{D_o} \cdot \frac{1}{D_i^2}}{2\pi L k_w} = -\frac{1}{D_o D_i 2\pi L k_w} \quad \text{A52.}$$

$$\frac{\partial R_w}{\partial L} = \frac{-\ln\left(\frac{D_o}{D_i}\right)}{2\pi L^2 k_w} \quad \text{A53.}$$

$$\frac{\partial R_w}{\partial k_w} = \frac{-\ln\left(\frac{D_o}{D_i}\right)}{2\pi L k_w^2} \quad \text{A54.}$$

The uncertainty of the inner Reynolds number is calculated as described in equation (A56) which is based on the definition of the Reynolds number in equation (A55).

$$Re_i = \frac{4\dot{m}_i}{\pi D_i \mu_i} \quad \text{A55.}$$

$$U_{Re_i} = \left[\left(\frac{\partial Re_i}{\partial \dot{m}_i} U_{\dot{m}_i}\right)^2 + \left(\frac{\partial Re_i}{\partial D_i} U_{D_i}\right)^2 + \left(\frac{\partial Re_i}{\partial \mu_i} U_{\mu_i}\right)^2\right]^{\frac{1}{2}} \quad \text{A56.}$$

The various differential terms of equation (A56) are described in equations (A57-A59).

$$\frac{\partial Re_i}{\partial \dot{m}_i} = \frac{4}{\pi D_i \mu_i} \quad \text{A57.}$$

$$\frac{\partial Re_i}{\partial D_i} = -\frac{4\dot{m}_i}{\pi {D_i}^2 \mu_i} \quad \text{A58.}$$

$$\frac{\partial Re_i}{\partial \mu_i} = -\frac{4\dot{m}_i}{\pi D_i {\mu_i}^2} \quad \text{A59.}$$

Similarly, the uncertainty of the outer tube Reynolds number is calculated using equation (A61) which is based on the annular Reynolds number in equation (A60).

$$Re_o = \frac{4\dot{m}_o}{\pi(D_a + D_o)\mu_o} \quad \text{A60.}$$

$$U_{Re_o} = \left[\left(\frac{\partial Re_o}{\partial \dot{m}_o} U_{\dot{m}_o}\right)^2 + \left(\frac{\partial Re_o}{\partial D_a} U_{D_a}\right)^2 + \left(\frac{\partial Re_o}{\partial D_o} U_{D_o}\right)^2 + \left(\frac{\partial Re_o}{\partial \mu_o} U_{\mu_o}\right)^2\right]^{\frac{1}{2}} \quad \text{A61.}$$

The differential terms of equation (A61) are described using equations (A62-A65).

$$\frac{\partial Re_o}{\partial \dot{m}_o} = \frac{4}{\pi(D_a + D_o)\mu_o} \quad \text{A62.}$$

$$\frac{\partial Re_o}{\partial D_a} = -\frac{4\dot{m}_o}{\pi(D_a + D_o)^2 \mu_o} \quad \text{A63.}$$

$$\frac{\partial Re_o}{\partial D_o} = -\frac{4\dot{m}_o}{\pi(D_a + D_o)^2 \mu_o} \quad \text{A64.}$$

$$\frac{\partial Re_o}{\partial \mu_o} = -\frac{4\dot{m}_o}{\pi(D_a + D_o)^2 {\mu_o}^2} \quad \text{A65.}$$

The Prandtl number uncertainty of the inner tube is calculated using equation (A66).

$$U_{Pr_i} = \left[\left(\frac{\partial Pr_i}{\partial Cp_i} U_{Cp_i}\right)^2 + \left(\frac{\partial Pr_i}{\partial k_i} U_{k_i}\right)^2 + \left(\frac{\partial Pr_i}{\partial \mu_i} U_{\mu_i}\right)^2\right]^{\frac{1}{2}} \quad \text{A66.}$$

The differential terms of equation (A66) are described using equations (A67-A69).

$$\frac{\partial Pr_i}{\partial Cp_i} = \frac{\mu_i}{k_i} \quad \text{A67.}$$

$$\frac{\partial Pr_i}{\partial k_i} = \frac{-\mu_i Cp_i}{{k_i}^2} \quad \text{A68.}$$

$$\frac{\partial Pr_i}{\partial \mu_i} = \frac{Cp_i}{k_i} \quad \text{A69.}$$

Similarly the outer tube Prandtl number is described using equations (A70-73).

$$U_{Pr_o} = \left[\left(\frac{\partial Pr_o}{\partial Cp_o} U_{Cp_o}\right)^2 + \left(\frac{\partial Pr_o}{\partial k_o} U_{k_o}\right)^2 + \left(\frac{\partial Pr_o}{\partial \mu_o} U_{\mu_o}\right)^2\right]^{\frac{1}{2}} \quad \text{A70.}$$

$$\frac{\partial Pr_o}{\partial Cp_o} = \frac{\mu_o}{k_o} \quad \text{A71.}$$

$$\frac{\partial Pr_o}{\partial k_o} = \frac{-\mu_o Cp_o}{{k_o}^2} \quad \text{A72.}$$

$$\frac{\partial Pr_o}{\partial \mu_o} = \frac{Cp_o}{k_o} \quad \text{A73.}$$

The uncertainty of the average heat transfer rate is calculated using equation (A74).

$$\begin{aligned} U_{\dot{Q}} = \Bigg[&\left(\frac{\partial \dot{Q}}{\partial \dot{m}_i} U_{\dot{m}_i}\right)^2 + \left(\frac{\partial \dot{Q}}{\partial Cp_i} U_{Cp_i}\right)^2 + \left(\frac{\partial Q}{\partial T_{i.in}} U_{T_{i.in}}\right)^2 + \left(\frac{\partial Q}{\partial T_{i,out}} U_{T_{i.out}}\right)^2 \\ &+ \left(\frac{\partial \dot{Q}}{\partial \dot{m}_o} U_{\dot{m}_o}\right)^2 + \left(\frac{\partial \dot{Q}}{\partial C_{po}} U_{C_{po}}\right)^2 + \left(\frac{\partial Q}{\partial T_{o.in}} U_{T_{o.in}}\right)^2 \\ &+ \left(\frac{\partial Q}{\partial T_{o,out}} U_{T_{o.out}}\right)^2\Bigg]^{\frac{1}{2}} \end{aligned} \quad \text{A74.}$$

where

$$\dot{Q} = \frac{1}{2}\left(\dot{Q}_o + \dot{Q}_i\right) \quad \text{A75.}$$

The differential terms of equation (A74) are described in equations (A76-A83).

$$\frac{\partial \dot{Q}}{\partial \dot{m}_i} = \frac{1}{2} C_{pi}\left(T_{i.in} - T_{i,out}\right) \quad \text{A76.}$$

$$\frac{\partial \dot{Q}}{\partial C_{pi}} = \frac{1}{2}\dot{m}_i\left(T_{i.in} - T_{i,out}\right) \quad \text{A77.}$$

$$\frac{\partial \dot{Q}}{\partial T_{i.in}} = \frac{1}{2}\dot{m}_i C_{pi} \quad \text{A78.}$$

$$\frac{\partial \dot{Q}}{\partial T_{i,out}} = -\frac{1}{2}\dot{m}_i C_{pi} \quad \text{A79.}$$

$$\frac{\partial \dot{Q}}{\partial \dot{m}_o} = \frac{1}{2}C_{po}\left(T_{o.in} - T_{o,out}\right) \quad \text{A80.}$$

$$\frac{\partial \dot{Q}}{\partial Cp_o} = \frac{1}{2}\dot{m}_o\left(T_{o.in} - T_{o,out}\right) \quad \text{A81.}$$

$$\frac{\partial \dot{Q}}{\partial T_{o.in}} = \frac{1}{2}\dot{m}_o C_{po} \quad \text{A82.}$$

$$\frac{\partial \dot{Q}}{\partial T_{o,out}} = -\frac{1}{2}\dot{m}_o C_{po} \quad \text{A83.}$$

To calculate the uncertainty of the log mean temperature difference, equation (A84) is used. The calculation is simplified using equations (A85) and (A86) to define the temperature differences.

$$U_{\Delta T_{lm}} = \left[\left(\frac{\partial \Delta T_{lm}}{\partial T_{i.in}}U_{T_{i.in}}\right)^2 + \left(\frac{\partial \Delta T_{lm}}{\partial T_{i.out}}U_{T_{i.out}}\right)^2 + \left(\frac{\partial \Delta T_{lm}}{\partial T_{o.in}}U_{T_{o.in}}\right)^2 + \left(\frac{\partial \Delta T_{lm}}{\partial T_{o.out}}U_{T_{o.out}}\right)^2\right]^{\frac{1}{2}} \quad \text{A84.}$$

$$\Delta T_1 = T_{i.in} - T_{o.out} \quad \text{A85.}$$

$$\Delta T_2 = T_{i.out} - T_{o.in} \quad \text{A86.}$$

The differential terms in equation (A84) are described by equations (A87-A90).

$$\frac{\partial \Delta T_{lm}}{\partial T_{i.in}} = \frac{\ln\left(\frac{\Delta T_1}{\Delta T_2}\right) - \left(\frac{\Delta T_1}{\Delta T_2}\right)(\Delta T_1 - \Delta T_2)}{\left(\ln\left(\frac{\Delta T_1}{\Delta T_2}\right)\right)^2} \quad \text{A87.}$$

$$\frac{\partial \Delta T_{lm}}{\partial T_{o.out}} = \frac{-\ln\left(\frac{\Delta T_1}{\Delta T_2}\right) - \left(\frac{\Delta T_2}{\Delta T_1}\right)(\Delta T_1 - \Delta T_2)}{\left(\ln\left(\frac{\Delta T_1}{\Delta T_2}\right)\right)^2} \quad \text{A88.}$$

$$\frac{\partial \Delta T_{lm}}{\partial T_{i.out}} = \frac{-\ln\left(\frac{\Delta T_1}{\Delta T_2}\right) - \left(\frac{\Delta T_2}{\Delta T_1}\right)(\Delta T_1 - \Delta T_2)}{\left(\ln\left(\frac{\Delta T_1}{\Delta T_2}\right)\right)^2} \quad \text{A89.}$$

$$\frac{\partial \Delta T_{lm}}{\partial T_{o.in}} = \frac{\ln\left(\frac{\Delta T_1}{\Delta T_2}\right) - \left(\frac{\Delta T_1}{\Delta T_2}\right)(\Delta T_1 - \Delta T_2)}{\left(\ln\left(\frac{\Delta T_1}{\Delta T_2}\right)\right)^2} \quad \text{A90.}$$

Using all the equations described in this chapter, the uncertainty of the inner heat transfer coefficient can be calculated.

The *x* and *y* values are plotted and the weighed linear least squares regression analysis is used to determine the coefficients of the Wilson Plot. There exists an uncertainty in both the *x* and *y* measurement values. To account for this combined uncertainty, equation (A91) is used. The value of u_j takes into account the combined measured uncertainty in both $u(y)$ and $u(x)$ using the weighted least squares method.

$$u_j = \sqrt{\{[u(y)]^2 + [au(x)]^2\}_j} \quad \text{A91.}$$

This is complicated however by the fact that *a* is featured in the equation of uncertainty (A91) and the uncertainty is featured in the equation of *a* (A92). As a result, the values of u_j and *a* have to be solved for iteratively using equations (A91) and (A92).

The *x* and *y* values are arranged to form a straight line graph as shown in equation (A13). The gradient of the straight line equation is defined as *a*, which is calculated using equation (A92).

$$a = \frac{\sum_{j=1}^{n} \frac{1}{u_j^2} \sum_{j=1}^{n} \frac{x_j y_j}{u_j^2} - \sum_{j=1}^{n} \frac{x_j}{u_j^2} \sum_{j=1}^{n} \frac{y_j}{u_j^2}}{\sum_{j=1}^{n} \frac{1}{u_j^2} \sum_{j=1}^{n} \frac{x_j^2}{u_j^2} - \left(\sum_{j=1}^{n} \frac{x_j}{u_j^2}\right)^2} \quad \text{A92.}$$

The intercept of the straight line equation is defined as *b* which is calculated using equation (A93).

$$b = \frac{\sum_{j=1}^{n} \frac{x_j^2}{u_j^2} \sum_{j=1}^{n} \frac{x_j}{u_j^2} - \sum_{j=1}^{n} \frac{x_j}{u_j^2} \sum_{j=1}^{n} \frac{x_j y_j}{u_j^2}}{\sum_{j=1}^{n} \frac{1}{u_j^2} \sum_{j=1}^{n} \frac{x_j^2}{u_j^2} - \left(\sum_{j=1}^{n} \frac{x_j}{u_j^2}\right)^2} \quad \text{A93.}$$

The uncertainty of *a* and *b* can be calculated using equations (A94) and (A95).

$$u(a) = \sqrt{\frac{\sum_{j=1}^{n} \frac{1}{u_j^2}}{\sum_{j=1}^{n} \frac{1}{u_j^2} \sum_{j=1}^{n} \frac{x_j^2}{u_j^2} - \left(\sum_{j=1}^{n} \frac{x_j}{u_j^2}\right)^2}} \quad \text{A94.}$$

$$u(b) = \sqrt{\frac{\sum_{j=1}^{n} \frac{x_j^2}{u_j^2}}{\sum_{j=1}^{n} \frac{1}{u_j^2} \sum_{j=1}^{n} \frac{x_j^2}{u_j^2} - \left(\sum_{j=1}^{n} \frac{x_j}{u_j^2}\right)^2}} \quad \text{A95.}$$

The coefficients of the Wilson Plot can be calculated once the parameters *a* and *b* are calculated. This is exhibited by equation (A96) and (A97).

$$C_i = \frac{1}{a} \quad \text{A96.}$$

$$C_o = \frac{1}{b} \quad \text{A97.}$$

The uncertainties of the Wilson Plot coefficients are calculated using equations (A98) and (A99) and are a function of the uncertainties calculated for the parameters *a* and *b*.

$$u(C_i) = \frac{\partial C_i}{\partial a} u(a) = \frac{1}{a^2} u(a) \quad \text{A98.}$$

$$u(C_o) = \frac{\partial C_o}{\partial b} u(b) = \frac{1}{b^2} u(ab) \quad \text{A99.}$$

Once the uncertainty values are calculated for the inner and outer tube Wilson Plot coefficients, the uncertainty of the inner and outer tube heat transfer coefficients can be calculated using equations (A100) and (A101).

$$U(h_i) = CFu(h_i) = \sqrt{\left[\frac{\partial h_i}{\partial h_i^*} u(h_i)\right]^2 \left[\frac{\partial h_i}{\partial C_i} u(C_i)\right]^2} \quad \text{A100.}$$

$$U(h_o) = CFu(h_o) = \sqrt{\left[\frac{\partial h_o}{\partial h_o^*}u(h_o)\right]^2 \left[\frac{\partial h_o}{\partial C_o}u(C_o)\right]^2} \quad \text{A101.}$$

The value of CF = 2 is incorporated as a coverage factor which is used for a 95% confidence level assuming a normal distribution and infinite number of data points. The t-distribution approaches a normal distribution with a number of data points larger than 30. Due to the large number of data points recorded during testing, it is assumed that a coverage factor of 2 is acceptable to use in this case.

A5. Uncertainty of the Wall Temperature using the Wilson Plot Results

The wall temperature is calculated using the Wilson Plot as described in section 3.6.4. The uncertainty of the wall temperature can be calculated by applying the general uncertainty equation (A4). This is defined in equation (A102).

$$U_{T_w} = \left[\left(\frac{\partial T_w}{\partial T_i(0)}U_{T_i(0)}\right)^2 + \left(\frac{\partial T_w}{\partial \Delta T_b(0)}U_{\Delta T_b(0)}\right)^2 + \left(\frac{\partial T_w}{\partial C^*}U_{C^*}\right)^2 + \left(\frac{\partial T_w}{\partial \dot{m}_i}U_{\dot{m}_i}\right)^2 + \left(\frac{\partial T_w}{\partial C_{pi}}U_{C_{pi}}\right)^2 + \left(\frac{\partial T_w}{\partial U_{ov}}U_{U_{ov}}\right)^2 + \left(\frac{\partial T_w}{\partial h_i}U_{h_i}\right)^2 + \left(\frac{\partial T_w}{\partial p_i}U_{p_i}\right)^2 + \left(\frac{\partial T_w}{\partial z}U_z\right)^2\right]^{\frac{1}{2}} \quad \text{A102.}$$

The uncertainty of the wall temperature with regards to the inner tube bulk temperature is described in equations (A103) and (A104).

$$\frac{\partial T_w}{\partial T_i(0)} = 1 \quad \text{A103.}$$

$$U_{T_i(0)} = U_{T_o}(0) = U_T \quad \text{A104.}$$

The uncertainty of the bulk temperature difference is described in equations (A105) to (A109).

$$U_{\Delta T_b(0)} = \left[\left(\frac{\partial T_b(0)}{\partial T_i(0)}U_{T_i(0)}\right)^2 + \left(\frac{\partial T_b(0)}{\partial T_o(0)}U_{T_o(0)}\right)^2\right]^{\frac{1}{2}} \quad \text{A105.}$$

where

$$\frac{\partial T_b(0)}{\partial T_i(0)} = 1 \quad \text{A106.}$$

$$\frac{\partial T_b(0)}{\partial T_o(0)} = -1 \quad \text{A107.}$$

$$\therefore U_{\Delta T_b(0)} = \sqrt{2}U_T \quad \text{A108.}$$

$$\frac{\partial T_w}{\partial \Delta T_b(0)} = -\frac{1}{C^* \dot{m}_i C_{pi}} + e^{U_{ov} p_i C^* z}\left[\frac{1}{C^* \dot{m}_i C_{pi}} - \frac{U_{ov}}{h_i}\right] \quad \text{A109.}$$

The uncertainty of the wall temperature with regards to C^* is described by equation (A110).

$$\frac{\partial T_w}{\partial C^*} = \Delta T_b(0)\left[\frac{1}{C^{*2} \dot{m}_i C_{pi}} - e^{-U_{ov} p_i C^* z}\left(\frac{1}{C^{*2} \dot{m}_i C_{pi}} + U_{ov} p_i z\left\{\frac{1}{C^* \dot{m}_i C_{pi}} + \frac{U_{ov}}{h_i}\right\}\right)\right] \quad \text{A110.}$$

where uncertainty in C^* is calculated using equation (A111):

$$U_{C^*} = \left[\left(\frac{\partial C^*}{\partial \dot{m}_i} U_{\dot{m}_i}\right)^2 + \left(\frac{\partial C^*}{\partial C_{pi}} U_{C_{pi}}\right)^2 + \left(\frac{\partial C^*}{\partial \dot{m}_o} U_{\dot{m}_o}\right)^2 + \left(\frac{\partial C^*}{\partial C_{po}} U_{C_{po}}\right)^2\right]^{\frac{1}{2}} \quad \text{A111.}$$

The terms of equation (A111) are defined as:

$$\frac{\partial C^*}{\partial \dot{m}_i} = -\frac{1}{\dot{m}_i{}^2 C_{pi}} \quad \text{A112.}$$

$$\frac{\partial C^*}{\partial C_{pi}} = -\frac{1}{\dot{m}_i C_{pi}^2} \quad \text{A113.}$$

$$\frac{\partial C^*}{\partial \dot{m}_o} = -\frac{1}{\dot{m}_o{}^2 C_{po}} \quad \text{A114.}$$

$$\frac{\partial C^*}{\partial C_{po}} = -\frac{1}{\dot{m}_o C_{po}^2} \quad \text{A115.}$$

The uncertainty of the wall temperature with regards to the mass flow rate and heat capacity rate for the inner tube is found in equations (A116) and (A117).

$$\frac{\partial T_w}{\partial \dot{m}_i} = \frac{\Delta T_b(0)}{C^* \dot{m}_i{}^2 C_{pi}}\left[1 - e^{U_{ov} p_i C^* z}\right] \quad \text{A116.}$$

$$\frac{\partial T_w}{\partial C_{pi}} = \frac{\Delta T_b(0)}{C^* \dot{m}_i C_{pi}^2}\left[1 - e^{U_{ov} p_i C^* z}\right] \quad \text{A117.}$$

The wall temperature uncertainty with respect to the overall heat transfer coefficient is described by equation (A118).

$$\frac{\partial T_w}{\partial U_{ov}} = \frac{\Delta T_b(0)}{h_i} e^{-U_{ov} p_i C^* z} \left[-1 + U_{ov} p_i C^* z\right] \quad \text{A118.}$$

The wall temperature uncertainty with respect to the inner tube heat transfer coefficient is found in equation (A119).

$$\frac{\partial T_w}{\partial h_i} = \frac{\Delta T_b(0)}{{h_i}^2} U_{ov} e^{-U_{ov} p_i C^* z} \quad \text{A119.}$$

The wall temperature uncertainty with respect to the perimeter is:

$$\frac{\partial T_w}{\partial p_i} = \frac{\Delta T_b(0)}{h_i} {U_{ov}}^2 C^* z e^{-U_{ov} p_i C^* z} \quad \text{A120.}$$

$$U_{p_i} = \frac{\partial p_i}{D_i} U_{D_i} \quad \text{A121.}$$

where

$$\frac{\partial p_i}{D_i} = \pi \quad \text{A122.}$$

The wall temperature uncertainty with respect to the position along the length of the tube is described by equation (A123).

$$\frac{\partial T_w}{\partial z} = \frac{\Delta T_b(0)}{h_i} {U_{ov}}^2 C^* e^{-U_{ov} p_i C^* z} \quad \text{A123.}$$

B. APPENDIX B – EXPERIMENTAL DATA

The experimental raw data that was recorded during testing can be found on the attached CD. All the measured data as well as the calculated data are included. An example of the data can be found below for a Reynolds number of 11 905 on the inner tube flow for the 8.3 mm tube.

Measured Variable	**Symbol**	**Units**	**Value**
Inner Tube:			
Reynolds Number	Re_i	[-]	11905.37
Mass Flow Rate	m_i	[kg/s]	0.045819334
Diameter	D_i	[m]	0.00829
Dynamic Viscosity	mu_i	[kg/m.s]	0.000591
Density	rho_i	[kg/m^3]	989.99
Specific Heat	Cp_i	[J/kg.K]	4179.695
Thermal Conductivity	k_i	[W/m.K]	0.637024189
Inlet Temperature	T_i_en	[°C]	57.73850015
Outlet Temperature	T_i_ex	[°C]	33.16353373
Pressure Drop	P_drop	[Pa]	5338.49
Nusselt Number	Nu	[-]	69.7046
Friction Factor	f	[-]	0.03090015
Prandtl Number	Pr	[-]	3.87837

The data for the 14.2 mm tube diameter is similarly calculated and also included on the attached disc.